



University of Kentucky  
UKnowledge

---

University of Kentucky Doctoral Dissertations

Graduate School

---

2007

## PORE ENGINEERING OF SURFACTANT TEMPLATED NANOPOROUS SILICA USING SUPERCRITICAL CARBON DIOXIDE

Kaustav Ghosh

*University of Kentucky*, [Kaustav.Ghosh@gmail.uky](mailto:Kaustav.Ghosh@gmail.uky)

[Right click to open a feedback form in a new tab to let us know how this document benefits you.](#)

---

### Recommended Citation

Ghosh, Kaustav, "PORE ENGINEERING OF SURFACTANT TEMPLATED NANOPOROUS SILICA USING SUPERCRITICAL CARBON DIOXIDE" (2007). *University of Kentucky Doctoral Dissertations*. 559.  
[https://uknowledge.uky.edu/gradschool\\_diss/559](https://uknowledge.uky.edu/gradschool_diss/559)

This Dissertation is brought to you for free and open access by the Graduate School at UKnowledge. It has been accepted for inclusion in University of Kentucky Doctoral Dissertations by an authorized administrator of UKnowledge. For more information, please contact [UKnowledge@lsv.uky.edu](mailto:UKnowledge@lsv.uky.edu).

ABSTRACT OF DISSERTATION

Kaustav Ghosh

The Graduate School  
University of Kentucky

2007

PORE ENGINEERING OF SURFACTANT TEMPLATED NANOPOROUS SILICA  
USING SUPERCRITICAL CARBON DIOXIDE

---

ABSTRACT OF DISSERTATION

---

A dissertation submitted in partial fulfillment of the  
requirements for the degree of Doctor of Philosophy in the  
College of Engineering  
at the University of Kentucky

By  
Kaustav Ghosh

Lexington, Kentucky

Director: Dr. Barbara L. Knutson, Professor of Chemical Engineering

Lexington, Kentucky

2007

Copyright © Kaustav Ghosh 2007

## ABSTRACT OF DISSERTATION

### PORE ENGINEERING OF SURFACTANT TEMPLATED NANOPOROUS SILICA USING SUPERCRITICAL CARON DIOXIDE

The use of compressed CO<sub>2</sub> processing to alter the pore size, structure and timescale of silica condensation in surfactant templated silica thin films and powders is investigated by systematically varying the template structure and CO<sub>2</sub> processing conditions. Tailoring the mesoporous materials increases its potential applications, as demonstrated in catalysis, drug delivery, chromatographic and electrode applications. This work demonstrates for the first time the applicability of fluorinated surfactants as templates for the synthesis of mesoporous silica thin films by dip coating. Well-ordered films with 2D hexagonal close-packed pore structure are synthesized in an acid-catalyzed medium using three cationic fluorinated templates of varied tail length and branching (C<sub>6</sub>F<sub>13</sub>C<sub>2</sub>H<sub>4</sub>NC<sub>5</sub>H<sub>5</sub>Cl, C<sub>8</sub>F<sub>17</sub>C<sub>2</sub>H<sub>4</sub>NC<sub>5</sub>H<sub>5</sub>Cl and (CF<sub>3</sub>)<sub>2</sub>CFC<sub>5</sub>F<sub>9</sub>C<sub>2</sub>H<sub>4</sub>NC<sub>5</sub>H<sub>5</sub>Cl). CO<sub>2</sub> processing of the fluorinated templated silica results in a significant and controlled increase in pore diameter relative to the unprocessed films. The pore expansion is significantly greater compared to the negligible expansion observed in hydrocarbon (C<sub>16</sub>H<sub>23</sub>NC<sub>5</sub>H<sub>5</sub>Br) templated silica. The greater swelling of the fluorinated templates is attributed to the favorable penetration of CO<sub>2</sub> in the 'CO<sub>2</sub>-philic' fluorinated tail and the relative solvation of each template is interpreted from their interfacial behavior at the CO<sub>2</sub>-water interface.

The CO<sub>2</sub> based pore expansion observed in fluorinated surfactant templated films is extended successfully to base-catalyzed silica powders templated with a fluorinated surfactant (C<sub>6</sub>F<sub>13</sub>C<sub>2</sub>H<sub>4</sub>NC<sub>5</sub>H<sub>5</sub>Cl). Pore expansion in silica powders is significantly less than in acid catalyzed films and demonstrates the effects of pH on surfactant self-assembly in CO<sub>2</sub> and increased silica condensation at basic conditions, which inhibits pore expansion.

Finally, the use of fluorescence probe molecules is demonstrated for in-situ monitoring of the of CO<sub>2</sub> processing of surfactant templated silica films to provide time dependent data on the local environment and dynamics of CO<sub>2</sub> penetration. CO<sub>2</sub> uptake occurs in surfactant tails even for hydrocarbon templates (C<sub>16</sub>H<sub>23</sub>N(CH<sub>3</sub>)<sub>3</sub>Br and C<sub>16</sub>H<sub>23</sub>NC<sub>5</sub>H<sub>5</sub>Br), which display negligible CO<sub>2</sub> based swelling of the resulting pores.

The timescale of silica condensation increases significantly in the presence of CO<sub>2</sub> suggesting opportunities for structure alteration through application of external forces, such as magnetic fields and change in substrate chemistry and system humidity.

**KEYWORDS:** Supercritical fluids, 'CO<sub>2</sub>-philic' fluorinated surfactants, mesoporous silica, surfactant solvation, fluorescence spectroscopy.

---

Kaustav Ghosh

---

10/16/2007

---

PORE ENGINEERING OF SURFACTANT TEMPLATED NANOPOROUS SILICA  
USING SUPERCRITICAL CARON DIOXIDE

By

Kaustav Ghosh

Dr Barbara Knutson

---

Director of Dissertation

Dr Barbara Knutson

---

Director of Graduate Studies

Date 10/16/2007

---

## RULES FOR THE USE OF DISSERTATIONS

Unpublished dissertations submitted for the Doctor's degree and deposited in the University of Kentucky Library are as a rule open for inspection, but are to be used only with due regard to the rights of the authors. Bibliographical references may be noted, but quotations or summaries of parts may be published only with the permission of the author, and with the usual scholarly acknowledgments.

Extensive copying or publication of the dissertation in whole or in part also requires the consent of the Dean of the Graduate School of the University of Kentucky.

A library that borrows this dissertation for use by its patrons is expected to secure the signature of each user.

Name

Date

---

---

---

---

---

---

---

---

---

---

DISSERTATION

Kaustav Ghosh

The Graduate School  
University of Kentucky

2007



PORE ENGINEERING OF SURFACTANT TEMPLATED NANOPOROUS SILICA  
USING SUPERCRITICAL CARON DIOXIDE

---

DISSERTATION

---

A dissertation submitted in partial fulfillment of the  
requirements for the degree of Doctor of Philosophy in the  
College of Engineering  
at the University of Kentucky

By  
Kaustav Ghosh  
Lexington, Kentucky

Director: Dr. Barbara L. Knutson, Professor of Chemical Engineering

Lexington, Kentucky

2007

Copyright © Kaustav Ghosh 2007

## ACKNOWLEDGEMENTS

First and foremost I would like to thank my advisor, Dr. Barbara Knutson for her continuous guidance and the unlimited patience that she showed during the course of this research. She has always encouraged me to come up with my own solutions and allowed me to explore research areas following my own personal interests which I believe was instrumental in developing my research skills. She has become an inspiration for me not only in research, but in all facets of life showing the way to overcome obstacles through dedication, hard work and patience. I am grateful that I got this opportunity to spend five important years of my life under her guidance.

I am also thankful to Dr. Stephen Rankin who was always ready to answer any question I had for him and provided many valuable inputs to my research. A special thanks to Dr. Geoff Bothun who was the best senior lab member / mentor possible and whose many valuable suggestions were important in getting me started on the right track in my research. I would also like to thank Dr. Hans Lehmler and his research group for synthesizing the many surfactants for this work. Thanks to my committee members, Dr. Douglass Kalika, Dr. Folami Ladipo and Dr. Janet Lumpp for their time and advice for completion of this dissertation. I would also like to acknowledge the contributions of Dr. Alan Dozier for help with TEM and Henry Francis and Jason Backus of Kentucky Geological Survey for their assistance with XRD.

I was extremely fortunate to have joined the Supercritical Fluids Lab and work with some great persons. Thanks to you all: Yeh Wei, Gifty, Vivian, Sarah, Kari, Satya,

Kim, Nick, Babacar and Amanda. You have all in your own separate ways contributed immensely to my Ph.D. experience and made my time here most enjoyable. I would also like to thank Venkat for allowing me to use his custom designed dip-coater for my research. Lexington and UK will always hold a special place in my heart and for that I am thankful to all my friends here. The long road trips and their even longer planning, unplanned outings, Friday night parties and the late night / early morning discussions will always be in my memories.

I would like to thank my parents Subhasis Ghosh and Manju Ghosh who have always convinced me that I can achieve anything I set my mind to. Even though far away, their love and support are very important to me and keeps me going. I am also thankful to my brother-in-law and my good friend, Soumya for having numerous stimulating conversations to keep me thinking. The final acknowledgements are reserved for the two most important persons in my life. A very special thanks to my sister, Priyanka growing up with whom has been a special time in my life. It has been really hard not seeing her for long periods of time during my stay in Lexington, but she has constantly encouraged me and felt proud of my accomplishments which has been very important to me. Finally, I would like to dedicate this dissertation to my wife and my best friend, Sonia. For the last four years, she has been constantly on my side, always ready to listen to the many frustrations and problems in my research and keep me focused and remind me of the important things in life. Without her support and love this work would never have been complete.

## TABLE OF CONTENTS

Acknowledgments.....	iii
List of Tables.....	viii
List of Figures.....	ix
Chapter One: Introduction.....	1
1.1 Research Hypothesis.....	3
1.2 Research Objectives .....	3
1.3 Overview of Dissertation Chapters .....	4
Chapter Two: Background.....	5
2.1 Porous Material.....	5
2.2 Surfactant Self Assembly .....	6
2.3 Mesoporous Silica Thin Film – Synthesis and Characterization .....	9
2.4 Tailoring of Surfactant Templated Materials.....	13
2.5 Compressed CO <sub>2</sub> in Surfactant Aggregates .....	15
2.6 Fluorescence Spectroscopy Probing of Surfactant Templates and CO <sub>2</sub> Dispersions .....	19
Chapter Three: Supercritical Carbon Dioxide Processing of Fluorinated Surfactant Templated Mesoporous Silica Thin Films .....	27
3.1 Summary.....	27
3.2 Introduction.....	27
3.3 Materials and Methods.....	29
3.4 Results and Discussion.....	31
3.5 Conclusions.....	37
Chapter Four: Tailoring Porous Silica Films through Supercritical Carbon Dioxide Processing of Fluorinated Surfactant Templates.....	39
4.1 Summary.....	39
4.2 Introduction.....	39
4.3 Materials and Methods.....	43
4.3.1 Materials.....	43
4.3.2 Cross-Polarized Microscopy.....	43
4.3.3 Thin Film Synthesis.....	43
4.3.4 Thin Film Characterization.....	44
4.3.5 Interfacial tension Measurements.....	45
4.3.6 Surfactant Solubility in CO <sub>2</sub> .....	45
4.4 Results and Discussion.....	46
4.4.1 Synthesis of Silica Thin Films Templated by Cationic Fluorinated Surfactants .....	46
4.4.2 Effects of CO <sub>2</sub> Processing on Thin Film Structure .....	51
4.4.3 Micelle-Based Interpretation of Pore Expansion.....	55
4.5 Conclusions.....	57

Chapter Five: Pore Size Engineering in Fluorinated Surfactant Templated Mesoporous Silica Powders through Supercritical Carbon Dioxide Processing ....	59
5.1 Summary.....	59
5.2 Introduction.....	59
5.3 Materials and Methods.....	61
5.3.1 Materials.....	61
5.3.2 Mesoporous Silica Synthesis and CO <sub>2</sub> processing.....	62
5.3.3 Material Characterization .....	62
5.4 Results and Discussion.....	63
5.5 Conclusions.....	73
 Chapter Six: Supercritical Carbon Dioxide Swelling of Fluorinated and Hydrocarbon Surfactant Templates in Mesoporous Silica Thin Films .....	75
6.1 Summary.....	75
6.2 Introduction.....	76
6.3 Materials and Methods.....	79
6.3.1 Materials.....	79
6.3.2 Substrate Preparation.....	79
6.3.3 Thin Film Synthesis.....	80
6.3.4 Thin Film Characterization.....	80
6.3.5 Contact angle measurement.....	81
6.4 Results and Discussion.....	81
6.4.1 Synthesis of Uniform Silica Thin Films by Fluorinated and Hydrocarbon Templates .....	81
6.4.2 Effects of CO <sub>2</sub> Processing on Thin Film Structure .....	87
6.5 Conclusions.....	93
 Chapter Seven: In-Situ Fluorescence Spectroscopy of Supercritical Carbon Dioxide Processing of Surfactant Templated Nano-Structured Silica Film..	95
7.1 Summary.....	95
7.2 Introduction.....	95
7.3 Materials and Methods.....	98
7.3.1 Chemicals.....	98
7.3.2 Film Synthesis .....	100
7.3.3 Atmospheric Fluorescence Measurements .....	100
7.3.4 High Pressure Fluorescence Spectroscopy .....	101
7.3.5 Nonradiative Energy Transfer (NRET) .....	102
7.4 Results and Discussion.....	102
7.4.1 Fluorescence Spectroscopy of Silica Films without CO <sub>2</sub> Processing .....	102
7.4.2 Timescales of Silica Condensation with CO <sub>2</sub> processing .....	105
7.4.3 High Pressure Nonradiative Energy Transfer .....	111
7.4.4 Silica Film Processing in Additional Solvent Environments .....	114
7.5 Conclusions .....	115
 Chapter Eight: Conclusions and Future Work.....	117

8.1 Conclusions.....	117
8.2 Future Work.....	120
Appendix A	
Solubility of Novel Nonionic Fluorinated Esters in Carbon Dioxide .....	123
Appendix B	
Investigation towards Alignment of Mesochannels in Mesoporous Silica Films Through Application of a Magnetic Field .....	128
References .....	132
Vita .....	145

## LIST OF TABLES

Table 3.1, Summary of d-spacing corresponding to (100) peak, lattice parameter and pore diameters of unprocessed thin films and CO <sub>2</sub> processed films before surfactant extraction as a function of processing conditions .....	36
Table 4.1, Summary of d-spacing and pore diameter for thin film templated with all three different surfactants as a function of CO <sub>2</sub> processing conditions .....	50
Table 5.1, Summary of pore structure of mesoporous silica powders as a function of CO <sub>2</sub> processing conditions .....	69
Table 6.1, Average contact angle measurements of CPB and HFOPC based solutions on glass and FDTS modified substrate .....	83
Table 6.2, Summary of pore diameter and absolute magnitude of pore expansion for thin film templated with all three surfactants as a function of CO <sub>2</sub> density...	91
Table A1, Structures of the nonionic fluorinated nicotinic acid esters in this study .....	124

## LIST OF FIGURES

Figure 2.1, Phase diagram and schematics of surfactant liquid crystal phases for CTAB .....	8
Figure 2.2, Thickness of film during dip-coating of a solution of silica, surfactant, alcohol, and water. Surfactant concentration increases with dip-coating time and distance above the reservoir surface .....	10
Figure 2.3, . Alkane penetration in surfactant tail based on mechanism proposed by Ulagappan et. al. <sup>153</sup> with a) short alkanes solublizing in tail and b) alkanes larger than decane forming separate core .....	15
Figure 2.4, Schematic of interfacial tension of surfactants at C/W interfaces as a function of HCB and other formulation variables .....	18
Figure 2.5, One form of Jablonski Diagram demonstrating fluorescence, phosphorescence and intersystem crossing .....	20
Figure 2.6, A form of Jablonski Diagram showing quenching and non-radiative energy transfer (NRET). $\Sigma k_i$ represents other nonradiative paths to the ground state .....	21
Figure 2.7, Schematic of the mechanism of non-radiative energy transfer (NRET) between an acceptor and donor .....	22
Figure 3.1, XRD patterns of thin films prepared without CO <sub>2</sub> processing (a) as-synthesized and (b) after surfactant extraction .....	32
Figure 3.2, TEM micrographs of (a) as-synthesized thin films not processed in CO <sub>2</sub> (b) extracted thin films not processed in CO <sub>2</sub> and (c) thin films processed in CO <sub>2</sub> at 172 bar and 45°C before surfactant extraction .....	33
Figure 3.3, XRD spectra of thin films before surfactant extraction (a) processed in CO <sub>2</sub> at 172 bar and 45°C, (b) processed in CO <sub>2</sub> at 172 bar and 25°C, (b) processed in CO <sub>2</sub> at 137 bar and 45°C, (d) processed in CO <sub>2</sub> at 103 bar and 45°C, (e) processed in CO <sub>2</sub> at 69 bar and 45°C and (f) not processed in CO <sub>2</sub> .....	35
Figure 4.1, Schematic of the homologous series of perfluoroalkylpyridinium chloride surfactants.....	42
Figure 4.2, XRD patterns of thin films prepared without CO <sub>2</sub> processing and templated with (a) HFOPC, (b) HFDoMePC and (c) HFDePC .....	47



Figure 4.3, TEM micrographs of thin films prepared without CO <sub>2</sub> processing and templated with (a) HFOPC, (b) HFDoMePC and (c) HFDePC and (d) for film templated with HFOPC and processed in CO <sub>2</sub> at 172 bar and 45 °C...	48
Figure 4.4, Nitrogen sorption isotherm of thin films prepared without CO <sub>2</sub> processing templated with (a) HFOPC, (b) HFDoMePC and (c) HFDePC. Open symbols are for adsorption and filled for desorption. The y-axis values have been offset by 130 units (trace b) and by 300 units (trace c) for clarity.....	49
Figure 4.5, XRD spectra of thin films templated with HFOPC and processed in CO <sub>2</sub> at (a) 172 bar and 45 °C, (b) 172 bar and 25 °C, (c) 137 bar and 45 °C, (d)103 bar and 45 °C, (e) 69 bar and 45 °C, and (f) not processed in CO <sub>2</sub> ...	52
Figure 4.6, Percentage increase of (a) d-spacing and (b) pore diameter of thin films processed in CO <sub>2</sub> relative to unprocessed films as a function of CO <sub>2</sub> density .....	53
Figure 4.7, Interfacial tension of all three surfactants at the CO <sub>2</sub> -water interface as a function of CO <sub>2</sub> pressure at 45 °C. Scaling on y-axis different above and below the break for clarity. Standard deviations of IFT values from this study (< ± 4%) not shown in figure for clarity. CO <sub>2</sub> -water interfacial tensions from this study are compared to those of da Rocha et.al. <sup>48</sup> and Chun and Wilkinson. <sup>76</sup> .....	55
Figure 5.1, XRD patterns of HFOPC templated silica powders synthesized (a) without CO <sub>2</sub> processing; and processed in CO <sub>2</sub> at 103 bar and 45 °C after aging for (b) 20 min, (c) 1 hr and (d) 24 hr .....	64
Figure 5.2, TEM micrographs of HFOPC templated mesoporous silica powders (a) without CO <sub>2</sub> processing and (b) processed in CO <sub>2</sub> at 103 bar and 45 °C ....	65
Figure 5.3, Nitrogen sorption isotherm of HFOPC templated silica powders prepared with CO <sub>2</sub> processing (103 bar and 45 °C) after aging for (a) 20 min, (b) 1 hr and (c) 24 hr. Filled symbols are for adsorption and open for desorption. The y-axis values have been offset by 600 units (trace b) and by 1000 units (trace c) for clarity .....	66
Figure 5.4, XRD patterns of mesoporous silica powders templated with HFOPC (a) before processing in CO <sub>2</sub> and processed in CO <sub>2</sub> at (b) 88 bar and 45 °C (ρ <sub>CO2</sub> = 0.31 g/ml), (c) 103 bar and 45 °C (ρ <sub>CO2</sub> = 0.54 g/ml), (d) 137 bar and 45 °C (ρ <sub>CO2</sub> = 0.71 g/ml), (e) 172 bar and 45 °C (ρ <sub>CO2</sub> = 0.78 g/ml), (f) 258 bar and 45 °C (ρ <sub>CO2</sub> = 0.86 g/ml), and (g) 344 bar and 45 °C (ρ <sub>CO2</sub> = 0.91 g/ml). (110) reflections have been expanded 3 times in some plots for clarity .....	68

Figure 5.5 Nitrogen sorption isotherm of mesoporous silica powders templated with HFOPC and processed in CO <sub>2</sub> at (a) 88 bar and 45 °C, (b) 103 bar and 45 °C, (c) 137 bar and 45 °C, (d) 172 bar and 45 °C, (e) 258 bar and 45 °C, and (f) 344 bar and 45 °C. Filled symbols are for adsorption and open for desorption. The y-axis values have been offset for clarity .....	70
Figure 5.6 Percentage increase of pore diameter of HFOPC templated acid-catalyzed films and base-catalyzed powders as a function of CO <sub>2</sub> density .....	72
Figure 6.1, Schematic of cetyl pyridinium bromide and perfluoroalkylpyridinium chloride surfactant .....	78
Figure 6.2, XRD patterns of thin films prepared without CO <sub>2</sub> processing templated with (a) HFCPC (b) HFOPC and (c) CPB .....	84
Figure 6.3, TEM micrographs of thin films templated with (a) HFCPC, (b) CPB and (c) HFOPC and (d) HFCPC and processed in CO <sub>2</sub> at 172 bar and 45°C, (e) CPB and processed in CO <sub>2</sub> at 172 bar and 45°C and (f) HFOPC and processed in CO <sub>2</sub> at 172 bar and 45°C .....	86
Figure 6.4, XRD spectra of thin films templated with (i) HFCPC and (ii) CPB and (a) not processed in CO <sub>2</sub> , (b) processed in CO <sub>2</sub> at 69 bar and 45 °C, (c) processed in CO <sub>2</sub> at 103 bar and 45 °C, (d) processed in CO <sub>2</sub> at 137 bar and 45 °C, and (e) processed in CO <sub>2</sub> at 172 bar and 45 °C .....	88
Figure 6.5, Percentage increase of pore diameter of thin films templated with all three surfactants as a function of CO <sub>2</sub> processing density .....	90
Figure 7.1, Schematic of CTAB, CPB, naphthalene and pyrene and its derivatives.....	99
Figure 7.2, Apparatus for high pressure thin film fluorescence measurements .....	101
Figure 7.3, Emission spectra of pyrene in a) CTAB and b) CPB templated film without CO <sub>2</sub> processing .....	103
Figure 7.4, Emission spectra of C <sub>10</sub> -pyr in a) CTAB and b) CPB and C <sub>16</sub> -pyr in c) CTAB and d) CPB templated film .....	105
Figure 7.5, a) Change in emission intensity and b) I <sub>1</sub> /I <sub>3</sub> values of pyrene spectra in CTAB templated film and processed in CO <sub>2</sub> at 103 bar and 45C for aging times less than 5 min and greater than 25 min .....	107
Figure 7.6, Change in emission intensity of C <sub>16</sub> -pyr in CPB templated film and processed in CO <sub>2</sub> at different pressures and 45°C as function of processing time ....	109

Figure 7.7, Emission spectra of C <sub>16</sub> -pyr in CTAB templated film excited at 290 nm and processed in CO <sub>2</sub> at 103 bar and 45°C (a) without dissolved naphthalene and (b) with naphthalene dissolved in CO <sub>2</sub> .....	112
Figure 7.8, I <sub>p</sub> / I <sub>n</sub> values due to NRET between naphthalene solubilized in processing CO <sub>2</sub> and C <sub>16</sub> -pyr in CTAB templated film as a function of time and processing pressure .....	113
Figure 7.9, Change in emission intensity of C <sub>16</sub> -pyr in CPB templated film and processed 3 different solvents as a function of time .....	115
Figure A.1, Cloud point and bubble point pressure for FONE-1, FONE-2 and FHNE-2 as a function of surfactant concentration at different temperatures .....	126
Figure B.1, XRD plots of silica thin film templated with HFOPC and with (a) no magnetic field and (b) in the presence of magnetic field of strength ~ 1T ...	130

## CHAPTER ONE

### INTRODUCTION

The synthesis of porous materials (ceramics, polymers, activated carbon, metal oxides, metal-organic matrices) with high surface area and a well-ordered structure, has been an important and active field of research for many years because of their wide variety of applications. The most extensive application of such materials has been in catalysis, both as active catalysts<sup>1-4</sup> and as catalyst support<sup>5-11</sup>, adsorption<sup>12-15</sup> and separations.<sup>16-20</sup> Applications have also been extended to novel areas such as fuel cells,<sup>21</sup> semiconductors,<sup>22</sup> and biological materials.<sup>23</sup> In 1992, the synthesis of well-ordered porous materials was demonstrated through the thermodynamically controlled co-assembly of surfactant templates with metal oxide precursors for the synthesis of porous silica, thus dictating a high degree of control over the final pore structure.<sup>24</sup> The surfactant templating technique was later extended to the formation of thin porous silica films with long range order.<sup>25,26</sup> Subsequently, porous silica materials have been tailored to increase their potential applications through choice of the surfactant template (cationic surfactants, e.g. CTAB<sup>24</sup>; anionic surfactants, e.g. SDS<sup>27</sup>; nonionic surfactants, e.g. Brij 56<sup>28</sup>; block copolymers, e.g. P123;<sup>28,29</sup> and fluorinated surfactants<sup>30,31</sup>), introduction of functional groups<sup>32-36</sup> or by introduction of an organic swelling agent to alter the pore structure with a given template.<sup>37-40</sup>

The many attractive properties of supercritical (sc) CO<sub>2</sub> compared to traditional organic solvents suggest its application for tailoring surfactant templated porous materials. Sc CO<sub>2</sub> is an inexpensive, nontoxic, nonflammable, chemically inert and environmentally friendly (unregulated by the U.S. Environmental Protection Agency) solvent. Additionally, sc CO<sub>2</sub> possesses high diffusivity, low viscosity, low surface tension and a pressure tunable solvent strength. Over the last two decades, application of CO<sub>2</sub> in diverse areas such as extraction of metals and drugs,<sup>41,42</sup> polymer synthesis and processing,<sup>43-45</sup> nanoparticle synthesis,<sup>46-48</sup> coatings,<sup>49</sup> catalysis,<sup>50,51</sup> photoresist drying<sup>52</sup> and processing of microelectronic devices<sup>53</sup> has been investigated. The application of sc CO<sub>2</sub> in processing inorganic porous materials has also significantly increased; its high

diffusivity allows quick diffusion into the nanometer sized pores while the absence of a liquid-vapor interface during removal of sc CO<sub>2</sub> prevents pore collapse.<sup>54-60</sup> Sc CO<sub>2</sub> has been applied to infuse precursors into preformed templates to synthesize nanoporous metals and oxides<sup>54,55</sup>, while nanoparticles dissolved in sc CO<sub>2</sub> have been successfully impregnated into small micropores of FSM-16 as a result of the favorable penetration of sc CO<sub>2</sub> compared to liquid solvents.<sup>54</sup> sc CO<sub>2</sub> has also been used as the solvent for alumina functionalization in mesoporous silica,<sup>56</sup> in catalysis applications in mesoporous silica<sup>57,58</sup> and as a solvent for surfactant extraction from surfactant templated porous silica.<sup>59,60</sup>

The use of sc CO<sub>2</sub> as a processing solvent is limited by its poor solvent power, particularly for polar solutes. Improvement of this solvent strength has been achieved in various studies by creating polar domains in CO<sub>2</sub> based reverse emulsions and micromulsions through the use of surfactants.<sup>51,61-64</sup> However, sc CO<sub>2</sub> is unable to form emulsions and micromulsions with most of the commercially available hydrocarbon surfactants<sup>65</sup> because the lower polarizability of CO<sub>2</sub> compared to organic solvents results in weak solvation of the surfactant tails by CO<sub>2</sub>.<sup>66</sup> Surfactants having low cohesive energy density and high free volume (e.g. siloxanes, surfactants with methyl groups and tail branching, oxygen containing molecules, e.g. carbonyls, ethers, and fluorocarbon groups) have favorable interactions with CO<sub>2</sub> and are termed 'CO<sub>2</sub>-philic'.<sup>64,67-74</sup> Alternatively, there has been limited investigation of CO<sub>2</sub> penetration in concentrated surfactant mesophases.<sup>75</sup>

Cationic fluorinated surfactants (e.g., perfluoralkyl pyridinium chlorides)<sup>31,76</sup> and nonionic fluorinated surfactants (FSO-100 (CF<sub>3</sub>-(CF<sub>2</sub>)<sub>4</sub>(EO)<sub>10</sub>) and FSN-100 (CF<sub>3</sub>(CF<sub>2</sub>)<sub>5</sub>(EO)<sub>14</sub>))<sup>30</sup> have recently been demonstrated as templates for the successful synthesis of mesoporous silica powders. Advantages of fluorinated templates include the ability to obtain a wide range of pore sizes in both microporous and mesoporous ranges,<sup>31</sup> a wide variety of pore structures (both hexagonal close-packed and novel mesh phase structures),<sup>31</sup> novel fluorinated functional group incorporation,<sup>77</sup> vinyl functionalized materials with increased accessibility relative to hydrocarbon surfactant (CTAB) templated powders,<sup>76</sup> and higher hydrothermal stability compared to hydrocarbon templated materials.<sup>78</sup> Potential application of such diverse materials has been suggested

for novel CO<sub>2</sub> adsorbents, packing materials in chromatography columns for separation of fluorocarbon and hydrocarbon compounds, and controlled drug delivery.<sup>77,79</sup> Perfluoroalkyl pyridinium chloride surfactants have also been suggested for other potential applications in novel gene and drug delivery systems.<sup>80</sup>

### **1.1 Research Hypothesis**

This dissertation examines the overall hypothesis that fluorinated surfactant templating can be extended to porous silica films and that subsequent processing of these films by compressed CO<sub>2</sub> will alter the pore structure. Significant interaction of CO<sub>2</sub> with the fluorinated templated materials is expected compared to traditional hydrocarbon templated materials. The pressure tunable solvent strength of CO<sub>2</sub> along with the use of templates with varying structure is expected to result in tailored silica materials.

### **1.2 Research Objectives**

The specific objectives of this research are:

1. To synthesize well-ordered porous silica thin films using fluorinated surfactants as templating agents.
2. To determine pore structure for fluorinated surfactant templated silica films and powders as a function of surfactant template and CO<sub>2</sub> processing conditions using X-ray diffraction (XRD), transmission electron microscopy (TEM) and nitrogen sorption measurements
3. To compare the pore expansion observed in fluorinated templates with that for traditional hydrocarbon surfactant templates at similar CO<sub>2</sub> conditions and to determine if pore size can be tailored by selective solvation of fluorocarbon groups in the template.
4. To develop an interpretation of the pore expansion behavior as a function of surfactant template and its interactions with CO<sub>2</sub> and thereby to provide a systematic approach to design future surfactant systems to generate specific tailored pore sizes.
5. To investigate the mechanism of CO<sub>2</sub> processing of surfactant templated silica films using high pressure spectroscopy techniques.

### 1.3 Overview of Dissertation Chapters

Chapter 2 provides a brief overview of synthesis and applications of surfactant templated materials, the thermodynamics of self-assembly and mesophase formation for surfactants, the tailoring of the mesostructure by solvents, compressed CO<sub>2</sub> processing of surfactant systems, and different techniques used in fluorescence spectroscopy to probe surfactant micelles and CO<sub>2</sub> systems.

Chapter 3 demonstrates the first synthesis of well-ordered acid-catalyzed silica thin film templated with a fluorinated surfactant, 1-(3,3,4,4,5,5,6,6,7,7,8,8,9,9,10,10,10-Heptadecafluoro-decyl)pyridinium chloride (C<sub>8</sub>F<sub>17</sub>C<sub>2</sub>H<sub>4</sub>NC<sub>5</sub>H<sub>5</sub>Cl) and subsequent CO<sub>2</sub> processing to expand the pore size as a function of CO<sub>2</sub> conditions while maintaining the long range structure before surfactant extraction. Chapter 4 continues with the CO<sub>2</sub> processing of nanoporous silica thin films using three cationic fluorinated surfactant templates (perfluoralkyl pyridinium chloride surfactants with systematic variation in tail length and branching) and pore expansion is compared as a function of template structure and CO<sub>2</sub> conditions. The relative pore expansion for each template as a function of processing conditions is further interpreted from the interfacial behavior of the surfactants at CO<sub>2</sub>-water interfaces.

Chapter 5 successfully extends the CO<sub>2</sub> processed pore expansion observed in porous silica films to base-catalyzed silica powders templated with the fluorinated surfactant 1-(3,3,4,4,5,5,6,6,7,7,8,8,8-tridecafluoro-octyl)-pyridinium chloride (C<sub>6</sub>F<sub>13</sub>C<sub>2</sub>H<sub>4</sub>NC<sub>5</sub>H<sub>5</sub>Cl) and compares pore expansion as a function of CO<sub>2</sub> conditions between mesoporous silica films and powders. Chapter 6 investigates the ability of CO<sub>2</sub> to preferentially solvate CO<sub>2</sub>-philic groups in concentrated surfactant mesophases by studying pore expansion as a function of the percentage of fluorocarbon segments in the surfactant template. Finally, Chapter 7 establishes high pressure steady state fluorescence spectroscopy as a powerful technique to investigate CO<sub>2</sub> penetration and delivery of solutes by CO<sub>2</sub> processing of surfactant templated films in real time.

## CHAPTER TWO

### BACKGROUND

The chapter briefly introduces the different types of porous materials, their applications and provides a description of the synthesis of surfactant templated mesoporous ordered materials. Self-assembly of surfactants to generate micelles and ordered liquid crystals are discussed next. The chapter continues with a detailed discussion of the synthesis of ordered mesoporous silica thin films and methods of tailoring the structure of templated porous silica. The interactions of compressed CO<sub>2</sub> with surfactant aggregates is discussed next followed by a brief review of different techniques in fluorescence spectroscopy and its application to probe surfactant micelles, templated materials and high pressure CO<sub>2</sub> systems.

#### 2.1 Porous Materials

Porous materials have been the subject of many investigations because of their wide application in a variety of industrial areas. Porous inorganic oxides and carbons have found application in catalysis,<sup>81</sup> adsorption, membrane separations<sup>82</sup> and in-vitro tissue engineering.<sup>83</sup> Porous polymers are applied as packing materials for chromatography,<sup>84</sup> adsorbents, ion exchange materials<sup>85</sup> and catalyst supports.<sup>86</sup> The large number of applications of the porous materials is due to their high surface area and porosities. Their unique dimensions determine their applications. Porous materials are classified into three groups according to their sizes: microporous materials having pore sizes less than 2 nm; mesoporous materials with pore sizes between 2 and 50 nm; and macroporous materials having pore sizes greater than 50 nm.

Zeolites are the most widely used microporous materials because their crystalline aluminosilicate network<sup>87</sup> and very narrow pore size distribution<sup>88</sup> provide important advantages in numerous applications in catalysis<sup>89</sup> and adsorption.<sup>90</sup> However most available zeolites have pore sizes between 4 Å to 7 Å<sup>81</sup> which limits their application for larger organic molecules. Porous materials synthesized by intercalation of layered



materials such as metal phosphates and clays<sup>91</sup> and porous glasses and gels<sup>92</sup> have pore size in the mesoporous range but their broad pore size distribution limit their applications.

In 1992, researchers from Mobil Corporation discovered the first controlled method to synthesize mesoporous materials with long range order.<sup>24</sup> Surfactants were used as pore templates with their self-assembled mesophases dictating the pore structure. The inorganic precursor formed a solid network around the templates through interaction with the surfactant head group and subsequent removal of the template resulted in the final ordered material. The synthesis of ordered mesoporous materials greatly increased the application of porous materials in catalysis, adsorption, separation, photocatalysis, hydrogen storage, solar cell technologies, drug delivery, biocatalysis and bioadsorption.<sup>93-100</sup>

## **2.2 Surfactant Self Assembly**

Surfactants are surface active molecules with one part having an affinity for polar media while the other region interacts favorably with non-polar media. The interactions direct the molecules to spontaneously form an oriented monolayer at the water-air interface thus lowering the surface tension. Surfactants are classified into four major groups according to the nature of their head groups: anionic (negatively charged head group), cationic (positively charged head group), non-ionic (no charge on the head group) and zwitterionic (both positive and negative charges on the head group).<sup>101</sup>

Surfactants present in very low concentration in aqueous solutions adsorb mainly at the interface and remains dispersed in solution as monomers. Increasing the surfactant concentration above the critical micelle concentration (cmc)<sup>101</sup> results in the formation of aggregates called micelles with the hydrophobic tails contained within the micelle interior and the hydrophilic headgroup facing the aqueous medium.<sup>102</sup> The formation of such micelle aggregates is a thermodynamically controlled process driven by the hydrophobicity of the surfactant tails.<sup>101</sup> Several researchers, most notably Nagarajan and Blankschtein, have investigated the thermodynamics of micelle formation and have determined the theoretical cmc and micelle structure of surfactants by investigating the Gibbs free energy change for the process.<sup>103-107</sup> Several interactions of the surfactants were determined to be important for the micelle formation process including the

hydrophobic interactions (enthalpic) between surfactant tails and water, conformational effects (entropic) associated with chain packing in the micelle core, interfacial effects at the micellar core-water interface, and finally steric (entropic) and electrostatic interactions (enthalpic) between surfactant headgroups.<sup>106</sup> Different combinations of these interactions leads to different micelle shapes such as spherical, cylindrical, lamellar, etc.

The micellar structure is related to the geometry of surfactant using the surfactant packing parameter,  $g = v/al$ ,<sup>108</sup> where  $v$  is the volume of the hydrophobic chain,  $l$  the length of the chain and  $a$  the head-group area per molecule.  $a$  is actually a thermodynamic quantity and can roughly be defined as  $a = (\alpha/\sigma)^{1/2}$ , where  $\alpha$  is a headgroup interaction parameter and  $\sigma$  is the interfacial free energy.<sup>109,110</sup> Spherical micelles are obtained for  $g < 1/3$ , a cylindrical structure is obtained for  $1/3 < g < 1/2$ , a bilayer is obtained for  $1/2 < g < 1$  and inverse structures are obtained for  $g > 1$ .<sup>108</sup> An increase in surfactant tail length makes the surfactant more hydrophobic resulting in easier self-assembly and a corresponding lower value of cmc. Branching of surfactant tails also result in micelle formation at a lower cmc and in aggregates that are more loosely packed.<sup>111</sup>

A progressive increase in surfactant concentration above the cmc results in the micelles packing together and forming a variety of liquid crystal structures. The resulting liquid crystal structures are functions of surfactant concentration and packing parameter. The different micelle structures and liquid crystal phases observed for a model hydrocarbon surfactant, cetyltrimethylammonium bromide (CTAB) is schematically presented in Figure 2.1. At the lowest surfactant concentration for micelle formation, spherical micelles are observed with a high curvature and headgroup area per molecule. With an increase in surfactant concentration, the curvature of the structures decreases and cylindrical micelles are formed. Liquid crystal structures are formed at even higher surfactant concentration and decreases in curvature with increase in concentration to form hexagonal, cubic and finally lamellar phase.<sup>112</sup>

Fluorinated surfactants are a special class of surfactants where one or more of the hydrogen atoms in the surfactant tail are replaced by fluorine. The presence of fluorine results in many unique properties including fluorinated surfactants being considerably

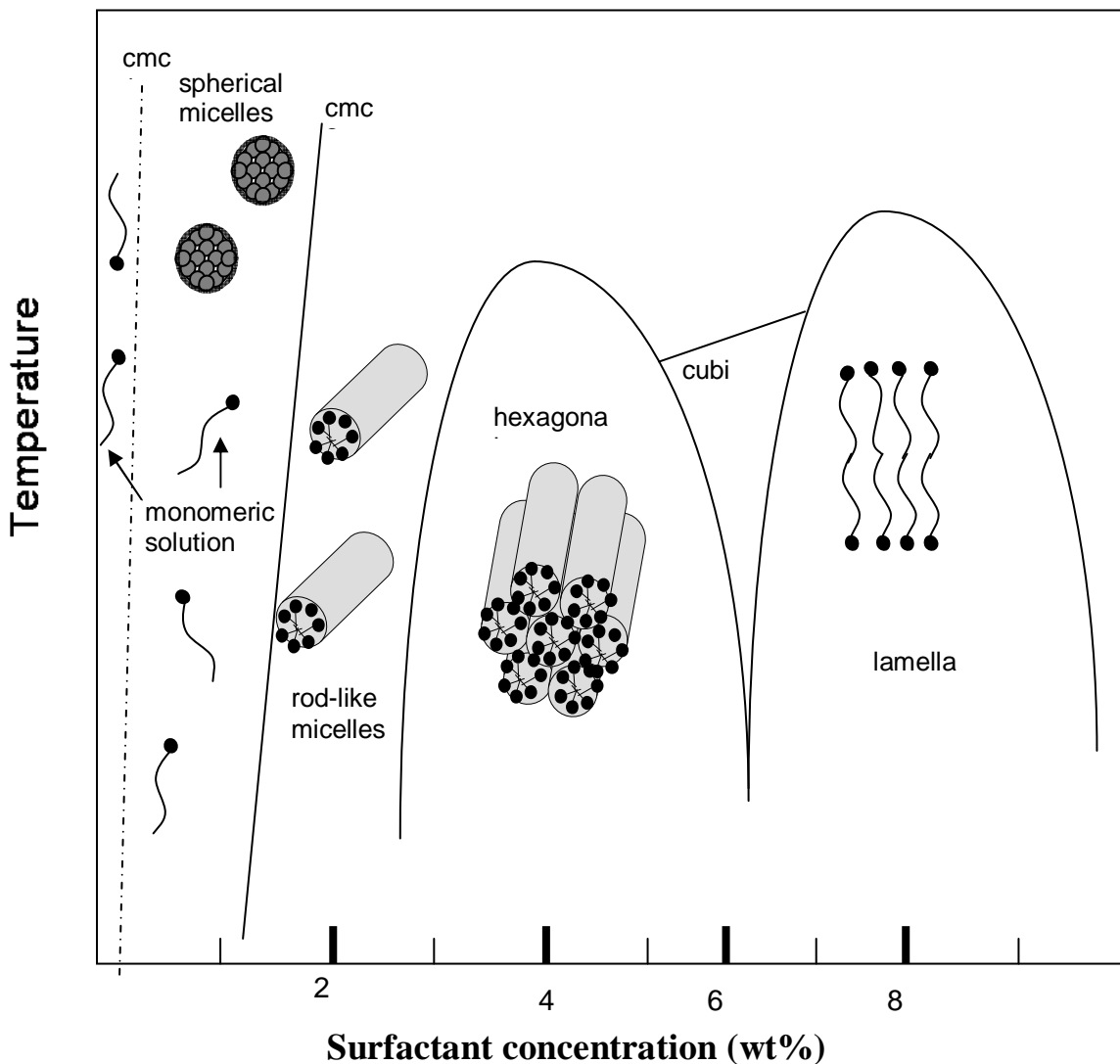


**Figure 2.1.** Phase diagram and schematics of surfactant liquid crystal phases for CTAB (adapted from Edler et. al.<sup>112</sup>)

more hydrophobic than hydrocarbon surfactants and thus forming self-assembled structures at lower cmc values.<sup>113</sup> Fluorinated tails are also more rigid due to a higher van der Waals radius of fluorine compared to hydrogen, resulting in lower surface tensions and also self-assembled structures having lower curvature compared to hydrocarbon surfactants.<sup>114,115</sup> This translates to fluorinated liquid crystals generally forming ‘mesh-phase’ structures (random mesh and rhombohedral mesh) at concentrations corresponding to cubic structures for the hydrocarbon surfactants. Other than advantageous self-

assembly properties, fluorinated surfactants are also more resistant to oxidation and have excellent thermal and chemical stability.<sup>116</sup>

### **2.3 Mesoporous Silica Thin Film – Synthesis and Characterization**

The synthesis of mesoporous silica powders via the surfactant templating route has received increasing attention ever since its first synthesis in 1992. The application of a variety of templates (cationic surfactants, nonionic polyethylene oxides alkyl ethers and triblock copolymers), different silica precursors (sodium silicate, TEOS and TMOS) and varying synthesis conditions (acidic or basic) have resulted in new families of mesoporous materials including HMS,<sup>117</sup> MSU,<sup>118</sup> KIT,<sup>119</sup> FSM,<sup>120</sup> SBA.<sup>95</sup> Studies have shown the ability to tailor the pore size (2 - 30 nm), shape and structure (hexagonal, cubic, disordered) for a variety of applications.<sup>121,122</sup> Fluorinated surfactants have also been applied recently as templates for synthesis of mesoporous silica and have demonstrated significant advantages. The high hydrophobicity of fluorocarbon groups has resulted in the successful use of a small single chain fluorinated surfactant,  $C_2H_5(CH_2)_2NC_5H_5Cl$  as a pore template to design porous silica with pore sizes as small as 1.6 nm. These pores are among the smallest formed by the surfactant templating route,<sup>123</sup> thus providing potential applications in catalysis.<sup>89</sup> Mesoporous silica with novel intermediate ‘mesh-phase’ structure was synthesized using another fluorinated surfactant template,  $C_8H_{17}(CH_2)_2NC_5H_5Cl$  and represents a structure difficult to obtain using traditional hydrocarbon templates.<sup>124</sup> Novel fluorinated functional groups have been incorporated in fluorinated templated silica powders and the materials were demonstrated to have application in chromatography towards separation of fluorocarbon and hydrocarbon compounds.<sup>77</sup>

The synthesis of surfactant templated mesoporous silica thin films with precisely controlled pore geometry has increased the application of porous silica even further to areas such as membranes, sensors, semiconductors, surface coatings, optical and electrical molecular devices.<sup>125-133</sup> Thin films were first prepared around the same time by Ogawa using spin coating<sup>25</sup> and Lu and colleagues through dip-coating<sup>26</sup> of surfactant and hydrolyzed precursor solutions on substrates. The synthesis of dip-coated silica thin film proceeds through an evaporation induced self-assembly process (EISA) and a

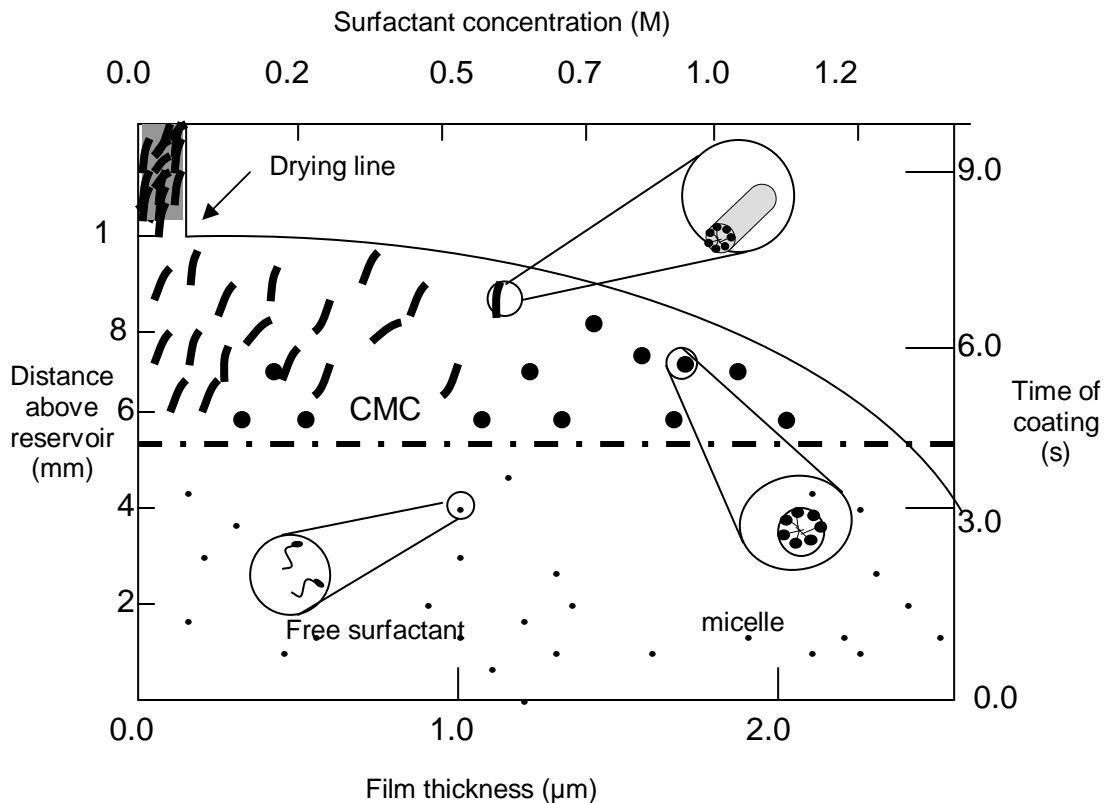


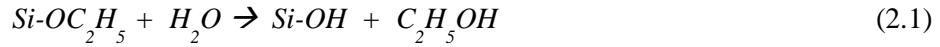
**Figure 2.2** . Thickness of film during dip-coating of a solution of silica, surfactant, alcohol, and water. Surfactant concentration increases with dip-coating time and distance above the reservoir surface (adapted from Lu et. al.<sup>26</sup>)

schematic of the the different processes occurring during EISA is presented in figure 2.2 (adapted from ref. 26). A homogenous solution of hydrolyzed silica and surfactant in a dilute acidic solution (pH ~ 2) of mainly ethanol and water is first prepared, such that the surfactant concentration is well below cmc and surfactants exist as monomers.<sup>26</sup> As the substrate is dip-coated with the silica solution, preferential evaporation of alcohol first increases the concentration of the surfactant above the cmc driving silica-surfactant micelle formation ( $t \sim 4.5$  s after start of dip-coating in Fig. 2.2) and further ethanol evaporation results in the formation of liquid crystalline silica-surfactant mesophases ( $t \sim 6$  s after dip-coating start). Continued evaporation and gravitational draining results in the formation of the initial silica-surfactant film mesostructure in about 10 s (Fig. 2.2). The pH of 2 for the dip-coating solution is near the iso-electric point of silica and keeps silica condensation rate at a minimum during this initial mesostructure formation and drives co-

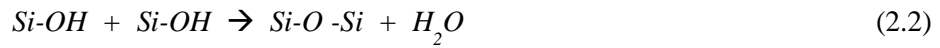
assembly between surfactant and hydrolyzed silica instead of separate silica precipitation.<sup>26</sup> The silica condensation begins mostly after the initial mesostructure is formed and proceeds for a considerable period called the Modulable Steady State (MSS) period, when the aggregate structure can still be modified by external forces.<sup>134</sup>

The silica hydrolysis and condensation reactions with tetraethoxy silane (TEOS) as precursor are given below:

*Hydrolysis:*



*Condensation:*



In acidic conditions, silica is protonated (represented as  $I^+$ ) and association with surfactant templates occurs through two different mechanisms depending on whether the surfactant is cationic or anionic.<sup>135</sup> A counter-ion ( $X^-$ ) is thought to be needed to mediate the self-assembly between positive silica ( $I^+$ ) and cationic surfactants ( $S^+$ ) to form  $S^+XI^+$ , whereas for an anionic surfactant ( $S^-$ ), direct interaction with silica occurs to form the co-assembled  $SI^+$ . Silica thin films with a final ordered structure varying from 2D hexagonal ( $p6m$ ) to 3D hexagonal ( $P63/mmc$ ) and cubic ( $Pm3n$ ) mesostructures have been synthesized through EISA.<sup>136-138</sup> The final porous structure is obtained after the template extraction or removal by calcination.

The numerous complex processes that occur in a very short time period during film synthesis by dip-coating has been followed in-situ by a variety of techniques including 1D XRD, small angle X-ray scattering (SAXS), grazing incidence small angle X-ray scattering (GISAXS), NMR, interferometry and spectroscopy probing to gain insight into the mechanism of formation of final film structure.<sup>134,137,139-142</sup> Brinker and coworkers have used spatially resolved 2D GISAXS experiments in combination with optical interferometry, to demonstrate that the formation of the final 2D hexagonally ordered silica thin films is nucleated initially by the formation of a lamellar phase oriented parallel to the substrate.<sup>139</sup> Babonneau and coworkers have performed in-situ characterization using SAXS combined with interferometry measurements to confirm the formation of an intermediate 3D hexagonal phase at the film/air interface during the final formation of a cubic mesostructure,<sup>137</sup> while in another study the formation of silica with

cubic pore order was demonstrated to proceed through the formation of lamellar and hexagonal intermediates.<sup>140</sup> Babonneau's group has also extensively investigated through various in-situ techniques the effects of variables such as solution aging time, ethanol vapor concentration,<sup>141</sup> pH<sup>141</sup> and CTAB/Si molar ratio<sup>134</sup> on the final film structure. In-situ <sup>17</sup>O NMR spectroscopy has been performed to analyze the hydrolysis behavior of TiCl<sub>4</sub> precursor in solution and the polymerization kinetics of titania during the formation of mesoporous titania film through dip-coating.<sup>142</sup>

Cagnol and coworkers investigated dip-coating of thin films using in-situ SAXS combined with interferometry and suggested that synthesis proceeds via four major steps.<sup>134</sup> The steps are 1) initial preparation of the solution, 2) evaporation of the volatile components during dip-coating which occurs in the first few seconds of dip-coating, 3) the MSS period which follows directly after evaporation and corresponds to the time when the volatile molecules equilibrate between the environment and film media and silica condensation is incomplete and 4) the formation of the final hybrid mesostructured film when the silica condensation is complete. The third stage (MSS) was identified as a very important step because even though the initial mesostructure is formed by that time, the silica structure is still flexible enough to be modified by external forces. Change of relative humidity or ethanol vapor pressure during the MSS period was shown to alter the final mesostructure.<sup>134</sup> The kinetics and timescales of silica condensation in thin films has also been investigated for various surfactant templates using in-situ FTIR spectroscopy.<sup>143</sup> Silica condensation times increase with size of the template molecule from CTAB to Brij 56 to P123, in which case the silica network was incompletely cured for > 1 h. Post-coating manipulation of the structure during this finite period of continuous silica condensation was demonstrated by change in orientation of the porous channels from parallel to a direction orthogonal to the substrate by placing the as-deposited film in contact with a chemically neutral substrate.<sup>143</sup> In-situ fluorescence spectroscopy probing has also been used to follow the chemical and structural changes during surfactant templated silica film synthesis and results from those studies also demonstrates the presence of a MSS period, as described in Section 2.6.

Ex-situ characterization to determine the final order and pore structure of surfactant templated thin films is mostly performed using 1D X-ray diffraction (XRD)

and transmission electron microscopy (TEM). 1D XRD is performed in the Bragg-Brentano geometry where the x-rays scattered from the sample are captured by a detector that moves in a circular path and perpendicular to the sample surface. Peaks in the scattering spectra are observed when diffraction occurs from patterns / pores / atoms spaced at regular distance  $d$  and Bragg's law (Eq. 2.3) is satisfied:

$$n\lambda = 2d\sin\theta \quad (2.3)$$

where  $\lambda$  is the wavelength of the x-rays,  $n$  is an integer and  $2\theta$  is the angle between the direct beam and the diffracted beam.<sup>144</sup> For ordered porous materials,  $d$  is one of the characteristic d-spacing values associated with a particular phase. Hillhouse has demonstrated that for 2D hexagonally ordered thin film with preferential orientation of the (100) plane of porous channels parallel to the substrate, the reflection from the (110) plane will be absent and only (100) peaks and its higher order reflections will be present in the pattern.<sup>145</sup> TEM uses electrons transmitted through the mesoporous samples to create images of the materials and has been used in conjunction with XRD to confirm the pore structure and orientation of the porous channels on substrates.<sup>143</sup>

## 2.4 Tailoring of Surfactant Templated Materials

Synthesizing ordered mesoporous thin films with precise orientation and geometry of pores significantly increases the potential applications of mesoporous silica, as discussed in the last section. Another method to expand the applications of surfactant templated mesoporous materials is to tailor the pore structure of the materials directly during synthesis without altering the template structure. Applications of tailored mesoporous materials have been demonstrated in drug delivery, chromatographic and electrode applications.<sup>146-148</sup>

Tailoring pore structure in surfactant templated mesoporous materials proceeds by altering the surfactant liquid crystal structure and changing the effective surfactant packing parameter. Numerous methods including the addition of electrolyte and alcohols to alter headgroup repulsion,<sup>149</sup> or addition of organic swelling agents in hydrophobic micelle core to increase the value of  $v$ <sup>37-39</sup> have been demonstrated as means of changing the packing parameter and hence pore structure.



The addition of long chain amines to as-synthesized MCM-41 silica materials was demonstrated to increase the pore size from 3.5 nm to at most 13.5 nm.<sup>150</sup> Pore expansion occurred through micelle expansion but was accompanied by a loss of pore order. Recently, P123 templated mesoporous titania thin films with tailored pore diameters between 8.3 nm to 14 nm have been synthesized through the addition of butanol, which acted as a co-surfactant during micelle formation.<sup>149</sup> The most common method for pore expansion has been the introduction of an organic agent that swells the micelles directly during material synthesis. Different organic compounds including aromatic molecules like benzene, substituted benzenes (e.g. triisopropylbenzene, etc.) and mesitylene or alkanes such as octane, nonane, decane, tridecane have been successfully used in separate studies to swell the micelle size of surfactant and copolymer templates.<sup>37-39,151</sup> Significant pore expansion in surfactant templated materials with pore sizes up to 9.1 nm for MCM-41 and up to 43 nm for SBA-15 materials was observed. The pore size of mesoporous silica templated with a nonionic fluorinated surfactant,  $\text{CF}_3(\text{CF}_2)_7\text{C}_2\text{H}_4(\text{OC}_2\text{H}_4)_9\text{OH}$  has also been expanded through the incorporation of a fluorinated solvent, perfluorodecalin, in the micelle.<sup>152</sup>

The interaction of organic agents with surfactant aggregates has been investigated in separate studies by Ulagappan et. al.<sup>153</sup> and by Kunieda and coworkers.<sup>40</sup> These results suggest a systematic guide towards selecting swelling agents for achieving specific pore expansion. Ulagappan et. al. studied interactions of alkanes in surfactant micelles and suggested a difference in alkane incorporation behavior with molecule size, as illustrated by the schematic in Figure 2.3.

Small alkanes (smaller than octane) were observed to result in negligible increase in micelle size suggesting alkane penetration in the surfactant tails (Fig. 2.3a), whereas alkanes larger than decane demonstrated a significant increase in micelle size indicating the formation of a separate core in the micelle (Fig. 2.3b). Kunieda et. al. also demonstrated that long saturated molecules like decane expand the size of liquid crystals suggesting the formation of a separate core in micelle aggregates. Kunieda's group further demonstrated that for aromatics, such as m-xylene, and alcohols, such as dodecanol, complete solubilization in the surfactant tail occurred and no swelling in micelle size was observed.

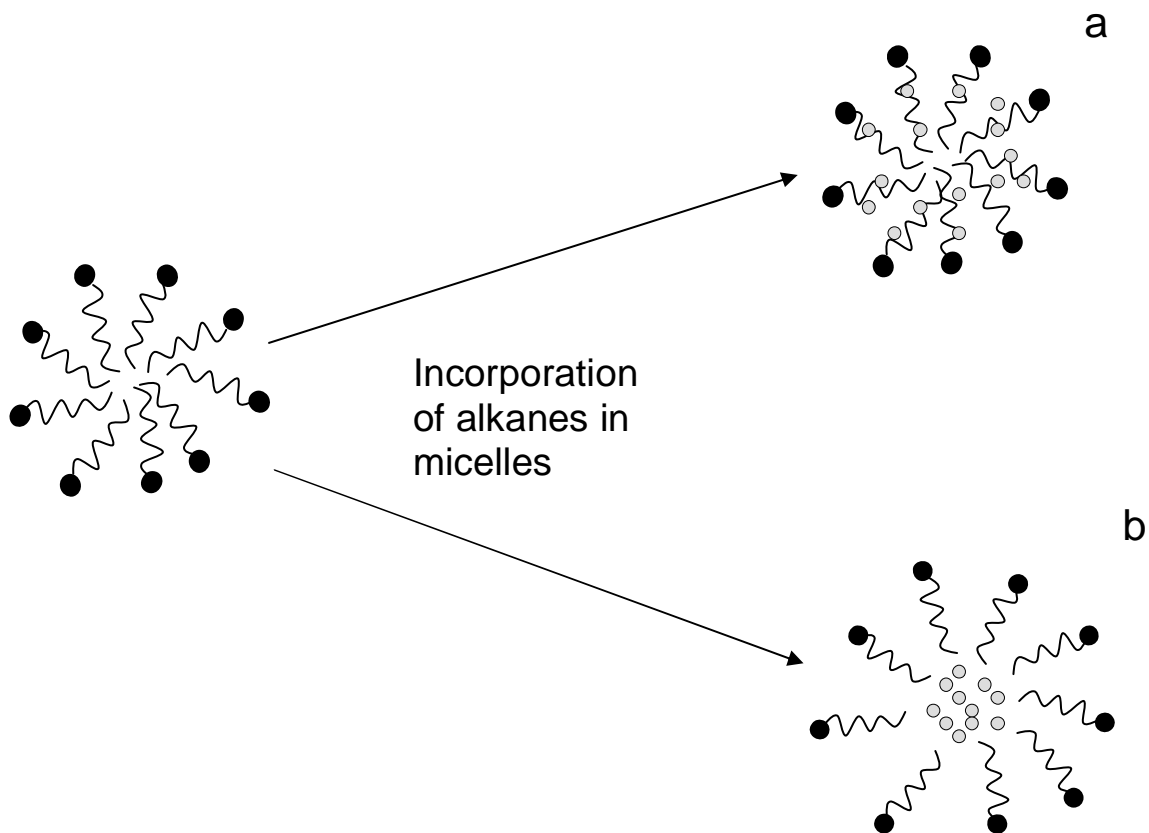


**Figure 2.3** . Alkane penetration in surfactant tail based on mechanism proposed by Ulagappan et. al.<sup>153</sup> with a) short alkanes solublizing in tail and b) alkanes larger than decane forming separate core

The difference between organic solvents solubilizing in the tail or forming a separate core in the micelle can be interpreted from the change in free energy of mixing of the solvents and surfactant tails.<sup>154</sup> The penetration of short alkanes in the tails of surfactant molecule is because of a favorable free energy difference between the smaller alkanes and surfactant tail. For molecules larger than decane however, the beneficial free energy of mixing of alkanes with the surfactant tails is very low and result in the alkanes being present in a separate core surrounded by surfactant molecules.

## 2.5 Compressed CO<sub>2</sub> in Surfactant Aggregates

The advantageous properties of sc CO<sub>2</sub> ( $T_c = 31.1^\circ\text{C}$ ,  $P_c = 78.8$  bar) as a processing solvent, including excellent mass transfer properties (high diffusivity, low viscosity), a pressure tunable solvent strength and the absence of a vapor-liquid interface

during depressurization suggests its application as an attractive solvent for tailoring surfactant templates in mesoporous silica. Sc CO<sub>2</sub> is also nontoxic, nonflammable and chemically inert and is considered to be an environmentally friendly process solvent. However, CO<sub>2</sub> is non-polar with a low dielectric constant and has weak van der Waals forces (i.e. low polarizability). These properties of CO<sub>2</sub> result in its low solvent strength and limits the applications of sc CO<sub>2</sub> as a processing solvent.

To take advantage of the tunable solvent properties of sc CO<sub>2</sub>, formation of water-in-CO<sub>2</sub> (W/C) dispersions such as microemulsions and emulsions have been investigated. Such dispersions have found numerous applications in a variety of areas including organic and enzymatic reactions,<sup>51</sup> nanoparticle syntheses,<sup>47</sup> emulsion templating<sup>155</sup> and formation of porous polymers.<sup>156</sup> The formation of W/C microemulsion and emulsion systems requires surfactants to satisfy several requirements. The surfactant aggregates need to have preferential curvature about water and the surfactant tails need to be significantly solvated by CO<sub>2</sub> so as to overcome attractive tail-tail interactions to prevent aggregation.<sup>64</sup> However, designing surfactant tails to have significant CO<sub>2</sub> penetration has been extremely challenging because the low cohesive energy density of CO<sub>2</sub> results in weak tail solvation.<sup>65</sup>

Initial efforts to design CO<sub>2</sub> based dispersions with several commercially available hydrocarbon surfactants met with limited success because of the weak interactions of CO<sub>2</sub> with hydrocarbon groups.<sup>65</sup> The first successful surfactant design with favorable interactions and high CO<sub>2</sub> solubility was reported in 1992 by DeSimone and coworkers when they demonstrated the solubility of poly(perfluoroalkyl acrylate) (Poly(FOA)) with over 2500 repeat units in compressed CO<sub>2</sub> at pressures below 150 bar.<sup>43</sup> Subsequently, experimental techniques such as high pressure small angle neutron scattering (SANS), NMR, and spectroscopic characterization using UV-Vis and fluorescence were used to investigate the formation of W/C emulsions and microemulsions.<sup>157-161</sup> Researchers successfully designed numerous 'CO<sub>2</sub>-philic' molecules capable of stabilizing dispersions in CO<sub>2</sub> including fluorinated surfactants (perfluoropolyether based surfactants and hybrid fluorocarbon-hydrocarbon) and fluorinated copolymers (PFOA). However, only a few of the surfactants screened in those

experiments were successful and initially it was difficult to design ‘CO<sub>2</sub>-philic’ surfactants.<sup>69</sup>

The first predictive method to design surfactants towards forming W/C dispersions was demonstrated by Johnston’s group by correlating interfacial tension of surfactants at CO<sub>2</sub>-water interfaces with the hydrophilic-CO<sub>2</sub> philic balance (HCB) of the surfactant.<sup>162</sup> The HCB is based on the balance between the interactions of surfactants with each phase (CO<sub>2</sub> and water) and self-interaction between the different phases and is defined as<sup>162,163</sup>

$$1/\text{HCB} = \frac{A_{TC} - A_{TT} - A_{CC}}{A_{HW} - A_{HH} - A_{WW}} \quad (2.4)$$

where  $A_{ij}$  is the interaction energy (treated here as a positive quantity for favorable interactions) for the various interactions between CO<sub>2</sub> (C), surfactant tail (T), water (W), and the surfactant headgroup (H).<sup>163</sup> Figure 2.4 (adapted from reference 67) demonstrates the effect of CO<sub>2</sub> pressure and temperature on the HCB and interfacial tension values.<sup>69</sup> At HCB = 1 the surfactant is at its most balanced state with the lowest interfacial tension. At this point of balance, dispersions can be varied from W/C to C/W by tuning different process variables, such as CO<sub>2</sub> pressure and temperature and system pH and salinity.<sup>67,69</sup> Increase of either salinity, CO<sub>2</sub> pressure or temperature or a decrease in pH leads to an increase in the favorable interactions between CO<sub>2</sub> and the surfactant and hence greater CO<sub>2</sub> penetration in surfactant (Fig. 2.4).<sup>67</sup> da Rocha and coworkers used the plot of interfacial tension values as a function of HCB as a guide for the design of a PDMS copolymer for formation of a C/W microemulsion.<sup>69</sup> The number of hydrophilic groups (EO) and hydrophobic groups (PO) in a PDMS-EO-PO copolymer was gradually changed to form a copolymer with the lowest IFT possible.

Another theoretical guide in designing surfactants for the stabilization of dispersions in CO<sub>2</sub>, the Fractional Free Volume (FFV) of a surfactant, was suggested by

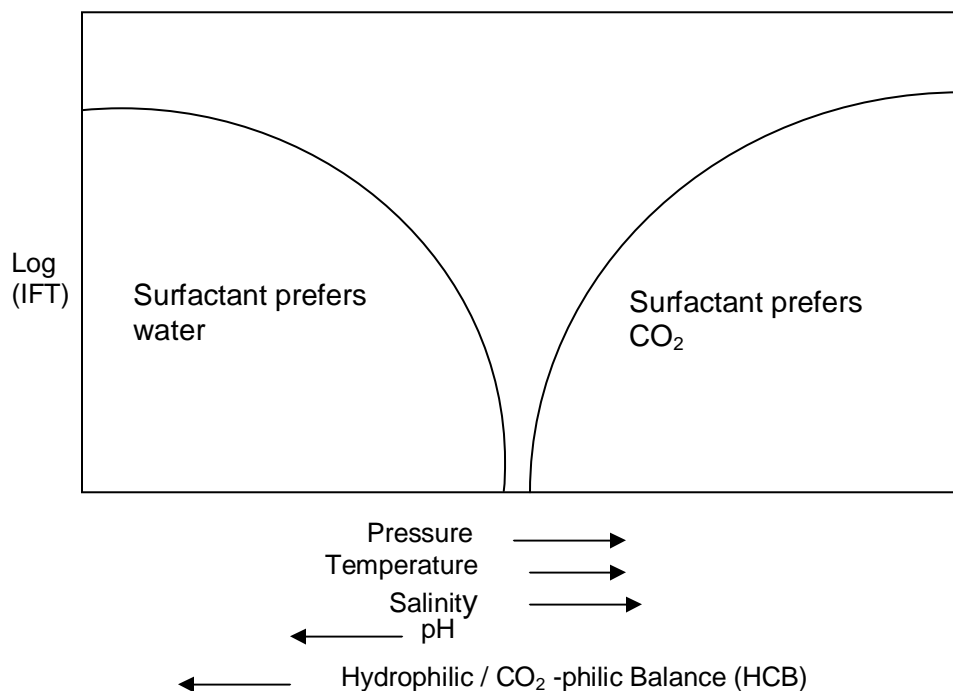


**Figure 2.4** . Schematic of interfacial tension (IFT) of surfactants at C/W interfaces as a function of HCB and other formulation variables. (adapted from Psathas et. al.<sup>67</sup>)

the same group.<sup>164</sup> FFV is defined as

$$\text{FFV} = 1 - \frac{V_t}{tA_h} \quad (2.5)$$

where  $V_t$  is the van der Waals volume of surfactant tail,<sup>164</sup>  $t$  is the length of the tail in an optimum gas phase configuration and  $A_h$  is the interfacial area per headgroup. A low FFV is required for the formation of W/C emulsions and microemulsions; increasing the stubbiness of the surfactant tail, which lowers the FFV, reduces the tail-tail overlap. The corresponding IFT decreases due to a reduction in the interpenetration between  $\text{CO}_2$  and water.

Recently, the use of theoretical paradigms like FFV and molecular simulations<sup>70</sup> and experimental investigations of  $\text{CO}_2$  interactions with surfactant aggregates have resulted in the design of different ‘ $\text{CO}_2$ -philic’ surfactants in addition to fluorinated molecules. Johnston’s research group has designed stubby methylated branched surfactants<sup>165-167</sup> and bulky trisiloxane surfactants<sup>168</sup> for stabilizing W/C emulsions and

microemulsions. Anand et. al. have also used branched methylated surfactants to disperse silver nanoparticles in CO<sub>2</sub>.<sup>169</sup> Small oxygenated hydrocarbon surfactants have also been established as ‘CO<sub>2</sub>-philes’.<sup>73</sup> Different molecular characteristics including a low cohesive energy density, specific interactions with CO<sub>2</sub> and high free volume were suggested in a recent review to be important for ‘CO<sub>2</sub>-philes’ thus suggesting more predictive ways to design ‘CO<sub>2</sub>-philic’ surfactants.<sup>74</sup> The increasing number of ‘CO<sub>2</sub>-philic’ surfactants suggest that applications of CO<sub>2</sub> for tailoring pore structure of surfactant templated materials through CO<sub>2</sub> processing of ‘CO<sub>2</sub>-philic’ fluorinated surfactants has potential for tuning pore geometry.

Fluorinated molecules are among the most ‘CO<sub>2</sub>-philic’ groups, as they possess all three ‘CO<sub>2</sub>-philic’ characteristics discussed above.<sup>74</sup> The large van der Waals radius of fluorine results in a stubby, high free volume molecule, while electronegative fluorine has specific interactions with the electron deficient carbon of CO<sub>2</sub>.<sup>74</sup> Fluorine also creates molecules with weak intramolecular interactions, thus resulting in fluorinated molecules having favorable interactions with CO<sub>2</sub> as demonstrated in numerous studies.

## **2.6 Fluorescence Spectroscopy Probing of Surfactant Templates and CO<sub>2</sub> Dispersions**

Fluorescence spectroscopy has proven to be an important tool for probing molecular assemblies such as micelles, vesicles, polymers and in biological applications such as DNA sequencing, cellular imaging and monitoring protein conformation.<sup>170-176</sup> The technique has been used to determine various system properties such as micropolarity, microviscosity, and also to probe inter and intra-molecular interactions. Briefly, fluorescence is the energy emission that occurs when an electron in an excited orbital (S<sub>1</sub>) returns to the ground-state orbital (S<sub>0</sub>) (Fig. 2.5).<sup>177</sup> Fluorescence spectroscopy follows the fluorescence emission of certain molecules in the system called fluorophores (generally polyaromatic hydrocarbons or heterocycles) to probe specific interactions of a system (e.g. solvatochromic probes estimate environment polarity, probes with nonzero anisotropies measure medium viscosity). Fluorescence emission can be accompanied by a number of other phenomena during the return of an excited electron to the ground state including phosphorescence, quenching, energy

transfer, internal conversion, intersystem crossing and solvent interactions.<sup>177</sup> Figures 2.5 and 2.6, representing two different schematics of the Jablonski diagram (adapted from ref. 177), illustrate all of these different phenomena. Researchers have used each of these different emission phenomena to investigate different molecular aspects of a system and have established the versatility of fluorescence spectroscopy. Another advantage of fluorescence is its high sensitivity which allows the use of very small concentration of fluorophores thus ensuring no destruction of other molecular interactions in the system.

‘Solvatochromism’<sup>178</sup> is the ability of some fluorescent probes to change its absorption and emission spectra through change in interactions with the surrounding solvent and has been used to investigate local polarity, solubility and reaction kinetics in various systems.<sup>179-181</sup> Solvatochromism behavior is either based on a decrease in the excited state energy due to an increase in solvent polarity or can be due to specific probe-solvent interactions.<sup>177</sup> The fluorescence of a probe molecule is the foundation of several ‘solvent polarity’ scales. The  $E_T(30)$  scale is based on the solvatochromic probe, pyridinium N-phenolate betaine dye,<sup>182</sup> while the  $\pi^*$  scale depends on nitroaromatic indicators.<sup>183</sup> The Py-scale is the result of variations in the relative intensities of pyrene emission bands with a change in the solvent polarity.<sup>184</sup>

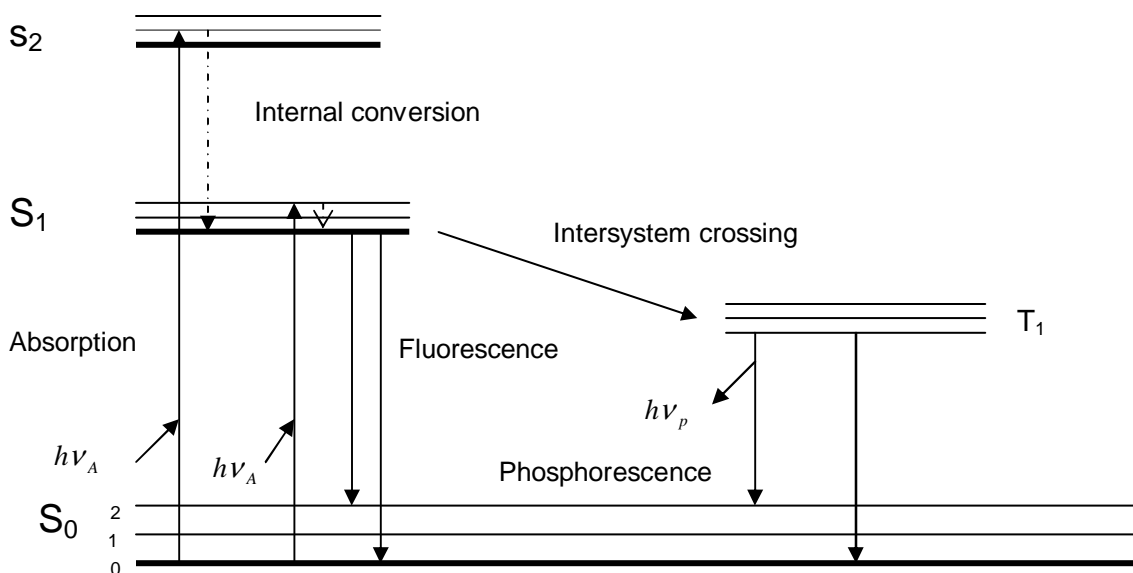


**Figure 2.5.** One form of Jablonski Diagram demonstrating fluorescence, phosphorescence and intersystem crossing (adapted from ref. 177)

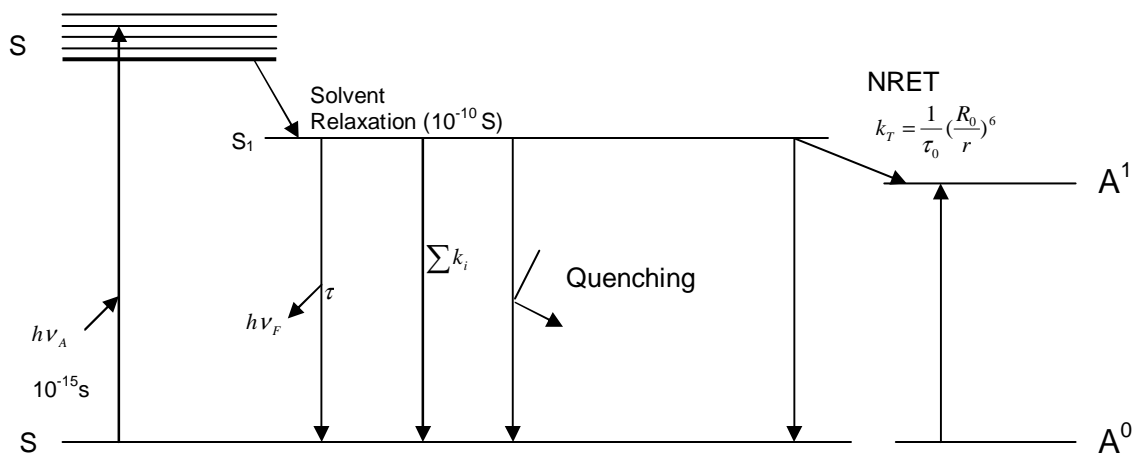


**Figure 2.6.** A form of Jablonski Diagram showing quenching and nonradiative energy transfer (NRET).  $\sum k_i$  represents other nonradiative paths to the ground state.(adapted from ref. 177)

The emission spectra of pyrene at low concentrations (below excimer formation) display five sharp vibronic bands. The intensity of the 0-0 emission band (I1 band) increases in comparison to the other bands in the presence of a polar solvent and the relative increase (as measured by the ratio of I1/I3 band ratio) has been correlated to solvent polarity.<sup>184-186</sup> The value of the I1/I3 ratio varies from 0.6 for a non-polar solvent like hexane to 1.8 for a polar solvent like water.<sup>184</sup> The polarity dependence of pyrene was determined to be primarily due to specific solute-solvent dipole-dipole coupling and some effects from the  $\pi$ -orbital interactions between solute and solvent.<sup>184-186</sup>

Another technique in fluorescence spectroscopy used frequently in micelle systems to determine aggregation numbers,<sup>187,188</sup> probe localization,<sup>189</sup> reaction kinetics,<sup>190</sup> diffusivity of reactants<sup>191</sup> and medium viscosity<sup>192</sup> is quenching, and its mechanism is demonstrated in Figure 2.6. Quenching is any process that decreases the emission intensity and can happen through various phenomena including excited-state reactions, molecular rearrangements, energy transfer, ground state complexation and collisional quenching.<sup>177</sup> Quenching can be either dynamic, resulting from diffusional encounters between probes and quenchers, or static, resulting from molecular binding between the fluorophore and the quencher. Both forms of quenching require contact



between the probe and quencher and illustrate the importance of quenching as a method to investigate localization and diffusivity of molecules. Fluorescence quenching can occur via several mechanisms depending on the quencher. Quenching by both oxygen and heavy atoms such as iodine, bromide probably occurs due to the fluorophore undergoing intersystem crossing to a triplet state where it is quenched in the solvent. Aromatic molecule such as pyridine quench mainly through an electron-transfer mechanism, and both static and dynamic quenching for aromatics has been observed. Fluorescence quenching is also an important technique in biological systems and has been applied to investigation of protein conformation and binding<sup>193,194</sup> and probe binding to DNA.<sup>195</sup> A detailed list of quencher-fluorophore pairs is provided elsewhere.<sup>177</sup>

Fluorescence non-radiative energy transfer (NRET) requires the presence of two probes in the system and is the transfer of energy from an excited donor to an acceptor through long range interactions between the donor and acceptor and without the appearance of a photon.<sup>177</sup> Figure 2.7 shows a schematic of the energy transfer process and demonstrates the two most important properties that need to be satisfied by the probes for significant NRET occurrence. First, the emission spectra of the donor must overlap the absorption spectra of the acceptor, as demonstrated by the darkened region in

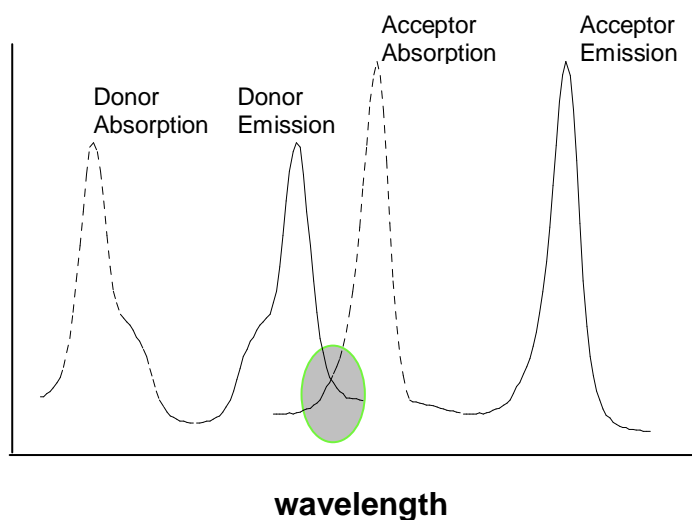


**Figure 2.7.** Schematic of the mechanism of non-radiative energy transfer (NRET) between an acceptor and donor (adapted from ref. 177)

Figure 2.7. Secondly, the two probes must be localized in the same environment and be in close proximity. For efficient energy transfer, the distance between the two probes should be less than their characteristic Forster distance,<sup>196</sup> which is defined as the distance at which energy transfer is 50% efficient. The rate of energy transfer from a donor to an acceptor is given by

$$k_T = (1/\tau) * (R_0/r)^6 \quad (2.6)$$

where  $k_T$  rate of transfer,  $\tau$  is decay time of the donor,  $R_0$  is the characteristic Forster distance and  $r$  is the distance between the probes. The strong dependence of energy transfer on distance has resulted in wide application of NRET to measure distance and hence localization and conformation of the two probes. NRET has been extensively used in biological systems in investigating folding,<sup>197</sup> orientation,<sup>198</sup> catalytic reaction rate and intramolecular interactions in proteins<sup>199</sup> and in following association reactions in DNA oligomers.<sup>200</sup> Energy transfer has also been extensively utilized in membrane systems e.g. in polypeptide membranes<sup>201</sup> and in membrane bound proteins<sup>202</sup> to measure the distance of closest approach between membrane bound proteins and acceptor bound lipids. NRET has also been used in polymer systems to investigate morphology.<sup>203,204</sup>

The efficiency (E) of energy transfer is generally defined as the fraction of photons absorbed by the donor that are transmitted to the acceptor and can be described by<sup>177</sup>

$$E = \frac{k_T}{\tau^{-1} + k_T} \quad (2.6)$$

For energy transfer between acceptor-donor pairs separated at a fixed distance, the above equation can be rewritten as<sup>177</sup>

$$E = 1 - \frac{F_A}{F} \quad (2.7)$$

where,  $F_A$  is the donor fluorescence intensity in presence and  $F$  is intensity in the absence of the acceptor.

The efficiency of energy transfer in membranes for unlinked donors and acceptors is expressed as<sup>177</sup>

$$E = 1 - \frac{1}{\tau} \int \frac{F(t)}{F(0)} dt \quad (2.8)$$

where,  $F(t)$  is the donor fluorescence intensity decay and  $F(0)$  is intensity in the absence of the acceptor. This form of describing energy transfer has been used to calculate the energy transfer efficiency as a function of surface density of energy acceptor in phospholipids membranes.<sup>205</sup>

For the specific acceptor-donor pair of pyrene and naphthalene, the efficiency of energy transfer has been previously calculated using the following formula:

$$E = I_P / I_N \quad (2.9)$$

where  $I_P$  is pyrene emission at 377 nm and  $I_N$  is naphthalene emission at 338 nm. Energy transfer efficiency using eqn. 2.9 has been calculated for several polymer systems labeled with pyrene and naphthalene.<sup>203,204</sup>

In-situ fluorescence spectroscopy has been applied to probe different aspects of the formation of dip-coated sol-gel thin films. The relative change in solvent composition during dip-coating of a solution of ethanol, water, SDS and hydrolyzed silica was monitored as a function of time during the synthesis of SDS templated lamellar silica thin films using pyranine and pyrene as probes for in-situ fluorescence spectroscopy.<sup>206</sup> Preferential evaporation of alcohol compared to water was observed during initial dip-coating. Using the 'solvatochromic' nature of pyrene, the study also demonstrated that the film structure proceeds through initial micelle formation, then breakup at intermediate times and finally formation of the lamellar structure. Zana and coworkers used pyrene and dipyranylpropane spectrofluorometry and fluorescence quenching measurements to investigate the change in micelle structure due to exchange of the counterions with excess silicate ions present in the system during synthesis of mesoporous silica.<sup>207</sup> The study provided insight into the interactions between cationic surfactants ( $S^+$ ), counterions ( $X^-$ ) and the silica source ( $I^+$  or  $I$ ) during porous silica synthesis. Pyrene fluorescence quenching was used to understand the mechanism of formation of mesoporous molecular sieves by surfactant templating at extremely low surfactant and silica concentrations,<sup>208</sup> while in another study time-resolved pyrene fluorescence quenching probed the synthesis of mesoporous alumina with SDS as template in an urea/water/SDS/alumina precursor system.<sup>209</sup> Fluorescence spectroscopy was also applied to measure the mobility of various probes (rhodamine 6G, sulforhodamine B, Oregon Green 514) embedded in sol-gel silica

films when placed in contact with different solvents (water or ethanol) by measuring anisotropy values.<sup>210</sup>

Fluorescence spectroscopy has been frequently used to investigate molecular interactions in supercritical fluids. Solvatochromic probes, including both the Kamlet-Taft  $\pi^*$  scale probes<sup>211</sup> and pyrene,<sup>212,213</sup> were used in fluorescence studies to demonstrate the presence of a solute-solvent clustering phenomena in sc CO<sub>2</sub>. Solute-solvent clustering has been observed in many supercritical fluids and is defined as an augmentation in local solvent density about a solute molecule compared to the bulk density.<sup>214</sup> The density-dependence of solute-solvent interactions in sc CO<sub>2</sub> was also monitored using the Py-polarity scale. Increasing CO<sub>2</sub> density resulted in increasing Py values (I1 / I3 ratio of pyrene emission bands), suggesting greater CO<sub>2</sub> solvation of pyrene. However, the increase was quite nonlinear, with rapid increase in Py value observed at reduced density values less than 0.5 indicating greater solute solvation by CO<sub>2</sub> in that density range, followed by much smaller increase in Py value at higher CO<sub>2</sub> densities.<sup>212,213</sup>

Fluorescence spectroscopy was also used to investigate compressed CO<sub>2</sub> penetration in AOT/water/isooctane reverse micelles.<sup>215</sup> Application of the solvatochromic probe, 6-propionyl-2-(dimethylamino)-naphthalene suggested continuous change in polarity of the micelles with CO<sub>2</sub> penetration, while the viscosity of the micelle core, as calculated from the polarized emission of 8-anilino-1-naphthalenesulfonic acid was observed to decrease with CO<sub>2</sub> uptake. In another study, pyrene fluorescence was used to interpret the local environment in the microregions of CO<sub>2</sub> swelled fluorocarbon micelles. Py values demonstrated that with increasing CO<sub>2</sub> penetration and micelle swelling, pyrene was located in an increasingly non-polar environment almost similar to pure CO<sub>2</sub> (Py = 0.9).<sup>155</sup> Compressed CO<sub>2</sub> penetration in thin films to alter the dynamics of solute movement has been investigated by following the diffusivity of pyrene in polystyrene films as a function of CO<sub>2</sub> penetration using steady state fluorescence quenching.<sup>216</sup>

High pressure fluorescence nonradiative energy transfer (NRET) with pyrene labeled polystyrene has been used to investigate the localization of various probes in polymer films during real time CO<sub>2</sub> processing.<sup>217</sup> NRET studies have also been extensively applied in both surfactant and block copolymer micellar systems to investigate

the partitioning of probes in different environments, to characterize the microenvironment of the micelles and also to study the structure of the micelles.<sup>218-220</sup>

Copyright © Kaustav Ghosh 2007

## CHAPTER THREE

### SUPERCRITICAL CARBON DIOXIDE PROCESSING OF FLUORINATED SURFACTANT TEMPLATED MESOPOROUS SILICA THIN FILMS

This chapter is based on work published as:

Ghosh, K.; Lehmler, J.H.; Rankin, S.E.; Knutson, B.L.; *Langmuir*, **2005**, *21*, 6145.

#### 3.1 Summary

The effect of processing mesoporous silica thin films with supercritical CO<sub>2</sub> immediately after casting is investigated, with a goal of using the penetration of CO<sub>2</sub> molecules in the tails of fluorinated surfactant templates to tailor the final pore size. Well-ordered films with 2D hexagonal close-packed pore structure are synthesized using a cationic fluorinated surfactant, 1-(3,3,4,4,5,5,6,6,7,7,8,8,9,9,10,10,10-heptadecafluorodecyl)pyridinium chloride, as a templating agent. Hexagonal mesopore structures are obtained for both unprocessed films and after processing the cast films in CO<sub>2</sub> at constant pressure (69 – 172 bar) and temperature (25°C to 45°C) for 72 hours, followed by traditional heat treatment steps. XRD and TEM analysis reveal significant increases in pore size for all CO<sub>2</sub> treated thin films (final pore diameter up to 4.22 ± 0.14 nm) relative to the unprocessed sample (final pore diameter of 2.21 ± 0.20 nm) before surfactant extraction. Similar pore sizes are obtained with liquid and supercritical fluid treatments over the range of conditions tested. These results demonstrate that combining the tunable solvent strength of compressed and supercritical CO<sub>2</sub> with the ‘CO<sub>2</sub>-philic’ nature of fluorinated tails allows one to use CO<sub>2</sub> processing to control the pore size in ordered mesoporous silica films.

#### 3.2 Introduction

Surfactant templating to create ordered mesoporous ceramics with pore sizes in the range of 2 – 50 nm was demonstrated in the early 1990’s<sup>24</sup> and extended the application of molecular sieves to larger chemical molecules. Mesoporous thin films are

of particular interest due to their potential applications in membrane separations, selective catalysis, sensing, adsorption, biological and optical functions.<sup>126,132,133,221</sup> These applications of mesoporous materials require pores of tailored structures, sizes and functionality.

Surfactant templated mesoporous materials are formed through a liquid phase co-assembly of the surfactant and an inorganic precursor. The hydrolyzed precursor associates itself with the hydrophilic head group in the aqueous phase and polymerizes to form a solid network while the hydrophobic tail groups of the surfactant pack close together to form an ordered mesophase. The structure of the surfactant template determines the size and shape of the pores that are left behind after extraction or calcination.<sup>89</sup> The most common technique for tailoring pore structures and sizes is expansion by introduction of an inert swelling agent, either during the preparation of the micellar solution or after addition of the precursor.<sup>37-39</sup> Hydrocarbon swelling agents (for example, dodecane and mesitylene) solubilize within the hydrocarbon tail of the surfactants or co-polymers<sup>40</sup> to achieve significant pore swelling. The addition of dopant molecules (such as carbazole and fluorine) and cosolvents (such as tetrahydrofuran and benzene) has also been reported to influence the final structure of thin films.<sup>222</sup> However, the use of these agents for tailoring pore structure sometime leads to either complete transition to a new mesophase or loss of long-range order.<sup>37,39,222</sup>

The tunable solvent strength of compressed and sc (supercritical) CO<sub>2</sub> suggests its use as a structure altering agent for the controlled expansion of pores formed by surfactant templating. Compressed or supercritical CO<sub>2</sub> ( $T_c = 31.1^\circ\text{C}$ ,  $P_c = 73.8$  bar) offers the additional benefits relative to traditional organic solvents of being nonflammable, nontoxic, environmentally acceptable and inexpensive. Watkins and coworkers have recently reported the synthesis of well ordered mesoporous silica films by the CO<sub>2</sub> processing of preformed block copolymer (comprising Pluronic surfactants) or Brij surfactant templates containing an acid catalyst.<sup>55</sup> The silica precursor was introduced into the preformed template using humidified CO<sub>2</sub> and condensed in the hydrophilic domains. Compressed CO<sub>2</sub> (introduced at 123 bar and 60°C for 2 hours) acted to swell the template and rapidly remove alcohol, a product of the condensation, leading to improved condensation within the films. In addition, Hanrahan and co-workers

controlled the pore expansion of mesoporous silica through scCO<sub>2</sub> processing of triblock copolymer templating agents (Pluronic surfactants, P123 and P85) in an acid catalyzed medium.<sup>223</sup> Significant swelling of the hydrocarbon copolymer template was achieved, resulting in an increase in pore diameter from 6.5 nm (unprocessed) up to 10 nm. However, pressures as high as 482 bar were used to achieve this level of pore expansion in the resulting mesoporous silica.

Many fluorinated moieties have been identified as “CO<sub>2</sub>-philic” based on their high solubility in CO<sub>2</sub>.<sup>74,224</sup> Ionic fluorinated surfactants have been successfully used for the formation of reverse microemulsions in CO<sub>2</sub>, with significant penetration of the small CO<sub>2</sub> molecules into the surfactant tail region.<sup>64,70,225,226</sup> Mesophases formed by fluorinated surfactants generally self-assemble more easily and form a broader range of nanoscale structures than their hydrocarbon analogs.<sup>114,227</sup> These mesophases are more stable, better organized and rigid.<sup>228</sup> Our group has demonstrated the base-catalyzed precipitation of silica particles with both 2D hexagonal cylindrical pores<sup>31</sup> and novel mesh phase pores,<sup>123</sup> by templating with 1-(3,3,4,4,5,5,6,6,7,7,8,8,9,9,10,10,10-heptafluorodecyl)pyridinium chloride (HFDePC). On the basis of their CO<sub>2</sub>-philic nature, ionic fluorinated surfactants such as HFDePC may be ideal candidates for CO<sub>2</sub>-controlled pore swelling during the synthesis of mesoporous materials.

We report for the first time the acid-catalyzed synthesis of mesoporous thin films using a cationic fluorinated surfactant, HFDePC, and the effect of sc CO<sub>2</sub> processing on the structure of the thin films templated by this surfactant. The thin films were synthesized in an acid catalyzed medium to minimize the siloxane condensation rate<sup>92</sup> and processed in CO<sub>2</sub> immediately after coating the sol on a glass substrate. The effect of CO<sub>2</sub> processing on the thin films was investigated at gaseous (45°C and 69 bar), liquid (25°C and 172 bar), and supercritical CO<sub>2</sub> (45°C and 103 to 172 bar) conditions and compared to non-CO<sub>2</sub> processed films with identical thermal histories.

### 3.3 Materials and Methods

The synthesis and characterization of 1-(3,3,4,4,5,5,6,6,7,7,8,8,9,9,10,10,10-heptafluorodecyl)pyridinium chloride (HFDePC) has been reported elsewhere.<sup>229</sup> In short, pyridine was alkylated with 1,1,1,2,2,3,3,4,4,5,5,6,6,7,7,8,8-heptafluoro-10-



iododecane to yield 1-(3,3,4,4,5,5,6,6,7,7,8,8,9,9,10,10,10-heptafluorodecyl)pyridinium iodide. The pyridinium iodide was converted into the corresponding chloride by ion exchange chromatography and used without further purification. Its purity was confirmed by mass spectrometry and melting point measurements. The silica precursor, tetraethoxysilane (TEOS) was purchased from Fluka and was over 99% pure. Hydrochloric acid (0.1 N standardized solution) was obtained from Alfa Aesar. Absolute ethyl alcohol was purchased from Aaper Alcohol and Chemical Co. (Shelbyville, KY). High purity carbon dioxide (99.99%) was obtained from Scott Gross Co. (Lexington, KY).

Thin mesoporous silica films were prepared on glass slides by dip coating based on the procedure of Lu et al.<sup>26</sup> Before coating, the glass slides were first treated in an ultrasonic cleaner and then sequentially cleaned with deionized water, isopropanol and acetone. In a typical preparation procedure a mixture of TEOS, ethanol, water and HCl (mole ratio 1 : 3.8 : 1 :  $5 \times 10^{-5}$ ) was refluxed at 65°C for 90 minutes and a clear solution with partially hydrolyzed silica was formed. Then, water and HCl were added and the mixture was aged at 25°C for 15 min and then at 50°C for an additional 15 min. Finally, HFDePC in the desired amount was directly dissolved in ethanol and this solution was added to the above aged silica sol with constant stirring. The final mole ratio obtained was 1 TEOS : 18 C<sub>2</sub>H<sub>5</sub>OH : 5 H<sub>2</sub>O : 0.004 HCl : 0.17 HFDePC. Slides were coated with the above prepared sol at 7.6 cm/sec.

Immediately after coating the thin films were divided into two treatment groups. One treatment group of thin films was pressurized by CO<sub>2</sub> in a 100 ml stainless steel Parr Mini Reactor (rated to 623 K and 207 bar) under controlled temperature and pressure for 72 hours. The effects of CO<sub>2</sub> pressure ranging from 69 to 172 bar and temperature of 25°C and 45°C on the final pore structure were observed. The second treatment group of thin films was not processed in CO<sub>2</sub> and dried in an oven at temperature of 25°C or 45°C for 72 hours. Thus, both processed and unprocessed batches of thin films were subjected to the same thermal treatment. After 72 hours, both treatment groups were dried at room temperature for 24 hours, then at 60°C for 24 hours and finally at about 120°C for a further 24 hours. The surfactant was then extracted from the as-synthesized films using a mixture of 45 ml of EtOH and 5 ml of concentrated HCl (36 wt%).

X-ray diffraction patterns were recorded on a Siemens 5000 diffractometer using with Cu K $\alpha$  radiation ( $\lambda = 1.54098 \text{ \AA}$ ) and a graphite monochromator. The transmission electron images were taken with a JEOL 2000FX instrument operating at 200 kV. Samples were prepared for TEM by scraping the films off the glass substrate and directly depositing them onto a lacey carbon grid. The pore diameters and d-spacings were calculated directly from regions of parallel channels in magnified TEM micrographs (300%) using ImageJ software.<sup>230</sup> Pore diameters were measured from the distance between the inside of two adjacent silica walls on the axis perpendicular to the parallel channels. Similarly, the d-spacing was calculated from the distance between the center of one silica wall and the center of the adjacent wall. The reported measurements were repeated in ten different areas of the micrographs and calibrated with TEM images of gold particles of known diameter (20 nm). Pore diameter and d-spacing measurements for all materials were replicated three times by characterizing samples synthesized in different batches.

### 3.4 Results and Discussion

The synthesis of ordered mesoporous silica thin films using a cationic fluorinated surfactant template under acidic conditions is first demonstrated in the absence of CO<sub>2</sub>. XRD spectra for as-synthesized and extracted thin films prepared using HFDePC as templating agent and aged at 45°C are shown in Figure 3.1. The trace of the as-synthesized sample (Fig 3.1a) shows one sharp reflection and has low intensity because of the presence of fluorinated surfactant in the sample.<sup>123</sup> Following extraction of the sample, the contrast of the XRD spectra increases and two sharp reflections are evident (Fig 3.1b), suggesting long range order in the mesoporous material. These two peaks can be indexed as (100) and (200) peaks of either a hexagonal or lamellar structure. However retention of the order of pore structure even after surfactant extraction suggests hexagonal pore structure; a lamellar structure would have collapsed after surfactant removal. The apparent absence of the (110) peak is consistent with the preferential alignment of the porous channels of the thin film with the (100) plane parallel to the substrate.<sup>145</sup>

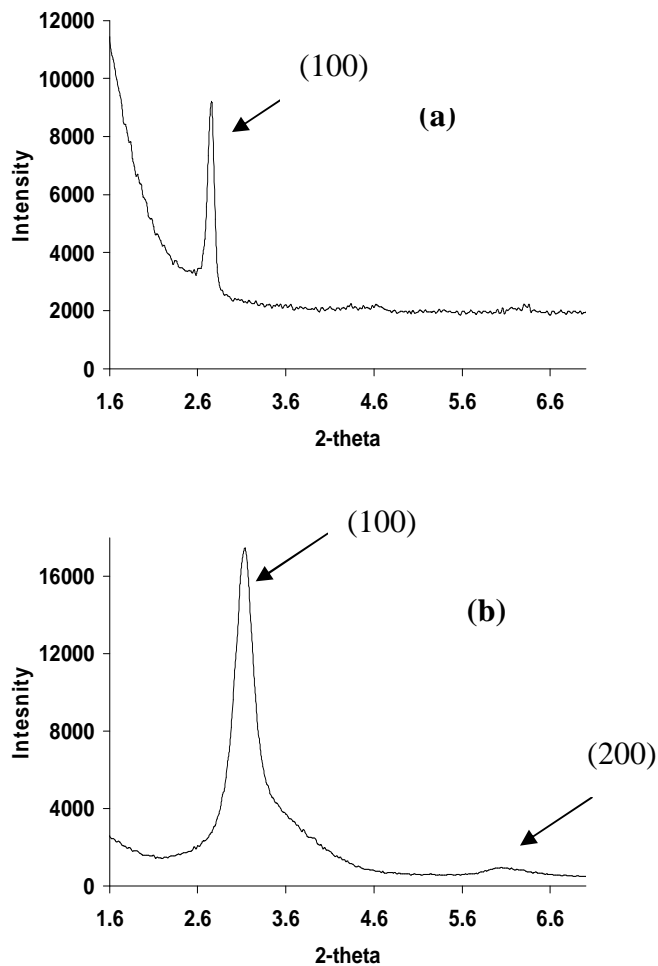


**Figure 3.1** XRD patterns of thin films prepared without CO<sub>2</sub> processing (a) as-synthesized and (b) after surfactant extraction

Although the order of the hexagonal structure is retained for the unprocessed thin films, surfactant extraction is accompanied by a slight contraction in the silica channels, as evident from a decrease in d-spacing from 3.15 nm for the as-synthesized film to about 2.87 nm for the extracted film. Aging the unprocessed thin films at different temperatures (25°C and 45°C) results in the same hexagonal structure for films at both conditions with similar d-spacing (approximately 3.15 nm). Table 3.1 presents a summary of the d-spacing, lattice parameter and pore diameter for the unprocessed and CO<sub>2</sub> processed thin films.

The long range order of the pore structure for thin films not processed in CO<sub>2</sub> and aged at 45°C is confirmed by TEM micrographs of as-synthesized and extracted films

(Fig 3.2). Regular arrays of uniform channels parallel to the channel axis, characteristic of a hexagonal structure, are evident in both the as-synthesized thin film (Fig. 3.2a) and extracted film (Fig. 3.2b) However, contrast is low in the as-synthesized film due to the

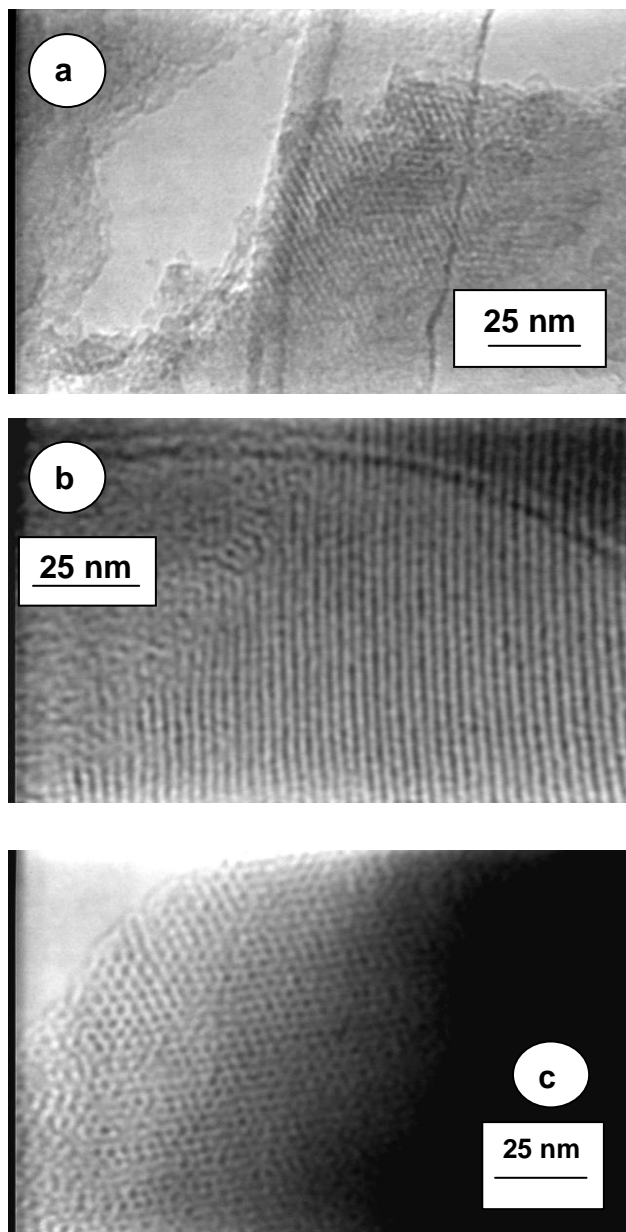


**Figure 3.2** TEM micrographs of (a) as-synthesized thin films not processed in CO<sub>2</sub> (b) extracted thin films not processed in CO<sub>2</sub> and (c) thin films processed in CO<sub>2</sub> at 172 bar and 45°C before surfactant extraction

presence of fluorinated surfactant. The pore diameter of the extracted thin film ( $2.02 \pm 0.17$  nm), determined from its TEM image, varies significantly from that of

hexagonally ordered mesoporous particles synthesized by precipitation using HFDePC as templating agent in a basic medium (2.78 nm).<sup>23</sup> The difference can be attributed to the silica being neutral or slightly positively charged in the present films, which is expected to lower the aggregation number in the cationic micelles formed from HFDePC relative to the negatively charged silica present in the previous case.

The XRD traces of as-synthesized thin films processed in gas, liquid, and supercritical CO<sub>2</sub> are presented in Fig. 3.3. An increase in d-spacing is observed at all conditions of CO<sub>2</sub> processing relative to films with an identical thermal history prepared without exposure to CO<sub>2</sub> (Table 3.1). Thin films processed in scCO<sub>2</sub> (103 bar and 172 bar, 45°C) and liquid CO<sub>2</sub> (172 bar, 25°C) had a similar increase in d-spacing, with the final value being about a 41% increase compared to the unprocessed film. Films with long range order are obtained at all conditions of CO<sub>2</sub> processing. For example, the XRD pattern of the film processed at 172 bar and 45°C has three sharp reflections, indexed as (100), (110) and (200) reflections (Fig. 3.3a) of a hexagonal structure. The presence of (110) peak in XRD spectra for the CO<sub>2</sub> processed film is surprising and could be an effect due to the swelling of the thin film by pressurized CO<sub>2</sub>, as observed previously for CO<sub>2</sub> processing of poly(dimethylsiloxane) thin films on silicon.<sup>231</sup> Swelling of the thin film above a certain critical thickness can lead to a decrease in the ordering ability of the substrate to confine the porous channels parallel to the substrate and result in three-dimensional unconstrained growth.<sup>232</sup> The thin film would then have multiple orientations and the XRD spectra would show the (110) reflection, as in the case of hexagonally ordered powder.

TEM images confirm the hexagonal ordering and the expansion of the pores of CO<sub>2</sub>-processed thin films (Figure 3.2c). The pore diameter of the thin film increases from 2.21 nm ( $\pm$  0.20 nm) for the unprocessed material to 4.22 nm ( $\pm$  0.14 nm) for thin film processed in CO<sub>2</sub> at 172 bar and 45°C, as calculated directly from the TEM images. This represents a pore size expansion of 91% in the processing of these thin films, which is much larger than obtained for a previous study on pore tailoring of mesoporous silica powder using CO<sub>2</sub>. In this previous study using a hydrocarbon template, pressures as high as 482 bar were required to achieve a 54% increase in pore size (from 6.5 nm to 10nm) in the formation of mesoporous silica powder.<sup>223</sup> The pore diameter of thin films

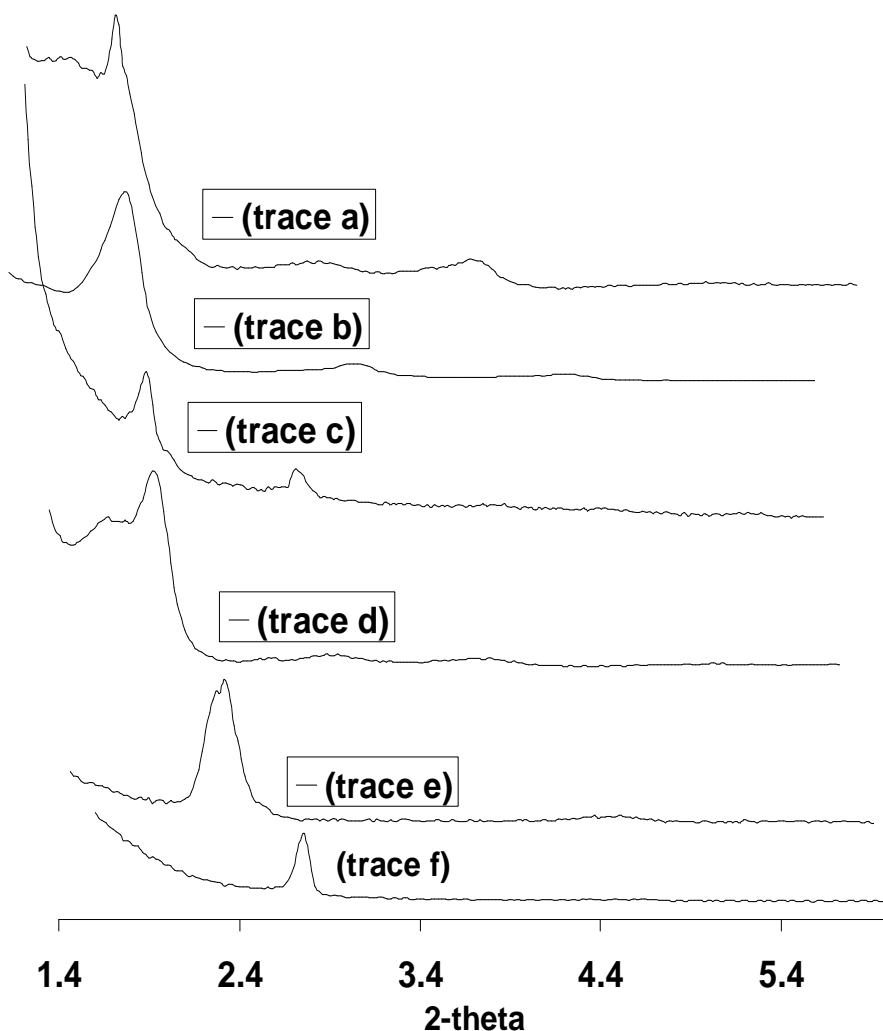


**Figure 3.3.** XRD spectra of thin films before surfactant extraction (a) processed in CO<sub>2</sub> at 172 bar and 45°C, (b) processed in CO<sub>2</sub> at 172 bar and 25°C, (c) processed in CO<sub>2</sub> at 137 bar and 45°C, (d) processed in CO<sub>2</sub> at 103 bar and 45°C, (e) processed in CO<sub>2</sub> at 69 bar and 45°C and (f) not processed in CO<sub>2</sub>

processed in CO<sub>2</sub> at other experimental conditions calculated from TEM images (not shown) also increases compared to the unprocessed sample (Table 3.1).

Broad broken peaks in the XRD spectra and TEM micrographs of CO<sub>2</sub>-processed thin films after extraction indicate partial collapse of the hexagonal structure (images not shown). An alternate pre-extraction procedure following CO<sub>2</sub> treatment, heating the films to 150 °C for 24 hours in vacuum followed by normal solvent extraction using EtOH/HCl

**Table 3.1:** Summary of d-spacing corresponding to (100) peak, lattice parameter and pore diameters of unprocessed thin films and CO<sub>2</sub> processed films before surfactant extraction as a function of processing conditions

Conditions of CO <sub>2</sub> processing	CO <sub>2</sub> Density (g/ml) <sup>233</sup>	d-spacing (nm)	Lattice Parameter (nm) <sup>+</sup>	Pore Diameter (nm) <sup>#</sup>
Unprocessed (45°C)	-	3.15	3.64	2.21 (± 0.20)
Unprocessed (25°C)	-	3.17	3.66	2.23 (± 0.20)
Unprocessed (45°C); extracted	-	2.87	3.32	2.02 (± 0.17)
Gaseous CO <sub>2</sub> ; 69 bar and 45°C	0.178	3.70	4.27	3.32 (± 0.15)
Supercritical CO <sub>2</sub> ; 103 bar and 45°C	0.544	4.28	4.94	4.03 (± 0.15)
Supercritical CO <sub>2</sub> ; 137 bar and 45°C	0.715	4.24	4.90	4.06 (± 0.14)
Supercritical CO <sub>2</sub> ; 172 bar and 45°C	0.779	4.45	5.14	4.22 (± 0.14)
Liquid CO <sub>2</sub> ; 172 bar and 25°C	0.894	4.41	5.10	4.20 (± 0.15)

<sup>+</sup> Lattice parameter of hexagonal structure calculated from the d-spacing values obtained in the XRD experiment by the formula:  $a = (2/\sqrt{3}) * d_{100}$

<sup>#</sup> Figure in bracket show the absolute value (in nm) of the maximum deviation of pore diameter from the average values calculated from ten different TEM images of the same sample.

mixture, appears to be more successful at maintaining the thin film structure. XRD spectra of these extracted CO<sub>2</sub>-processed thin films (images not shown) have one sharp peak for the (100) reflection with an intensity count about 4 times greater than the films before extraction. The large increase in contrast of XRD spectra suggests successful extraction of the surfactant and conservation of order for the thin film. Further characterization of these CO<sub>2</sub>-processed thin films and optimization of the pre-extraction techniques to maintain structure will be the subject of future investigations.

The solvating power of CO<sub>2</sub> for the fluorinated surfactant tail is hypothesized to control the expansion of pores in the mesoporous silica thin films. The thickness of the silica walls (before surfactant extraction) as calculated from the difference of the lattice parameter and pore diameter is observed to decrease from 1.43 nm for unprocessed film to 0.90 nm in the presence of liquid CO<sub>2</sub> (172 bar and 25°C). This decrease suggests that increase of d-spacing with CO<sub>2</sub> pressure is primarily due to swelling of fluorinated tail and is consistent with the proposed hypothesis. Although an increase in pore size or d-spacing due to tail solvation is expected with increasing CO<sub>2</sub> density,<sup>64,70</sup> no significant difference in the pore diameter was observed for the liquid and scCO<sub>2</sub> processing conditions investigated. The lack of a difference may either be because the fluorocarbon tails are swollen so effectively by CO<sub>2</sub> that they are saturated even at the density of sc CO<sub>2</sub>, or because the micelle swelling is constrained by the silica matrix.

Finally, we note that while we have shown CO<sub>2</sub> processing to alter pore size in fluorinated surfactant templated films, recent computer simulations by Johnston and coworkers suggests that CO<sub>2</sub> solvates both fluorinated tail and hydrocarbon tail almost equally well.<sup>234</sup> Thus, CO<sub>2</sub> may have more general applicability as a structure altering agent of surfactant templated thin films, with the potential to tailor the pore size of a large range of mesoporous materials.

### 3.5 Conclusions

Mesoporous silica thin films with well ordered hexagonal structure were synthesized using a cationic fluorinated surfactant under acidic conditions. This synthesis extends the advantages of fluorinated surfactant templating, such as high thermal stability and a broad range of nanoscale structures, to thin films. CO<sub>2</sub> processing of the mesoporous silica film directly after coating expanded the pores and increased the d-spacing of the thin films. The expansion is achieved through solvation of ‘CO<sub>2</sub>-philic’ fluorinated surfactant tail by CO<sub>2</sub>. Compressed CO<sub>2</sub>, with its high diffusivity, provides a large degree of control over the pore size while maintaining the long range structure, unlike some previous investigations using traditional organic solvents as pore swelling agents.<sup>235</sup> The pore expansion increased as the CO<sub>2</sub> processing conditions were changed from gaseous (69 bar and 45°C) to supercritical or liquid state. Processing in liquid or sc



CO<sub>2</sub> induced a 90% increase in the pore diameter of the as-synthesized materials (from  $2.21 \pm 0.20$  nm to  $4.22 \pm 0.14$  nm). Applications of thin films with tunable pore sizes are envisioned in the fields of membrane separation or catalysis. Future work is aimed at investigating the contribution of the constrained silica matrix on the final pore size obtained after swelling. An improved description of the unrestricted pore expansion as a function of CO<sub>2</sub> temperature and pressure would enable us to optimize processing conditions and identify new surfactant systems for further synthesis and pore size control of mesoporous silica films.

Copyright © Kaustav Ghosh 2007

## CHAPTER FOUR

### TAILORING POROUS SILICA FILMS THROUGH SUPERCRITICAL CARBON DIOXIDE PROCESSING OF FLUORINATED SURFACTANT TEMPLATES

This chapter is based on work published as:

Ghosh, K.; Vyas, S.; Lehmler, J.H.; Rankin, S.E.; Knutson, B.L. *J. Phys. Chem. B.* **2007**, *111*, 363.

#### 4.1 Summary

The tailoring of porous silica thin films synthesized using perfluoroalkylpyridinium chloride surfactants as templating agents is achieved as a function of carbon dioxide processing conditions and surfactant tail length and branching. Well-ordered films with 2D hexagonal close-packed pore structure are obtained from sol gel synthesis using the following cationic fluorinated surfactants as templates: 1-(3,3,4,4,5,5,6,6,7,7,8,8,8-Tridecafluoro-octyl)-pyridinium chloride (HFOPC), 1-(3,3,4,4,5,5,6,6,7,7,8,8,8-Dodecafluoro-7-trifluoromethyl-octyl)-pyridinium chloride (HFDoMePC) and 1-(3,3,4,4,5,5,6,6,7,7,8,8,9,9,10,10,10-Heptadecafluoro-decyl)-pyridinium chloride (HFDePC). Processing the sol gel film with CO<sub>2</sub> (69 – 172 bar, 25 °C and 45 °C) immediately after coating results in significant increases in pore diameter relative to the unprocessed thin films (increasing from 20% to 80% depending on surfactant template and processing conditions). Pore expansion increases with CO<sub>2</sub> processing pressure, surfactant tail length, and surfactant branching. The varying degree of CO<sub>2</sub> induced expansion is attributed to the solvation of the 'CO<sub>2</sub>-philic' fluorinated tail and is interpreted from interfacial behavior of HFOPC, HFDoMePC and HFDePC at the CO<sub>2</sub>-water interface.

#### 4.2 Introduction

Surfactant templated mesoporous thin films have generated much interest because of their broad range of potential application in membrane separation, adsorption, catalysis, biomimetics, and chemical and optical sensors.<sup>126,129,132,133,221,236-239</sup> Recently

synthesized ultralow-k dielectric trimethylsilylated mesoporous silica thin films and cross-linked methylsilsesquioxane low k dielectric thin films with high mechanical strength have also found application in the microelectronics industry as insulator metal interconnects.<sup>240,241</sup> The evaporation induced self-assembly (EISA) process for synthesizing surfactant templated films permits control of the final mesostructure through a variety of parameters such as initial sol composition, pH, aging time, and relative humidity.<sup>134,137,138,140,242</sup> Tailoring the pore size and structure of surfactant templated thin films, while maintaining their narrow pore size distribution and large surface area, will increase their potential applications, as demonstrated for tailored mesoporous silica powders in chromatographic and electrode applications.<sup>147,148</sup>

Porous silica film synthesis by EISA is initiated by coating a substrate with a dilute solution of the surfactant and silica precursor. Evaporation drives the concentration of the surfactant above the critical micelle concentration (cmc). Through a co-assembly process, the hydrolyzed silica precursors associates with the hydrophilic head groups of the surfactants and the hydrophobicity of the surfactant tail drives the formation of micelles. Further solvent evaporation results in a co-assembled mesophase. The precursor then polymerizes to form a solid silica network in the aqueous portions of the surfactant mesophase and, upon subsequent removal of the surfactant, a templated porous silica material is obtained. The most common technique for tailoring pore size is the introduction of an inert swelling agent directly during the formation of the co-assembled micelle. Hydrocarbon swelling agents (e.g., polypropylene oxide, dodecane and mesitylene) either solubilize within the tail of traditional hydrocarbon surfactant templates or form an inner core surrounded by a layer of surfactant molecules.<sup>37-39,243</sup> When pore expansion occurs through the formation of an inner core rich in the swelling agent, progressive solvent addition can lead to variability in the final pore size. The addition of too much swelling agent can cause complete transition to a new mesophase or loss of long-range order.<sup>37,39,222</sup>

The tunable solvent strength of compressed and sc (supercritical) CO<sub>2</sub> ( $T_c = 31.1^\circ\text{C}$ ,  $P_c = 73.8$  bar) suggests its use for the controlled expansion of pores formed by surfactant templating. Compressed and sc CO<sub>2</sub> has processing advantages relative to organic solvents; it possesses a high diffusivity while also being nonflammable, nontoxic,

environmentally acceptable, and inexpensive. The ability of CO<sub>2</sub> to expand mesoporous silica pores has been demonstrated for hydrocarbon copolymer templates (P123, P85 and F127) of mesoporous silica powders.<sup>75,223</sup> The dilation of hydrocarbon surfactant templates by CO<sub>2</sub> has also been used to infuse reactive precursor into hydrocarbon-based nanocast templates<sup>55</sup> and to introduce a gold nanocrystal dispersion into the cylindrical pores of mesoporous silica.<sup>244</sup> More recently, we have demonstrated the ability to swell the pores of fluorinated surfactant (HFDePC) templated silica films using CO<sub>2</sub> processing.<sup>245</sup> A 90% increase in pore diameter was observed for films processed in sc CO<sub>2</sub> at 172 bar and 45°C prior to surfactant extraction. In comparison, pressures as great as 482 bar were required to achieve a pore expansion of 54% in silica templated with a hydrocarbon surfactant (Pluronic copolymer, P123).<sup>75</sup>

The dramatic pore expansion achieved in fluorinated surfactant templated silica suggests a favorable penetration of CO<sub>2</sub> molecules into the fluorinated tails compared to hydrocarbon surfactants. Indeed, many fluorinated moieties have been identified as “CO<sub>2</sub>-philic” based on their high solubility in CO<sub>2</sub>, and their weak dispersion forces, which are similar to that of CO<sub>2</sub>.<sup>74,224</sup> CO<sub>2</sub> processing of fluorinated surfactant templated materials has the potential to combine the high degree of solvation of fluorinated tails with the tunable solvent strength of CO<sub>2</sub> to achieve a broad range of pore sizes in nanoporous ceramics. The high diffusivity of sc CO<sub>2</sub> suggests its effective transport into the surfactant tails compared to traditional organic solvents, a property that has already been exploited in the functionalization of mesoporous ceramics.<sup>246-248</sup>

CO<sub>2</sub> solvation of surfactant templates leading to pore expansion in mesoporous silica draws many analogies to the formation and swelling of self-assembled aggregates (e.g., micelles) in CO<sub>2</sub>. Reverse microemulsion behavior in CO<sub>2</sub> has been the focus of numerous investigations because the aqueous core provides a polar environment for organic and enzymatic reactions,<sup>51,61</sup> extraction,<sup>249</sup> nanoparticle syntheses<sup>47,48,250</sup> and ‘green’ applications of carbon dioxide technology.<sup>251</sup> The weak solvation of traditional hydrocarbon surfactant tails by CO<sub>2</sub> is not sufficient to promote CO<sub>2</sub>-continuous microemulsion formation. The design of fluorinated and CO<sub>2</sub>-philic surfactants for reverse microemulsion formation and the subsequent swelling behavior of micellar systems has provided a great deal of insight into the penetration of CO<sub>2</sub> molecules into

the surfactant tail region.<sup>64,70,225,226</sup> The emulsion and microemulsion formation behavior of a series of surfactants and block co-polymers has been correlated with interfacial tension (IFT) at the CO<sub>2</sub>-water interfaces.<sup>67-69,71</sup> Low IFT values are required for reverse microemulsion formation as it decreases the Gibbs free energy penalty associated with the large surface area formed.

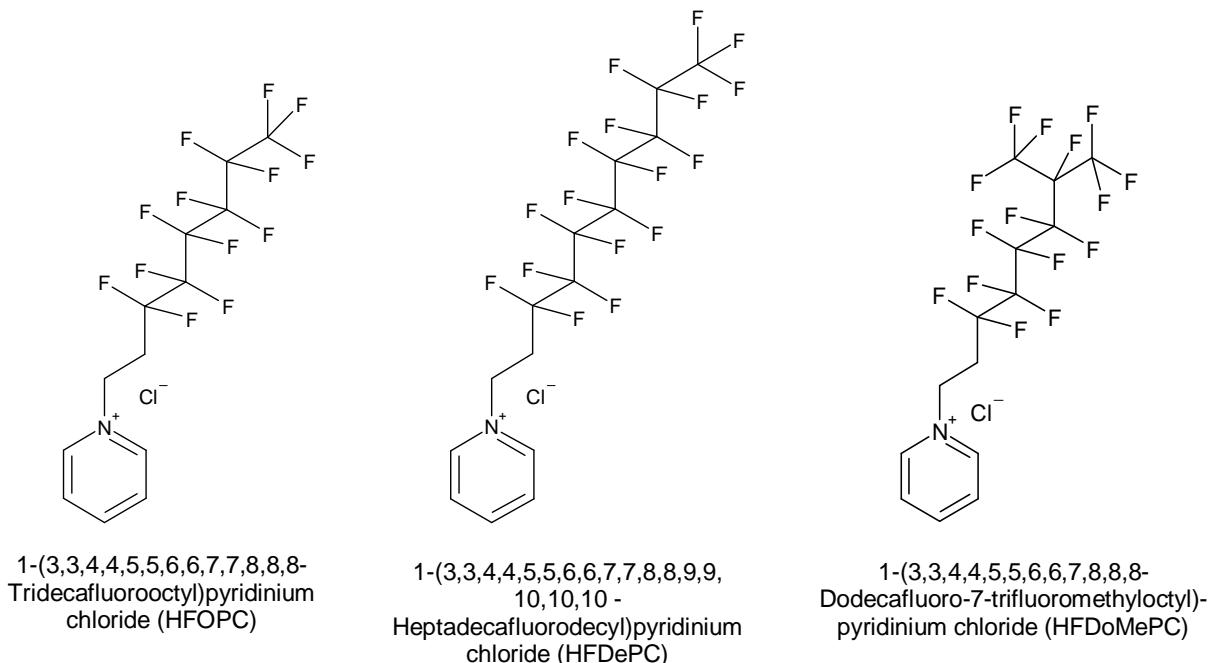


**Figure 4.1.** Schematic of the homologous series of perfluoroalkylpyridinium chloride surfactants

In this paper we report the acid-catalyzed synthesis of mesoporous thin films using a series of perfluoroalkylpyridinium chloride surfactants as pore templates and describe the effect of CO<sub>2</sub> processing on the structure of the thin films. The three surfactant templates, HFOPC, HFDoMePC and HFDePC (Figure 4.1), were chosen to systematically study the ability to tailor pore sizes with changes in CO<sub>2</sub> processing conditions, fluorinated template tail length, and surfactant branching. Pore expansion is interpreted from the change in the hydrophilic-CO<sub>2</sub>-philic balance (HCB) of each surfactant as a function of processing conditions, as described by the relative solubilities

of HFOPC, HFDoMePC and HFDePC in water and CO<sub>2</sub> and the interfacial activities of the surfactants at the CO<sub>2</sub>-water interface.

### 4.3 Materials and Methods

**4.3.1 Materials.** The fluorinated surfactants 1-(3,3,4,4,5,5,6,6,7,7,8,8,8-Tridecafluorooctyl)pyridinium chloride (HFOPC; C<sub>6</sub>F<sub>13</sub>(CH<sub>2</sub>)<sub>2</sub>NC<sub>5</sub>H<sub>5</sub><sup>+</sup> Cl<sup>-</sup>), 1-(3,3,4,4,5,5,6,6,7,7,8,8,9,9,10,10,10-Heptadecafluoro-decyl)pyridinium chloride (HFDePC; C<sub>8</sub>F<sub>17</sub>(CH<sub>2</sub>)<sub>2</sub>NC<sub>5</sub>H<sub>5</sub><sup>+</sup> Cl<sup>-</sup>) and 1-(3,3,4,4,5,5,6,6,7,8,8,8-Dodecafluoro-7-trifluoromethyloctyl)pyridinium chloride (HFDoMePC; (CF<sub>3</sub>)<sub>2</sub>CFC<sub>4</sub>F<sub>8</sub>(CH<sub>2</sub>)<sub>2</sub>NC<sub>5</sub>H<sub>5</sub><sup>+</sup> Cl<sup>-</sup>)) were synthesized as described previously.<sup>229</sup> Briefly, for each surfactant, anhydrous pyridine was alkylated with the corresponding 1H,H,2H,2H-perfluoroalkyl iodide. The pyridinium iodide was converted into the corresponding chloride by ion exchange chromatography. The purity of all three surfactants was confirmed by mass spectrometry and melting point measurements (as detailed elsewhere).<sup>31</sup> Tetraethoxysilane (TEOS, purity > 99%) was purchased from Gelest. Absolute ethyl alcohol purchased from Aaper Alcohol and Chemical Co. (Shelbyville, KY), deionized ultrafiltered water from Fisher Scientific and hydrochloric acid (0.1 N standardized solution) obtained from Alfa Aesar were used for thin film synthesis. Carbon dioxide (Coleman grade, 99.99+%) was purchased from Scott Gross Co. (Lexington, KY). Concentrated aqueous HCl (Fisher Scientific) was used for surfactant extraction.

**4.3.2 Cross-Polarized Microscopy.** Samples of HFDoMePC / H<sub>2</sub>O mixtures were observed between crossed polaroids for birefringency and subsequent identification of mesophases at room temperature (23 ± 1 °C). Samples were prepared at four different concentrations (30 wt%, 40 wt%, 50 wt% and 60 wt%) of HFDoMePC by mixing known amounts of HFDoMePC and water in a vial for 24 hours to form a homogenous mixture. The mixture was then placed on a glass slide in between the channels of a spacer. The spacer was covered by a cover-slip to prevent any evaporation of the sample and allowed to equilibrate for 72 hours to form the observed mesophase.

**4.3.3 Thin Film Synthesis.** Thin porous silica films were synthesized by dip coating on glass slides based on the procedure of Lu et al.<sup>26</sup> The glass slides were cleaned by treating them in an ultrasonic cleaner and then sequentially rinsing them in water, isopropanol and

acetone. Initially, TEOS, ethanol, water and HCl (mole ratio 1: 3.8: 1:  $5 \times 10^{-5}$ ) were refluxed at 65 °C for 90 minutes and a clear solution of partially hydrolyzed silica was formed. Water and HCl were then added in calculated quantities, resulting in a pH of approximately 2 in the final solution, and the mixture was aged at 25 °C for 15 min and then at 50 °C for an additional 15 min. Finally, a solution of the surfactant in ethanol was added to the previously hydrolyzed silica sol under constant stirring. The final mole ratio obtained was 1 TEOS : 12 C<sub>2</sub>H<sub>5</sub>OH : 5 H<sub>2</sub>O : 0.004 HCl : x surfactant (x varying between 0.15 – 0.21, depending on surfactant). This solution was then dip-coated onto the slides.

Immediately after coating, the thin films were divided into two treatment groups. One treatment group of thin films was pressurized by CO<sub>2</sub> in a 100 ml stainless steel Parr Mini Reactor (rated to 623 K and 207 bar) under controlled temperature and pressure for 72 hours. The effects of CO<sub>2</sub> pressure (69 to 172 bar) and temperature (25 °C or 45 °C) on the final pore structure were observed. The second treatment group of thin films, which was not processed in CO<sub>2</sub>, was dried in an oven at temperature of 25 °C or 45 °C for 72 hours. This ensured uniform thermal conditions for both batches of thin films. Both treatment groups were next heated to 150°C in vacuum (heating started at 30°C and oven temperature was ramped by 30°C every 6 hours) to ensure condensation of the silica wall. The surfactant was then extracted from the as-synthesized films by washing twice with acidic ethanol (5 ml of concentrated HCl in 45 ml of EtOH) .

**4.3.4 Thin Film Characterization.** X-ray diffraction patterns were recorded on a Siemens 5000 diffractometer using Cu K $\alpha$  radiation ( $\lambda = 1.54098 \text{ \AA}$ ) and a graphite monochromator. Transmission electron microscope (TEM) images were taken with a JEOL 2000FX instrument operating at 200 kV. TEM samples were prepared by scraping the films off the glass substrate and directly depositing them onto a lacey carbon grid. The pore diameters were calculated from the TEM micrographs using ImageJ software, as reported previously.<sup>230,245</sup> The pore diameters determined by TEM were confirmed by nitrogen sorption measurements (on Micromeritics Tristar 3000 system) for thin films not processed in CO<sub>2</sub>, which could readily be prepared in quantities sufficient for nitrogen sorption analysis (> 10 mg). Nitrogen sorption samples were prepared by scraping the films off the glass substrate and degassing at 140 °C for 4 hours under flowing nitrogen

prior to measurement. The method proposed by Dubinin and Kaganer<sup>252</sup> was used to calculate pore size for the microporous materials templated by HFOPC while the BJH method with a modified statistical film thickness equation (KJS method)<sup>253</sup> was used to calculate the pore size distributions for the mesoporous films templated by HFDePC and HFDoMePC.

**4.3.5 Interfacial Tension Measurements.** Interfacial tensions at the carbon dioxide/water interface in the presence of the three cationic fluorinated surfactants were determined as a function of CO<sub>2</sub> pressure (69 bar to 172 bar) at 45 °C. The IFTs were measured at 1.5 wt% surfactant in water, calculated to be above cmc for each surfactant.<sup>113</sup> IFT analysis was performed using JEFRI high-pressure pendant drop tensiometer (DB Robinson Design & Manufacturing Ltd., Edmonton, Canada) in which the drop phase fluid (surfactant + water) was introduced into a CO<sub>2</sub> continuous phase. A detailed description of the tensiometer is available elsewhere.<sup>254</sup> An experimental run was initiated by loading CO<sub>2</sub> into the view cell at the desired pressure using a high pressure syringe pump (ISCO Model 500D, Lincoln, NB). Before forming droplets, the aqueous surfactant solution was presaturated with CO<sub>2</sub> at the experimental temperature and pressure. Pendant drops were subsequently formed on the end of the capillary tube (diameter 0.02 cm) by slightly increasing the pressure in the drop phase cylinder relative to the pressure in the view cell. Images of the pendant drop were recorded after approximately 20 min. The interfacial tensions were calculated from analysis of the pendant drop dimensions using a numerical solution to the Laplace equation.<sup>254,255</sup>

**4.3.6 Surfactant Solubility in CO<sub>2</sub>.** The solubility of the cationic fluorinated surfactants in CO<sub>2</sub> at 25 °C and 45 °C was examined using a Pressure Volume Temperature (PVT) apparatus (DB Robinson Design & Manufacturing Ltd., Edmonton, Canada), as described previously.<sup>256</sup> Cloud point pressure was used to indicate the miscibility of surfactants with CO<sub>2</sub>.<sup>256</sup> Pressures of 55 bar to 355 bar were traversed at 25 and 45 °C and at concentrations as low as 1 wt% surfactant. The fluorinated surfactants were immiscible with CO<sub>2</sub> at these conditions.



## 4.4 Results and Discussion

### 4.4.1 Synthesis of Silica Thin Films Templated by Cationic Fluorinated Surfactants.

Fluorinated surfactants generally possess higher thermal stability, self-assemble more easily and form aggregate structures with lower curvature compared to hydrocarbon surfactants.<sup>113,114</sup> The self assembly behavior of fluorinated surfactants results in low critical micelle concentrations and low surface tensions, and the formation of fluorinated mesophases with a broader range of structures including novel 'intermediate' phases. Our research team has previously demonstrated the homologous series of perfluoroalkylpyridinium chloride surfactants as templates in the base-catalyzed sol gel synthesis of porous silica powders, resulting in hexagonal close-packed and mesh phase structures,<sup>31</sup> pore sizes in both microporous and mesoporous range,<sup>31</sup> and vinyl functionalized materials with increased accessibility relative to hydrocarbon surfactant (CTAB) templated powders.<sup>76</sup> The synthesis of ceramic thin films by templating with a homologous series of fluorinated surfactants has the potential to control pore size through surfactant tail length and branching, while exploiting the advantageous properties of fluorinated mesophases.

In the present work, the phase behavior of the binary fluorinated cationic surfactant/water system guides the synthesis recipe for the acid-catalyzed thin films. Previous syntheses of mesoporous silica films by triblock copolymer templating and CTAB have demonstrated that the final structure of the materials corresponds to the mesophase observed in the surfactant water phase diagram when the surfactant volume fraction is equated to that in the film after removal of the volatile solvents.<sup>257,258</sup> The binary water-surfactant diagrams were obtained from literature for the surfactants HFOPC<sup>259</sup> and HFDePC<sup>114</sup> and volume fractions of 0.7 for HFOPC and 0.67 for HFDePC were selected, corresponding to the center of the hexagonal domain in the phase diagram. A surfactant concentration for formation of hexagonal mesophase in the HFDoMePC/water system was determined as 55 wt% HFDoMePC (volume fraction of 0.64) using cross-polarized microscopy.

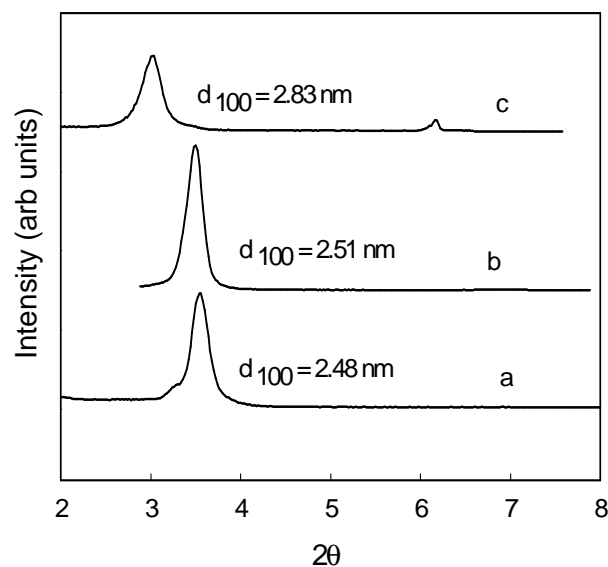


**Figure 4.2.** XRD patterns of thin films prepared without CO<sub>2</sub> processing and templated with (a) HFOPC, (b) HFDoMePC and (c) HFDePC.

The XRD patterns of thin films templated with the three cationic fluorinated surfactants at 45°C after extraction are presented in Figure 4.2. Thin films templated with HFOPC and HFDoMePC display one sharp reflection, indicating the formation of ordered structure. XRD pattern of film templated with HFDePC shows one sharp reflection corresponding to (100) plane and a second weaker reflection that can be indexed to the (200) reflection. The presence of ordering after surfactant extraction and position of the two reflections are consistent with the formation of hexagonal structure for the HFDePC templated film; a lamellar structure would have collapsed after surfactant removal. Representative TEM images for all three surfactant templated thin films confirm the presence of well-ordered 2-D hexagonal structure (Fig. 4.3).

The one reflection observed in XRD plots of HFOPC and HFDoMePC templated films can then be indexed to the (100) plane of a hexagonal mesostructure. It is worth noting that this is truly an example of evaporation-induced self-assembly; forming ordered bulk materials by polymerization at similar pH and surfactant: silica values has been very difficult due to the slow assembly of these surfactants in concentrated solution at moderately elevated temperatures.

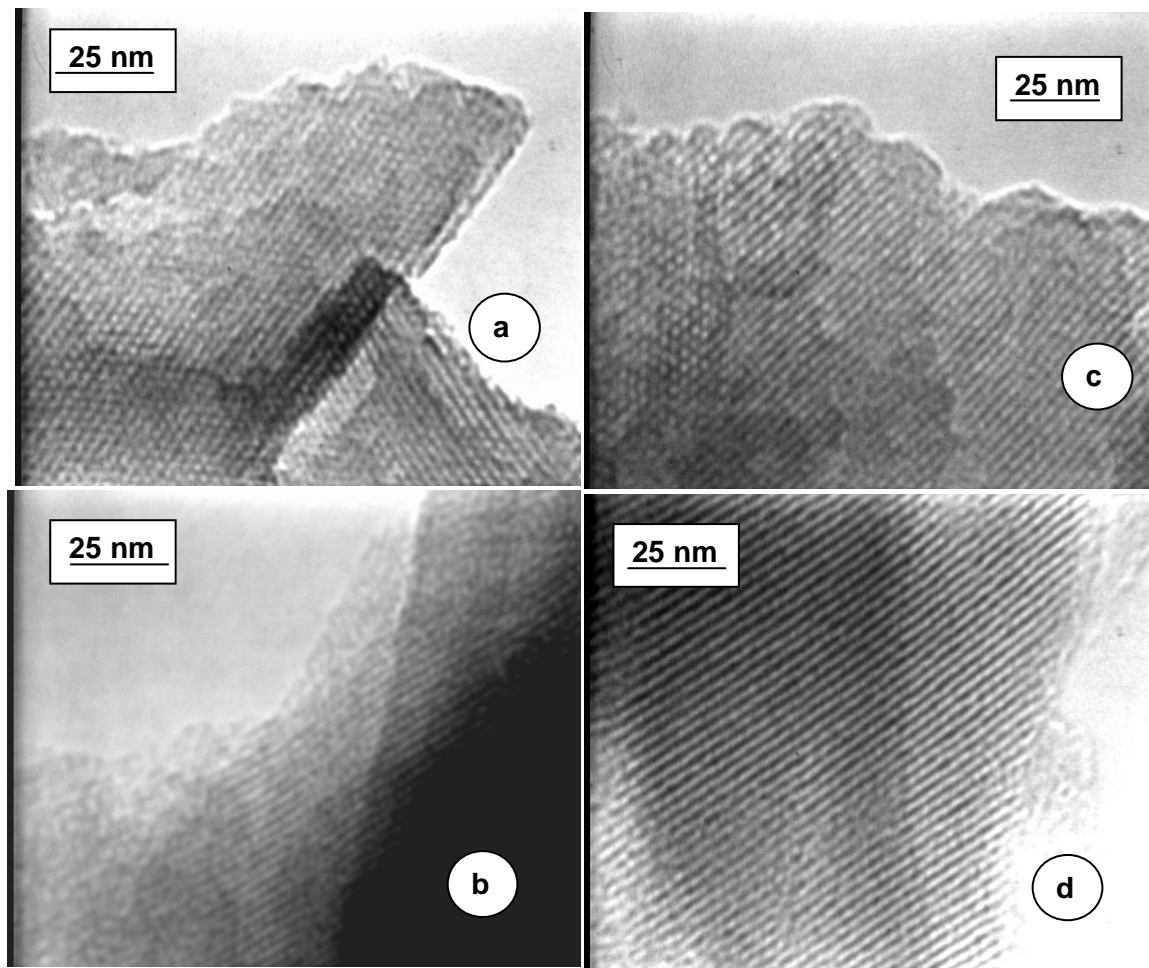


**Figure 4.3.** TEM micrographs of thin films prepared without CO<sub>2</sub> processing and templated with (a) HFOPC, (b) HFDoMePC and (c) HFDePC and (d) for film templated with HFOPC and processed in CO<sub>2</sub> at 172 bar and 45 °C.

The nitrogen sorption analysis reveals a Type I isotherm for the HFOPC-templated thin film, characteristic of microporous materials (Figure 4.4), and its pore diameter was estimated as 1.91 nm using the method of Dubinin and Kaganer.<sup>252</sup> Type IV isotherms, characteristic of mesoporous materials, were observed for films templated with both HFDePC and HFDoMePC. The KJS method (modified BJH method),<sup>253</sup> applicable to the calculation of physical properties of mesoporous material with uniform cylindrical pores, was used to analyze the N<sub>2</sub> sorption data for both samples. Pore diameters obtained from these N<sub>2</sub> adsorption experiments are 1.98 nm and diameters calculated from N<sub>2</sub> sorption measurements compare favorably with those calculated from

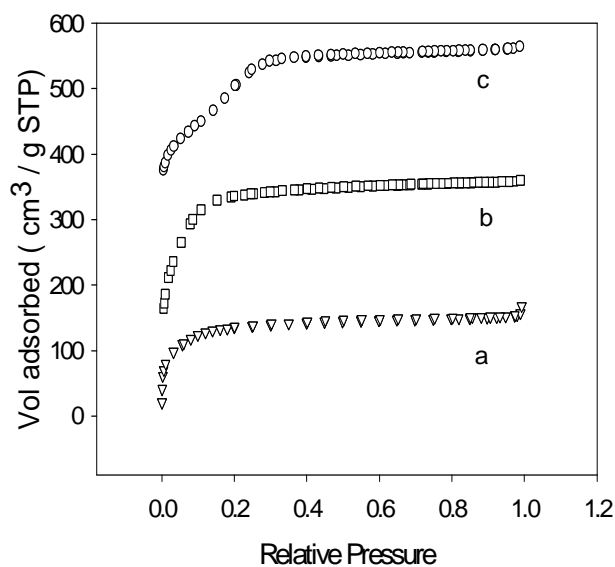


**Figure 4.4.** Nitrogen sorption isotherm of thin films prepared without CO<sub>2</sub> processing templated with (a) HFOPC, (b) HFDoMePC and (c) HFDePC. Open symbols are for adsorption and filled for desorption. The y-axis values have been offset by 130 units (trace b) and by 300 units (trace c) for clarity.

TEM images (as listed in Table 4.1). Aging the thin films at 25 °C results in the same hexagonal structure for all three surfactants, with d-spacing values and pore sizes similar to values obtained at 45 °C (Table 4.1).

Templating with a longer-tailed surfactant, the decyl chain surfactant (HFDePC), resulted in a larger pore diameter relative to the octyl chain surfactant (HFOPC). This is an expected trend because the pore size is determined by the length of the hydrophobic tail group of the surfactant.<sup>31</sup> The tail length for each surfactant molecule was calculated from their optimum configuration using SPARTAN.<sup>260</sup> The surfactant molecule was first created in an all trans configuration in SPARTAN and next an energy minimization was performed on the molecule to using the classical MMFF94 force field to obtain the optimum configuration. Finally the tail length of each surfactant was calculated by noting the distance between the pyridinium nitrogen atom and the last atom in the tail. HFOPC and a branched version of this surfactant, HFDoMePC (containing an additional CF<sub>2</sub> group) was determined to have similar surfactant tail lengths, However the pore diameter for HFDoMePC templated film is larger compared to HFOPC templated film, suggesting

**Table 4.1:** Summary of d-spacing and pore diameter for thin film templated with all three different surfactants as a function of CO<sub>2</sub> processing conditions

CO <sub>2</sub> -processing conditions	Density of CO <sub>2</sub> (g/ml) <sup>23</sup> <sub>3</sub>	HFOPC film		HFDePC film		HFDoMePC film	
		d-spacing (nm)	Pore diameter <sup>a</sup> (nm)	d-spacing (nm)	Pore diameter <sup>a</sup> (nm)	d-spacing (nm)	Pore diameter <sup>a</sup> (nm)
Unprocessed (45 °C)	-	2.48	1.91 (0.092)	2.83	2.16 (0.082)	2.51	1.96 (0.086)
Unprocessed (25 °C)	-	2.46	1.90 (0.088)	2.86	2.18 (0.085)	2.53	1.96 (0.084)
69 bar and 45 °C (gas)	0.178	2.78	2.33 (0.086)	3.50	3.06 (0.080)	2.88	2.51 (0.087)
103 bar and 45 °C (sc)	0.544	2.9	2.58 (0.098)	3.94	3.57 (0.084)	3.12	2.84 (0.089)
137 bar and 45 °C (sc)	0.715	2.96	2.69 (0.094)	3.98	3.68 (0.078)	3.21	2.99 (0.082)
172 bar and 45 °C (sc)	0.779	3.06	2.78 (0.090)	4.06	3.86 (0.084)	3.32	3.18 (0.09)
172 bar and 25 °C (liq)	0.894	3.06	2.76 (0.094)	4.05	3.84 (0.082)	3.33	3.17 (0.084)

<sup>a</sup> Values in the parenthesis are standard deviations of pore diameters obtained from ten different TEM images of the same sample.

that branching expands the core of the micelle template.<sup>31</sup> The d-spacing values, as calculated from the XRD plots, also increase slightly from HFOPC templated film (2.48 nm) to HFDoMePC films (2.51 nm), and are significantly larger for HFDePC (2.83 nm) synthesized film. The similar trends in pore diameter are expected, as the surfactant chain length contributes to both parameters. However, the d-spacing (distance between the (100) planes of the hexagonal close-packed structure) includes both the diameter of the pores and the thickness of the silica walls.

This trend in pore size with surfactant chain length was also observed during the base-catalyzed synthesis of hexagonally ordered silica particles in a homogenous medium.<sup>31</sup> In that study, the d-spacing for the HFOPC templated powders (2.66 nm) was also smaller than both the branched HFDoMePC powders (2.81 nm) and longer chain HFDePC templated powders (2.96 nm). The larger d-spacing for base catalyzed powders compared to acid catalyzed films as observed for each template can be attributed to the silica being neutral or slightly positively charged in the acid-catalyzed films, which is expected to lower the aggregation number in the cationic micelles relative to the negatively charged silica present in base catalyzed synthesis.

#### **4.4.2 Effects of CO<sub>2</sub> Processing on Thin Film Structure**

The ability to tailor the pore size of fluorinated surfactant templated thin films by CO<sub>2</sub> processing immediately after coating was examined for this homologous series of cationic surfactants. Varying the properties of the surfactant tail (tail length and branching) and the solvent strength of CO<sub>2</sub> are expected to result in treated thin films having a wide range of pore sizes. CO<sub>2</sub> processing and the resulting penetration of surfactant tail for pore expansion in thin films occurs during the modulable steady state (MSS) of the film, a period reached a few seconds after sol coating, when the silica network is not too rigid and the final structure can be modified by external influence.<sup>134</sup> The higher diffusivity of sc CO<sub>2</sub> is expected to be an advantage compared to organic swelling agents as it allows more rapid penetration into the surfactant tail during silica condensation.

Figure 4.5 compares XRD plots of thin films templated with HFOPC as a function of CO<sub>2</sub> treatment conditions immediately after coating. At least one sharp peak corresponding to the (100) reflection is observed for all extracted films, indicating that the hexagonal ordering is preserved after CO<sub>2</sub> processing. A decrease in 2 $\theta$  value for the (100) reflection, corresponding to an increase in d-spacing, is evident for CO<sub>2</sub> processed films relative to the unprocessed film. The largest increase in d-spacing is observed for the film treated at the highest pressure investigated (2.48 nm for the unprocessed film relative to 3.06 nm for CO<sub>2</sub> processing at 172 bar). Liquid CO<sub>2</sub> (25°C) and sc CO<sub>2</sub> (45°C) treatment at 172 bar result in similar d-spacing values. (Table 4.1)

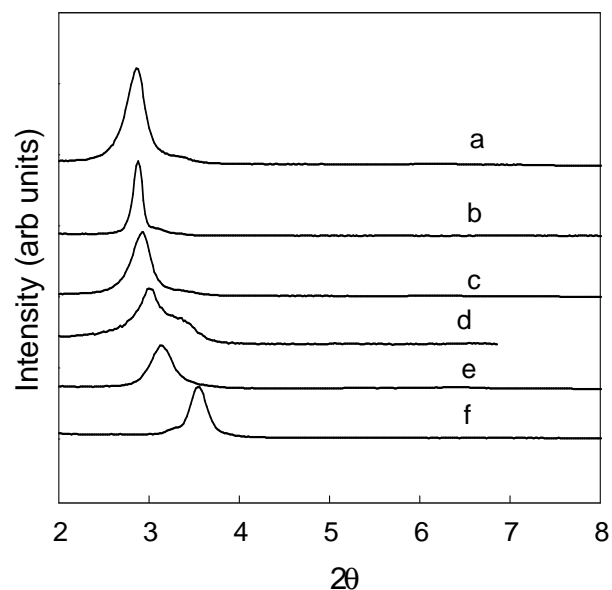


**Figure 4.5.** XRD spectra of thin films templated with HFOPC and processed in CO<sub>2</sub> at (a) 172 bar and 45 °C, (b) 172 bar and 25 °C, (c) 137 bar and 45 °C, (d) 103 bar and 45 °C, (e) 69 bar and 45 °C, and (f) not processed in CO<sub>2</sub>.

TEM images confirm the long range structure of the CO<sub>2</sub>-processed films (representative TEM images are shown in Figure 4.3), and were used to determine the corresponding pore size (Table 4.1). The pore diameters measured directly from the TEM images increase with CO<sub>2</sub> pressure. For example, the largest pore diameter observed for the HFOPC templated film is 2.76 nm for CO<sub>2</sub> treatment at 172 bar and 45°C compared to 1.91 nm for the unprocessed film (Figure 4.2, Table 4.1).

The increase in d-spacing (Figure 4.6a) with CO<sub>2</sub> processing mirrors the increase in pore size (Figure 4.6b). Both measures of pore expansion increase steadily at lower CO<sub>2</sub> densities, but level off at higher CO<sub>2</sub> density ( $\rho_{\text{CO}_2} > 0.6$  g/ml). However, the magnitude of the increase of pore diameter with CO<sub>2</sub> processing (20% - 80% at the conditions investigated) is significantly greater than the increased d-spacing (10% - 45%). The difference results from the fact that the thickness of the silica wall, as measured from the difference between the lattice parameter ( $a = 2/\sqrt{3} \cdot d\text{-spacing}$ ) and the pore diameter, actually decreases between 5% - 25% (depending on CO<sub>2</sub> pressure and

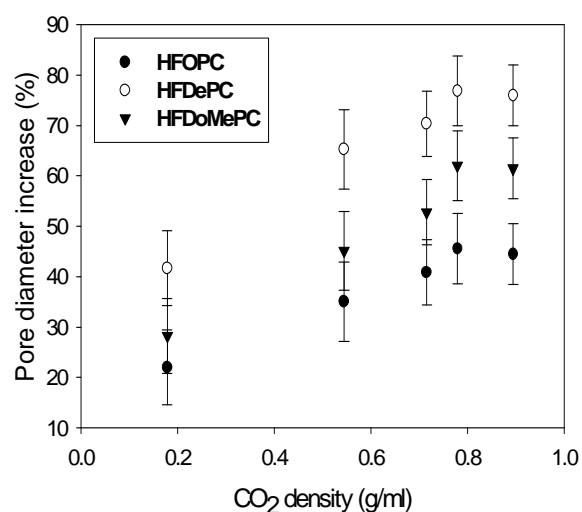
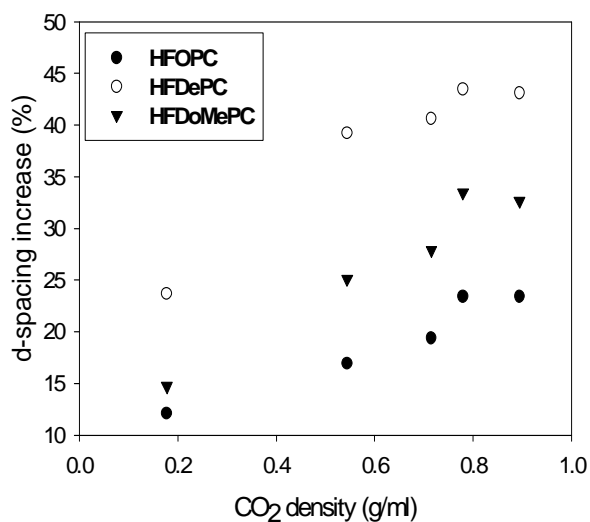


**Figure 4. 6.** Percentage increase of (a) d-spacing and (b) pore diameter of thin films processed in CO<sub>2</sub> relative to unprocessed films as a function of CO<sub>2</sub> density.

surfactant) with increasing pressure. Thus, the observed swelling effect of CO<sub>2</sub> during synthesis is limited to the pores.

The increase in pore expansion with increasing CO<sub>2</sub> pressure (Figure 4.6) can be interpreted from the driving force for the localization of CO<sub>2</sub> molecules in the surfactant tails. For example, investigations of alkane incorporation within a CTAB (hydrocarbon) micellar system have shown that short alkane swelling agent penetrate the tails of



surfactant molecules.<sup>153,261</sup> In contrast, the free energy of mixing of alkanes in tails is unfavorable for alkanes larger than decane. Hence the larger alkane molecules form a core at the center of the micelle.<sup>153</sup> CO<sub>2</sub> is a small molecule and has a favorable free energy of mixing with the fluorinated tails as indicated by the high solubility of a large number of fluorinated surfactants in CO<sub>2</sub>.<sup>74,224</sup> Thus, CO<sub>2</sub> would be expected to be solubilized in the fluorinated surfactant tails of the templates, as observed in perfluoropolyether surfactant cylindrical micelles.<sup>154</sup> The larger pore expansion observed with increased CO<sub>2</sub> density is consistent with its increased solvent strength,<sup>160</sup> resulting in a higher degree of surfactant tail solvation.

Pore expansion reaches a near-constant value at CO<sub>2</sub> densities greater than approximately 0.6 g/ml. Similarly, CO<sub>2</sub> sorption during swelling of bulk and polymer films like poly(methylmethacrylate) (PMMA),<sup>262-264</sup> polycarbonates (PC),<sup>262,264</sup> and poly(dimethylsiloxane) (PDMS),<sup>231,265</sup> and CO<sub>2</sub> solubility in hydrocarbon copolymer agents like poly(propylene oxide) (PPO),<sup>75</sup> also increases rapidly at lower pressure and then levels off at higher pressure. Another reason for the observed limit in pore expansion could be that the increased solvent strength with increasing CO<sub>2</sub> pressure may be offset by the decreased diffusivity of CO<sub>2</sub> with pressure in supercritical and liquid conditions. An additional explanation is that micelle swelling could be constrained by the silica matrix, which is fixed to a glass slide.

Figure 4.6 also compares the pore expansion in the silica thin films as a function of surfactant tail length and branching of the template. The film templated with the longer -decyl tail surfactant HFDePC has a greater degree of pore expansion relative to the -octyl tail HFOPC templated film. CO<sub>2</sub> is capable of solvating the entire length of the fluorinated tail.<sup>70</sup> Therefore, an increase in number of fluorocarbon groups in the surfactant tail leads to an expected increase in pore expansion by CO<sub>2</sub>. The pore expansion for the branched tail surfactant HFDoMePC templated film is also larger than that of HFOPC templated film (Figure 4.6) even though the unsolvated tail length of both surfactants are approximately equal. This result can also be explained by noting that previous studies of water-in-CO<sub>2</sub> microemulsions have shown that branching increases surfactant solubility in CO<sub>2</sub> resulting in greater solvation of the stubby branched tails compared to straight chain surfactants.<sup>163</sup>

### 4.4.3 Micelle-Based Interpretation of Pore Expansion

Previous micellization studies in the presence of CO<sub>2</sub> provide insight into the driving force and limitations of CO<sub>2</sub>-based pore expansion in templated thin films. Similar to micellization,<sup>160</sup> the driving forces for pore expansion through surfactant tail solvation by CO<sub>2</sub> can be interpreted as a balance between the favorable free energy of CO<sub>2</sub> penetration of the surfactant tails and the unfavorable free energy penalty associated with micelle swelling. Interfacial tension at CO<sub>2</sub>-water interfaces and solubility studies have been used to interpret properties of self-assembled aggregates such as CO<sub>2</sub>-continuous microemulsions as a function of pressure, temperature, and surfactant structure.<sup>67-69,71</sup> Figure 4.4.7 reports the interfacial tensions (IFTs) of the surfactant templates used in this study, HFOPC, HFDoMePC and HFDePC, at CO<sub>2</sub>-water interfaces relative to pure CO<sub>2</sub>-water interface data at 45 °C.<sup>69,266</sup> The IFT values for all three fluorinated surfactants decrease with an increase in CO<sub>2</sub> pressure and also with an increase of fluorocarbon groups and branching of the tail, as observed in previous studies.<sup>68,71</sup> The lowest IFT value is observed for the branched chain surfactant, HFDoMePC (3.80 mN/m at 172 bar and 45 °C).

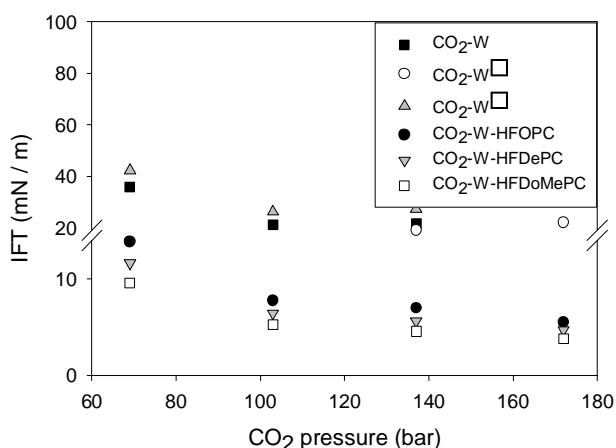


**Figure 4.7.** Interfacial tension of all three surfactants at the CO<sub>2</sub>-water interface as a function of CO<sub>2</sub> pressure at 45 °C. Scaling on y-axis different above and below the break for clarity. Standard deviations of IFT values from this study (< ± 4%) not shown in figure for clarity. CO<sub>2</sub>-water interfacial tensions from this study (■) are compared to those of da Rocha et.al.<sup>69</sup> (◇) and Chun and Wilkinson<sup>266</sup> (△).

The lowest possible value of IFT for a particular surfactant at CO<sub>2</sub>-water interfaces is observed at the most balanced state of hydrophilic-CO<sub>2</sub>-philic balance (HCB),<sup>69</sup> where the surfactant has equal affinity for both phases; inversion of colloidal dispersions between CO<sub>2</sub>-in-water and water-in-CO<sub>2</sub> with change in formulation variables (CO<sub>2</sub> pressure, temperature, system pH and salinity) can occur at this balanced state.<sup>67,267</sup> In general, the curvature (H) at the CO<sub>2</sub>-water interface predicts the existence of colloidal dispersions of CO<sub>2</sub>-in-water (H>0) or water-in-CO<sub>2</sub> (H<0) and can be described from the packing parameter.<sup>67</sup> The distribution of the surfactant between oil and water phases has roughly been used to determine the sign of the curvature (Bancroft's rule),<sup>268</sup> although Kahlweit suggests that the ratio of cmcs in the two phases (and not the ratio of monomers) is a more accurate predictor of curvature.<sup>269</sup> Thus, for a surfactant with higher solubility in aqueous phase compared to CO<sub>2</sub>, the surfactant lies on the aqueous side of HCB (HCB > 1). The homologous series of cationic fluorinated templates in this study was observed to have minimal solubility at concentrations lower than 1 wt% (at 25°C and 45°C and pressures from 55 – 355 bar) in CO<sub>2</sub>, while being highly soluble in water (solute concentration > 40 wt%).<sup>114</sup> Hence, these surfactants lie on the aqueous side of the HCB. The observed decrease in IFT with increasing CO<sub>2</sub> pressure indicates movement towards a more balanced state of HCB (i.e. towards the CO<sub>2</sub>-philic side or more favorable penetration of CO<sub>2</sub> molecules in the surfactant tail).<sup>67</sup>

Similarly, the decrease in the IFT at the CO<sub>2</sub>/water interface with increasing surfactant tail length is consistent with the larger degree of pore expansion observed for the HFDePC - templated film. However, the IFT values for the branched surfactant, HFDoMePC, are lower than for the -decyl tail surfactant, HFDePC, suggesting that degree of pore expansion for HFDoMePC templated film should be greater. This apparent contradiction between IFT values and the observed pore expansion may be explained from the solvation and geometric effects of micelle assembly in CO<sub>2</sub>. Branching of surfactant tail leads to an increased solubility of surfactant in CO<sub>2</sub> along with a corresponding lowering of aqueous solubility.<sup>163</sup> For surfactants present on the aqueous side of HCB, this would indicate a movement towards the CO<sub>2</sub>/water interface and along with the ability of the stubby branched tails to minimize tail overlap<sup>163,164</sup> leads

to the observed decrease in interfacial tension for HFDoMePC. The geometric dependence of micelle swelling can be described by the penalty in Gibbs free energy during formation of self-assembled aggregates, which is directly related to the creation of interfacial area. For the straight tail surfactant, swelling by CO<sub>2</sub> is limited along the radial direction. However, solvation along the branches of a branched surfactant results in a lesser increase in interfacial area, thus resulting in a smaller free energy penalty. Therefore, the solvation of the branched surfactant can result in a smaller pore diameter increase (expansion is distributed along both branches) compared to the straight chain surfactant, but the CO<sub>2</sub> penetration and hence volume swelling over both branches of HFDoMePC can be greater (consistent with the IFT measurements). CO<sub>2</sub>-water interfacial activity and solubility of surfactants in CO<sub>2</sub> can thus be used to interpret the trends in pore expansion as a function of surfactant template structure and CO<sub>2</sub> density.

#### 4.5 Conclusions

Nanoporous silica thin films with well ordered hexagonal structure were synthesized by dip-coating using a homologous series of cationic fluorinated surfactants as templating agents under acidic conditions. The nanoporous silica films were processed in CO<sub>2</sub> directly after coating, which resulted in pressure tunable swelling of the 'CO<sub>2</sub>-philic' fluorinated templates leading to thin films with pore diameters in the range of 1.91 ( $\pm$  0.20) nm to 3.86 ( $\pm$  0.20) nm. The pore expansion of thin films increased with an increase in CO<sub>2</sub> pressure and with the tail length of surfactant templates. Branching of the surfactant template resulted in increased swelling of the micelle core, compared to linear tail surfactants, which is consistent with previous studies of CO<sub>2</sub> solvation of fluorinated tails.<sup>224,244</sup> The long-range ordering of the thin films was retained after pore expansion, unlike some previous investigations using traditional organic solvents as pore swelling agents.<sup>37,39,222</sup>

Sol-gel processing of templated materials provides the opportunity to capture self-assembled structures into kinetically stable materials.<sup>270,271</sup> Capturing the effects of CO<sub>2</sub> on self-assembly has practical application (i.e., pore expansion or CO<sub>2</sub>-directed self assembly) and addresses the limited investigations of the effect of CO<sub>2</sub> on surfactant mesophases.<sup>75,272</sup> In contrast, numerous investigations have focused on the effect of CO<sub>2</sub>

on self-assembled aggregates (micelles and microemulsions).<sup>68,70,226,251,273</sup> The interpretation of CO<sub>2</sub>-induced pore expansion using micelle-based approaches (i.e. interfacial activity and phase behavior, as relevant to the HCB) may provide a systematic guide to design surfactant systems whose resulting co-assembled structures may be altered through CO<sub>2</sub> solvation.

Copyright © Kaustav Ghosh 2007

## CHAPTER FIVE

### PORE SIZE ENGINEERING IN FLUORINATED SURFACTANT TEMPLATED MESOPOROUS SILICA POWDERS THROUGH SUPERCRITICAL CARBON DIOXIDE PROCESSING

#### 5.1 Summary

Pore expansion of fluorinated surfactant templated mesoporous silica powders is demonstrated as a function of pressurized CO<sub>2</sub> processing conditions. Mesoporous silica powder is synthesized by sol-gel reaction induced precipitation in a base-catalyzed medium using 1-(3,3,4,4,5,5,6,6,7,7,8,8,8-tridecafluoro-octyl)-pyridinium chloride (HFOPC) as template and, immediately after filtration, the precipitated material is processed in gaseous and supercritical CO<sub>2</sub> (88 – 344 bar, 45°C) for 48 h. Characterization of the silica powders by XRD, TEM and N<sub>2</sub> adsorption reveals the formation of well-ordered materials with 2D hexagonal close-packed pore structure before and after CO<sub>2</sub> processing. An optimal aging time (time from addition of silica precursor to the sol until the filtration of the hydrolyzed sol) of 20 min prior to CO<sub>2</sub> processing is identified. Proper aging time results in silica powder with significant pore expansion at all processing pressures while retaining the long range structure of the material. The pore diameter of the mesoporous material increases with increasing CO<sub>2</sub> pressure (from 2.60 nm (unprocessed) to 3.21 nm at 344 bar), but appears to level off above 100 bar. The pore expansion behavior is attributed to favorable CO<sub>2</sub> penetration in the 'CO<sub>2</sub>-philic' fluorinated tails of the surfactant template. The CO<sub>2</sub> expansion of base catalyzed silica powders is significantly less than we previously observed for acid catalyzed, evaporation-driven thin film synthesis using fluorinated cationic surfactant templates. The effect of pH on self-assembly and increased silica condensation in basic conditions may inhibit pore expansion by CO<sub>2</sub>.

#### 5.2 Introduction

The base-catalyzed sol-gel synthesis of mesoporous silica proceeds through a co-assembly process, in which the surfactant molecules form well-ordered supramolecular

templates and the hydrolyzed silica precursor associates with the surfactant head group.<sup>24</sup> Under basic conditions, hydrolyzed silica precursors initially precipitate with surfactant micelles to form composite particles that are solidified by condensation of the silica network. Finally, removal of the surfactant templates results in mesoporous silica with the desirable properties of uniform pore size distribution and high surface area. The ordered nanostructured materials have diverse applications in the fields of separations, adsorption, catalysis, biomimetics and sensing.<sup>129,132,133,221,238</sup> The ability to tailor the mesoporous materials has further increased their applications, as recently demonstrated in drug delivery, chromatographic and electrode applications.<sup>146-148</sup> Traditionally, the synthesis of pore expanded surfactant templated materials is accomplished through the addition of an inert swelling agent (e.g., polypropylene oxide or dodecane) in the micellar solution. The swelling agent interacts favorably with the surfactant tails or forms an inner core in the micelle.<sup>37-39,243</sup> However, agents for tailoring pore structure affect the surfactant self-assembly in solution and may lead to either complete transition to a new mesophase or loss of long-range order.<sup>37,39,222</sup>

The tunable solvent strength of compressed and sc (supercritical) CO<sub>2</sub> (T<sub>c</sub> = 31.1°C, P<sub>c</sub> = 73.8 bar) suggests its use for the controlled expansion of pores formed by surfactant templating. Additional advantages of sc CO<sub>2</sub> relative to organic process solvents include its high diffusivity and the absence of a liquid-vapor interface during depressurization enabling preservation of long-range structure. CO<sub>2</sub> is also nonflammable, nontoxic, environmentally acceptable, and inexpensive. CO<sub>2</sub> is also nonflammable, nontoxic, environmentally acceptable, and inexpensive.

Sc CO<sub>2</sub> has previously been used to expand mesoporous silica powders templated by hydrocarbon copolymer surfactants (P123, P85 and F127), where pore expansion of 54% was achieved for processing pressures of 482 bar.<sup>75,223</sup> Recently, we have observed significant pore expansion (20% - 80%) as a function of CO<sub>2</sub> processing conditions (69 - 172 bar, 45°C) for silica films templated with cationic fluorinated surfactants with varying tail length and branching.<sup>245,274</sup> The dramatic pore expansion achieved in fluorinated surfactant templated silica at lower CO<sub>2</sub> processing pressures compared to hydrocarbon templates suggests a favorable penetration of CO<sub>2</sub> molecules into the fluorinated tails. Indeed, many fluorinated moieties have been identified as “CO<sub>2</sub>-philic”

based on their high solubility in CO<sub>2</sub>, and their weak dispersion forces, which are similar to that of CO<sub>2</sub>.<sup>74,224</sup> Thus, the high degree of solvation of fluorinated tails by CO<sub>2</sub> can be exploited to tailor mesoporous ceramics. The favorable transport properties and tunable solvent strength of sc CO<sub>2</sub> processing are also advantageous for infusing silica precursors into preformed ordered templates for synthesis of mesoporous silica films<sup>55</sup> and the extraction of surfactant templates from uncalcined ordered mesoporous silica.<sup>275,276</sup> Thus, CO<sub>2</sub> technology is potentially a versatile tool in processing mesoporous ceramics.

All prior investigations of the CO<sub>2</sub>-activated pore expansion of silica materials employed an acid-catalyzed sol gel process (pH ~ 2-3). Acid catalysis is well-suited to the use of high pressure CO<sub>2</sub>, which acidifies aqueous solutions (pH ~ 3) due to the formation and dissociation of carbonic acid.<sup>277</sup> Extending CO<sub>2</sub> processing to base catalyzed silica powders, however, could introduce pH variations in the system. Previous studies have shown that the addition of NaOH to a water-CO<sub>2</sub> system can raise pH values to above 8 for CO<sub>2</sub> pressure of 482 bar at 22°C.<sup>278</sup> In addition, materials synthesis in a basic media is characterized by more rapid condensation of the silica matrix, which could ultimately constrain pore expansion compared to acid catalyzed films.

In this paper we report the CO<sub>2</sub>-activated pore expansion of base-catalyzed mesoporous silica powders templated using a cationic fluorinated surfactant, HFOPC. The effect of the aging time of the hydrolyzed sol on processibility using CO<sub>2</sub> is examined and an appropriate aging time is identified. The swelling behavior of these silica powders is compared to the pore swelling in acid catalyzed thin films. The change in pore structure of silica powders as a function of CO<sub>2</sub> processing conditions is used to interpret CO<sub>2</sub> penetration in surfactant mesophases.

## 5.3 Materials and Methods

### 5.3.1 Materials

1-(3,3,4,4,5,5,6,6,7,7,8,8,8-Tridecafluorooctyl)pyridinium chloride (HFOPC; C<sub>6</sub>F<sub>13</sub>(CH<sub>2</sub>)<sub>2</sub>NC<sub>5</sub>H<sub>5</sub><sup>+</sup> Cl<sup>-</sup>), was synthesized as described previously.<sup>229</sup> Briefly, anhydrous pyridine was alkylated with 1H,1H,2H,2H-tridecafluoroalkyl iodide. The pyridinium iodide was converted into the corresponding chloride by ion exchange chromatography and the purity was confirmed by mass spectrometry and melting point measurements (as



detailed elsewhere).<sup>31</sup> Tetraethoxysilane (TEOS, purity > 99%, Gelest), NH<sub>3</sub> (28 – 30% solution from Malinckrodt), absolute ethanol (Aaper Alcohol and Chemical Co.), deionized ultrafiltered water and HCl (Fisher Scientific) were also used in the material synthesis. Carbon dioxide (Coleman grade, 99.99+%) was purchased from Scott Gross Co. (Lexington, KY).

### **5.3.2 Mesoporous Silica Synthesis and CO<sub>2</sub> processing**

Mesoporous silica powders were synthesized using NH<sub>3</sub> as a catalyst and HFOPC as a template, as described previously.<sup>76</sup> Briefly, TEOS was added to a mixture of NH<sub>3</sub> and de-ionized ultra-filtered (DIUF) H<sub>2</sub>O in molar ratios of 1 TEOS: 2.65 NH<sub>3</sub>: 149 DIUF H<sub>2</sub>O.<sup>76</sup> After letting the sol-gel reaction proceed for a fixed amount of time (aging time), the solution was filtered and the powdered silica filtrate was divided into two batches. One batch was treated at 45°C at ambient pressure for 48 h; the other batch was processed in CO<sub>2</sub> at a constant pressure (88 to 344 bar) and 45°C, also for 48 h. Samples treated with CO<sub>2</sub> at less than 172 bar were processed in a 100 mL stainless steel Parr Mini Reactor. At higher pressures, CO<sub>2</sub> processing was conducted in a 16 mL Micro Reactor (High Pressure, SS Series, rated to 2064 bar). The Micro Reactor is not suitable for holding a glass slide, and was therefore not used in the previous investigation of CO<sub>2</sub> processing of dip coated films. Thus, an advantage of extending CO<sub>2</sub> processing to base-catalyzed particle precipitation was the ability to investigate CO<sub>2</sub> processing at higher pressures. After completion of CO<sub>2</sub> processing, the powders were depressurized. For both reactors, the pressurization and depressurization steps were performed slowly (~ 25 bar/min) to prevent collapse of silica structure. Both the CO<sub>2</sub> treated and the untreated batches of synthesized materials were then heated in vacuum at 100°C for 24 h (temperature ramped by 30°C every 6 h) and then extracted by washing twice with acidic ethanol (5 ml of concentrated HCl in 95 ml of EtOH).

### **5.3.3 Material Characterization**

X-ray diffraction patterns were recorded on a Siemens 5000 diffractometer using Cu K $\alpha$  radiation ( $\lambda = 1.54098 \text{ \AA}$ ) and a graphite monochromator. Transmission electron microscope (TEM) images were taken with a JEOL 2000FX instrument operating at 200 kV. Samples were prepared by directly depositing the powders onto a lacey carbon grid. Nitrogen adsorption measurements were conducted using a Micromeritics Tristar 3000

system. Samples were degassed at 140°C for 4 h under flowing nitrogen prior to adsorption measurement. The pore size distribution and surface area of the mesoporous silica were determined by analyzing the nitrogen adsorption results using the BJH method with a modified statistical film thickness equation (KJS method).<sup>253</sup>

## 5.4 Results and Discussion

Fluorinated surfactants generally self-assemble more easily and form aggregate structures with lower curvature compared to hydrocarbon surfactants.<sup>113,114</sup> Our research team has exploited properties of fluorinated surfactant templating to form unusually small uniform pores (1.6 nm),<sup>123</sup> to capture novel intermediate mesh phase structures,<sup>31</sup> to alter accessibility of organic functional groups,<sup>124</sup> and to demonstrate pore structure refinement by CO<sub>2</sub> processing.<sup>274</sup> The synthesis of base-catalyzed porous silica powders through templating with a homologous series of perfluoroalkylpyridinium chloride surfactants, including HFOPC, resulted in hexagonal close-packed and mesh phase structures.<sup>31</sup> Separate investigations demonstrated the pore expansion of acid catalyzed porous silica films through CO<sub>2</sub> penetration of the ‘CO<sub>2</sub>-philic’ fluorinated templates, including HFOPC.<sup>245,274</sup>

In extending CO<sub>2</sub> processing to base-catalyzed silica powders, we first investigated the effects of aging time (time from addition of silica precursor to the sol until the filtration of the hydrolyzed sol) of silica synthesis on the ability to process the powders with CO<sub>2</sub>. While a minimum aging time is required to allow sufficient hydrolysis for the formation of the initial silica structure in base-catalyzed precipitation of particles, the extent of silica condensation in an over-aged solution may inhibit expansion of the silica structure by CO<sub>2</sub>. In contrast, the mesostructure of thin films is formed within the first few seconds after dip coating. Therefore, for the acid catalyzed films, there is no minimum aging time before CO<sub>2</sub> processing, and longer aging times merely result in increased condensation, thereby limiting pore expansion.<sup>274</sup>

The effect of aging time on the CO<sub>2</sub>-activated pore expansion behavior of templated silica was evaluated at CO<sub>2</sub> processing conditions of 103 bar and 45°C for 48 h. XRD was used to determine the long range order and pore expansion of mesoporous silica powders with and without CO<sub>2</sub> processing (Fig. 5.1) at aging times of 20 min, 1 h

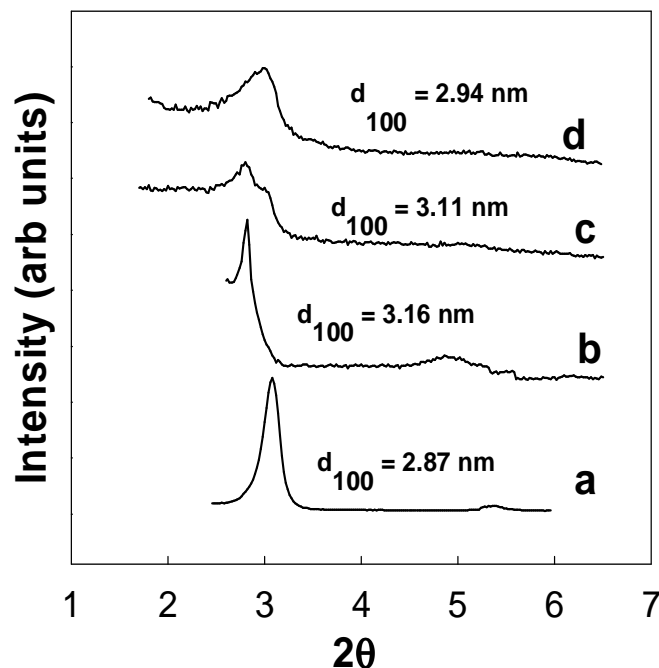


**Fig. 5.1.** XRD patterns of HFOPC templated silica powders synthesized (a) without CO<sub>2</sub> processing; and processed in CO<sub>2</sub> at 103 bar and 45 °C after aging for (b) 20 min, (c) 1 hr and (d) 24 hr.

and 24 h. The minimum aging time investigated, 20 min, is the approximate onset of uniform cloudiness in the sol solution, indicating significant hydrolysis and silica precipitation. The longest aging time, 24 h, was selected to match conditions from our previous study and represents complete hydrolysis of the silica precursor and the formation of the final ordered structure.<sup>76</sup> The XRD plot for the sample aged 20 min prior to CO<sub>2</sub> processing (Fig. 5.1b) shows a significant increase in d-spacing (3.16 nm) compared to the unprocessed sample (2.87 nm). In addition, the presence of (100) and (110) reflections in both the unprocessed material and the material aged 20 min indicates that long range hexagonal ordering is retained. TEM images confirm 2D-hexagonal structure for the HFOPC templated mesoporous silica (Fig. 5.2a) and the retention of order following CO<sub>2</sub> processing of the 20 min aged sample (Fig. 5.2b).

A broad, broken peak is observed for the sample aged for 1 hr prior to CO<sub>2</sub> processing (Fig. 5.1c), characteristic of a broad distribution of pore sizes. This peak can

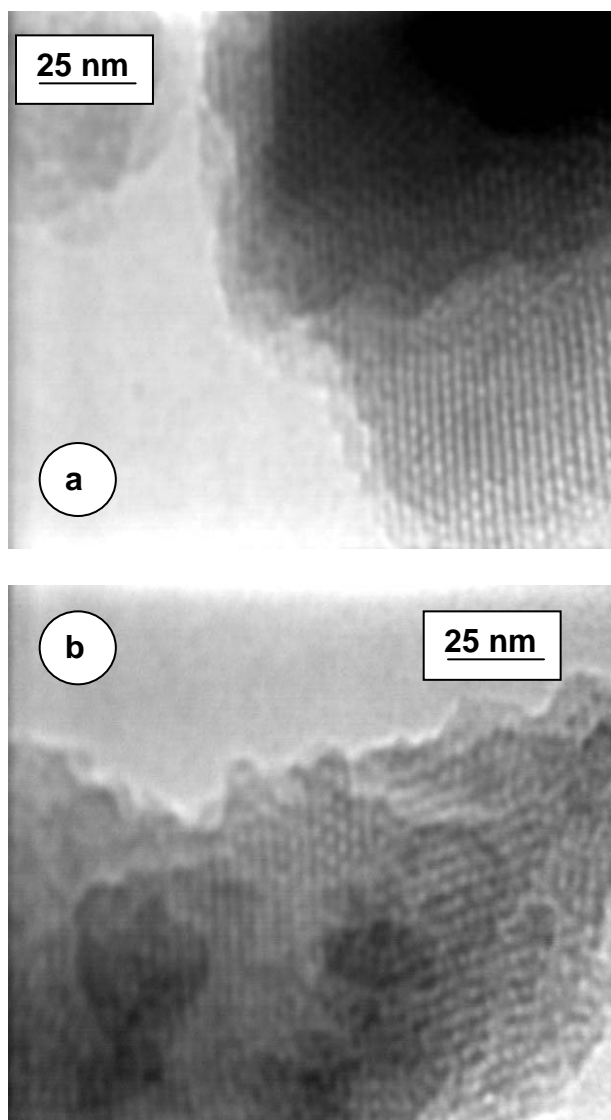


**Figure 5.2.** TEM micrographs of HFOPC templated mesoporous silica powders (a) without CO<sub>2</sub> processing and (b) processed in CO<sub>2</sub> at 103 bar and 45°C.

be indexed to the (100) reflection with a d-spacing of 3.11 nm. Non-uniform pore expansion during CO<sub>2</sub> processing could explain the breadth of the (100) reflection. Regions where CO<sub>2</sub> penetrates the surfactant tails before significant silica condensation may experience pore expansion, while pore expansion would be limited in areas where significant silica condensation has occurred. For the 24 h aged sample, CO<sub>2</sub> processing

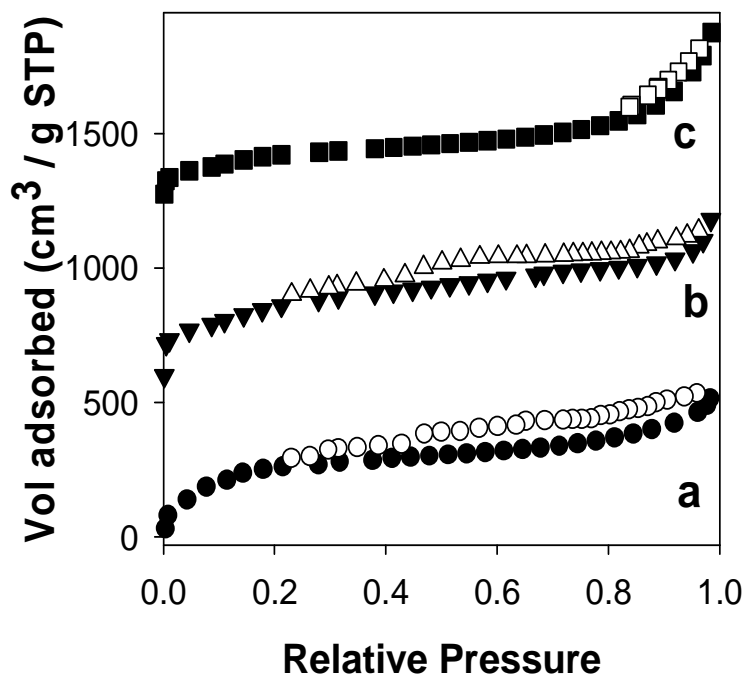


**Figure 5.3.** Nitrogen sorption isotherm of HFOPC templated silica powders prepared with CO<sub>2</sub> processing (103 bar and 45 °C) after aging for (a) 20 min, (b) 1 hr and (c) 24 hr. Filled symbols are for adsorption and open for desorption. The y-axis values have been offset by 600 units (trace b) and by 1000 units (trace c) for clarity.

increased the d-spacing only slightly (2.94 nm) (Fig. 5.1d) relative to the unprocessed sample (2.87 nm). More complete silica condensation throughout the sample due to longer aging time restricts the pore expansion. However, the breadth of the peak suggests that the order of the silica structure deteriorated after CO<sub>2</sub> processing compared to the unprocessed powder, which was aged for a similar period of 24 h.

The effect of aging time can also be observed from the N<sub>2</sub> adsorption isotherms of the silica powders. The 20 min and 1 h aged samples processed in CO<sub>2</sub> at 103 bar and 45°C display Type IV isotherms (Figure 5.3), characteristic of ordered mesoporous materials.<sup>253</sup> The pore diameter of the 20 min aged sample increases from 2.60 nm for the unprocessed particles to 2.98 nm (Fig. 5.3a), similar to the increased d-spacing observed by XRD. The surface area also increases, from 811 m<sup>2</sup>/g for the unprocessed powder to 1117 m<sup>2</sup>/g for the powders processed in CO<sub>2</sub> after 20 min of aging. The pore diameter of the 1 h aged sample does not change significantly with CO<sub>2</sub> processing (2.66 nm) and the

surface area actually decreases ( $550 \text{ m}^2/\text{g}$ ). (Fig. 5.3b), This result is counterintuitive to the XRD analysis, which reveals an increase in d-spacing with  $\text{CO}_2$  processing from 2.87 nm for the unprocessed powder to 3.10 nm for 1h aged powder. This difference could be the result of non-uniform pore expansion by  $\text{CO}_2$ , an observation confirmed from XRD analysis. For the 24 h aged sample, both the pore diameter (1.55 nm) and the surface area ( $176 \text{ m}^2/\text{g}$ ) decrease significantly after  $\text{CO}_2$  processing (103 bar and  $45^\circ\text{C}$ ) compared to the unprocessed sample (Fig. 5.3c). This suggests partial collapse of the silica structure, a finding confirmed by the loss of long-range order in the XRD plot. The investigation of aging time suggests that  $\text{CO}_2$  processing should begin as soon as precipitation of the base-catalyzed templated silica is observable. All subsequent comparisons of effects of  $\text{CO}_2$  processing on mesoporous silica are based on an aging period of 20 min.

The ability to tune the pore expansion of the mesoporous silica powders was investigated as a function of  $\text{CO}_2$  processing conditions. The XRD patterns of mesoporous silica powders as a function of  $\text{CO}_2$  treatment (no  $\text{CO}_2$  processing, gaseous  $\text{CO}_2$  processing at 88 bar and  $45^\circ\text{C}$ , and sc  $\text{CO}_2$  processing at  $45^\circ\text{C}$  and pressures of 103 bar, 137 bar, 172 bar, 258 bar and 344 bar) are presented in Figure 5.4. XRD results indicate well ordered 2D hexagonal structure, with the presence of at least two peaks that can be indexed to the (100) and (110) reflections. TEM images verify the 2D hexagonal structure inferred from the XRD results. Figure 5.2b presents a representative TEM image of mesoporous silica powder processed in  $\text{CO}_2$  at 103 bar and  $45^\circ\text{C}$ . Regular arrays of uniform channels parallel to the channel axis and a cross-sectional view of the hexagonal channels confirm the long range hexagonal order of the  $\text{CO}_2$  processed powders.

An increase in d-spacing of the periodic nanostructure, corresponding to a decrease in the  $2\theta$  value of the (100) reflection, is observed for all  $\text{CO}_2$  processed powders relative to the unprocessed powders (Fig. 5.4 and Table 5.1). The d-spacing increases substantially with pressure at lower processing pressures (from 2.87 nm for the unprocessed powders to 3.11 nm for gaseous  $\text{CO}_2$  processing at 88 bar and  $45^\circ\text{C}$  and to 3.16 nm for sc  $\text{CO}_2$  processing at 103 bar at  $45^\circ\text{C}$ ). Thereafter, the degree of d-spacing increase with pressure is much lower, achieving a d-spacing of 3.30 nm at the highest processing pressure of 344 bar at  $45^\circ\text{C}$ .  $\text{CO}_2$  density at a given temperature is a better

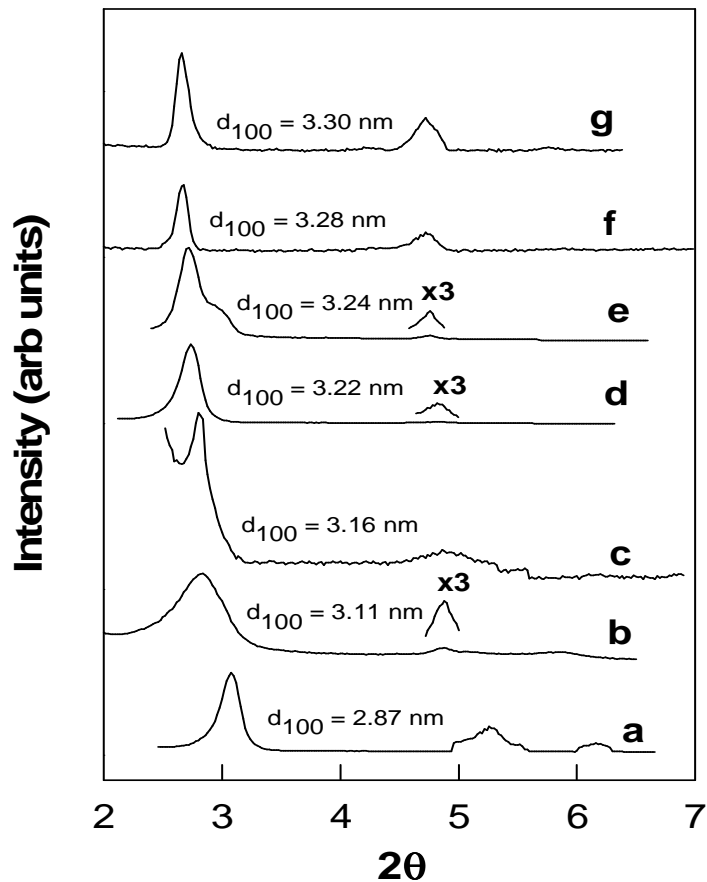


**Figure 5.4.** XRD patterns of mesoporous silica powders templated with HFOPC (a) before processing in CO<sub>2</sub> and processed in CO<sub>2</sub> at (b) 88 bar and 45 °C ( $\rho_{\text{CO}_2} = 0.31$  g/ml), (c) 103 bar and 45 °C ( $\rho_{\text{CO}_2} = 0.54$  g/ml), (d) 137 bar and 45 °C ( $\rho_{\text{CO}_2} = 0.71$  g/ml), (e) 172 bar and 45 °C ( $\rho_{\text{CO}_2} = 0.78$  g/ml), (f) 258 bar and 45 °C ( $\rho_{\text{CO}_2} = 0.86$  g/ml), and (g) 344 bar and 45 °C ( $\rho_{\text{CO}_2} = 0.91$  g/ml). (110) reflections have been expanded 3 times in some plots for clarity.

description of its tunable solvent strength, or the ability to solvate the fluorinated tails, than pressure. However, the d-spacing increase with CO<sub>2</sub> density (Table 5.1) is not linear. The most significant increase of d-spacing with density is observed in the low density regime of gaseous CO<sub>2</sub> (8.4 % d-spacing increase at 0.31 g/ml (88 bar, 45°C). The increase with density is less sizable at higher processing pressures (15.0 % d-spacing increase at 0.92 g/ml (344 bar, 45°C).

N<sub>2</sub> adsorption isotherms of the CO<sub>2</sub>-processed mesoporous silica powders (Fig 5.5) display Type IV isotherms, indicative of ordered mesoporous materials. The

**Table 5.1** Summary of pore structure of mesoporous silica powders as a function of CO<sub>2</sub> processing conditions

CO <sub>2</sub> conditions	$\rho_{\text{CO}_2}$ (g/ml) <sup>2</sup> <sub>33</sub>	d <sub>100</sub> (nm)	d <sub>p</sub> (nm)	S <sub>t</sub> (m <sup>2</sup> /g)	v <sub>m</sub> (cm <sup>3</sup> /g)	t (nm)
No CO <sub>2</sub>		2.87	2.6	811	0.28	0.71
88 bar, 45°C	0.31	3.11 (0.24) <sup>a</sup>	2.83 (0.23) <sup>b</sup>	1052	0.59	0.76
103 bar, 45°C	0.54	3.16 (0.29) <sup>a</sup>	3.03 (0.43) <sup>b</sup>	1117	0.71	0.62
137 bar, 45°C	0.72	3.22 (0.35) <sup>a</sup>	3.11 (0.51) <sup>b</sup>	1225	0.79	0.61
172 bar, 45°C	0.78	3.24 (0.37) <sup>a</sup>	3.12 (0.52) <sup>b</sup>	1187	0.77	0.62
258 bar, 45°C	0.86	3.28 (0.41) <sup>a</sup>	3.17 (0.57) <sup>b</sup>	1279	0.80	0.62
344 bar, 45°C	0.91	3.30 (0.43) <sup>a</sup>	3.21 (0.61) <sup>b</sup>	1315	0.83	0.60

d<sub>100</sub> is d-spacing, d<sub>p</sub> is the pore diameter, S<sub>t</sub> is the specific surface area, v<sub>m</sub> is the mesopore volume, t is thickness of silica wall, values in parenthesis are increase in d-spacing<sup>a</sup> and pore diameter<sup>b</sup> compared to unprocessed powder. Maximum standard deviation for d-spacing or pore diameter at any CO<sub>2</sub> processing condition < 0.04 nm.

adsorption data for the mesoporous powders were analyzed by the KJS method (Kelvin equation modified BJH) which uses the high resolution  $\alpha_s$ -plot method and has been established previously to accurately analyze pore properties of mesoporous materials.<sup>253</sup> Similar to the d-spacing values, pore diameter, pore volume, and specific surface area of the silica powders (Table 5.1) increase for all CO<sub>2</sub> processed samples compared to the unprocessed powder and the increase is generally greater at higher CO<sub>2</sub> densities. The expansion of the pore diameter and d-spacing with CO<sub>2</sub> pressure follow similar trends; the pore diameter increase with CO<sub>2</sub> pressure is most significant in the low pressure regime (e.g, d<sub>p</sub>=2.83 nm for gaseous CO<sub>2</sub> processing 88 bar relative to d<sub>p</sub>=2.60 nm for the unprocessed samples). At higher processing pressures the degree of pore diameter increase with pressure is reduced, with a maximum pore diameter of 3.23 nm observed at 344 bar. The similarity of the trends in pore size and d-spacing with pressure is expected. The increase in d-spacing, which comprises both the pore diameter and the thickness of the silica walls, is dominated by the pore diameter increase due to



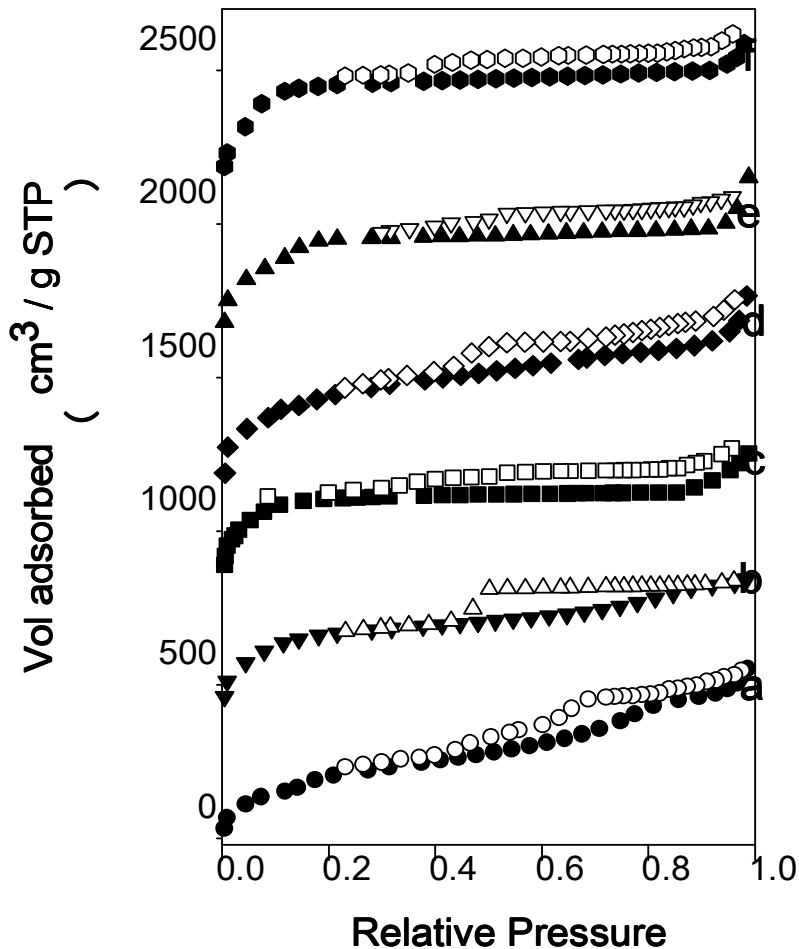


**Figure 5.5.** Nitrogen sorption isotherm of mesoporous silica powders templated with HFOPC and processed in CO<sub>2</sub> at (a) 88 bar and 45 °C, (b) 103 bar and 45 °C, (c) 137 bar and 45 °C, (d) 172 bar and 45 °C, (e) 258 bar and 45 °C, and (f) 344 bar and 45 °C. Filled symbols are for adsorption and open for desorption. The y-axis values have been offset for clarity.

solvation of the surfactant tails. The thickness of the silica walls decreases with CO<sub>2</sub> pressure (Table 5.1), which results in a lower d-spacing increase (on a percentage basis) relative to the pore diameter increase.

Limits of pore expansion by CO<sub>2</sub> were observed in our previous study of fluorinated surfactant templated thin films.<sup>245</sup> In that study, increasing CO<sub>2</sub> pressure beyond approximately 100 bar did not lead to further significant increases in pore size.<sup>245</sup> In the case of thin films, further pore expansion may be inhibited by the constraining

effect of the silica matrix fixed to the glass substrate. Alternatively, this phenomena may reflect trends in solvation of the surfactant tail, analogous to the leveling off of CO<sub>2</sub> swelling of polymers with increasing pressure.<sup>279,280</sup> For example, CO<sub>2</sub> uptake in the polypropylene oxide core of a P123 liquid crystal phase is most pronounced at pressures up to 100 bar and then increases only slightly with increasing pressure.<sup>75</sup> CO<sub>2</sub> solubility in bulk polymers such as polystyrene<sup>279,281</sup> and polybutadiene<sup>282</sup> is generally characterized by an 'S' shaped isotherm; CO<sub>2</sub> sorption increases uniformly up to the inflection point near the critical pressure of CO<sub>2</sub> (~ 80 bar) and then increase only slightly at higher pressures. However, for polymers such as poly(methylmethacrylate) (PMMA)<sup>282</sup> and poly-(dimethylsiloxane) (PDMS),<sup>231</sup> which exhibit specific favorable interactions and high miscibility with CO<sub>2</sub>, CO<sub>2</sub> sorption is significant not only below the CO<sub>2</sub> critical pressure but also increases at a substantial rate above the critical pressure. This trend is a characteristic of the good solvent quality of CO<sub>2</sub> for PMMA and PDMS.<sup>231,282</sup> Hence, the pore expansion trend in the current study (considerable expansion below 100 bar and a lesser, yet significant, increase with pressure at higher pressures) is consistent with the miscibility of fluorocarbons tails with CO<sub>2</sub>, similar to PMMA and PDMS.

Figure 5.6 compares the pore expansion of silica powders in the current study templated with HFOPC with that observed for acid catalyzed films, also synthesized with the same fluorinated surfactant template at comparable CO<sub>2</sub> processing densities. The similarity of the expansion trends for powder precipitation and thin film synthesis again suggests that surfactant tail solvation, and not the constraining effect of the glass substrate on the thin films, dominate the observed pore expansion. Although the pore expansion trends with CO<sub>2</sub> pressure are alike for silica thin film synthesis and particle precipitation, the percentage pore expansion at a given CO<sub>2</sub> processing condition is less for the silica powders compared to the films (Fig 5.6). For example, the pore diameters of the silica powder increases 20% compared to a 42% increase in the thin films processed in CO<sub>2</sub> at 172 bar and 45°C. However, the absolute pore diameter of the films is always less compared to the powder at the same CO<sub>2</sub> processing condition (e.g. 3.12 nm for base catalyzed powders compared to 2.71 nm for the films for CO<sub>2</sub> processing at 172 bar<sup>274</sup>).

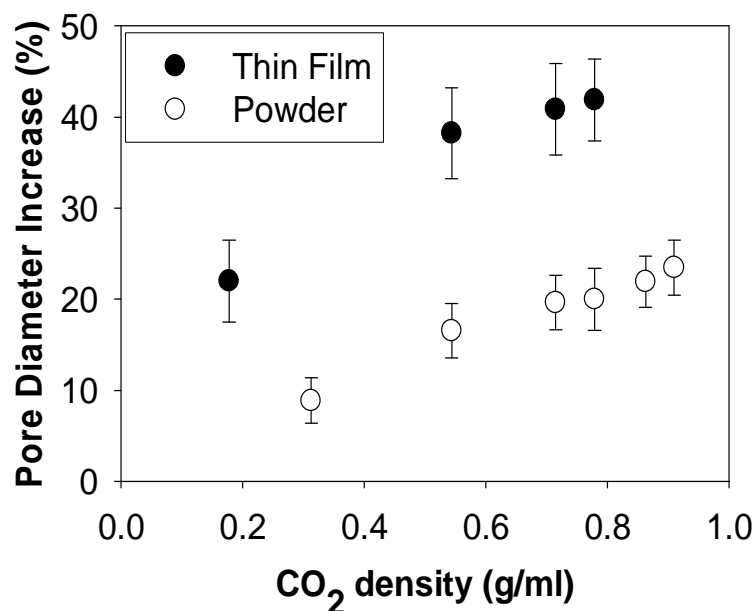


**Figure 5.6.** Percentage increase of pore diameter of HFOPC templated acid-catalyzed films and base-catalyzed powders as a function of CO<sub>2</sub> density.

The effect of pH on self-assembly, sol gel reactions, hydrolysis and condensation may explain this difference in pore expansion and absolute pore diameter between acid and base catalyzed samples after CO<sub>2</sub> processing. In acid catalyzed film synthesis, the silica is neutral or slightly positively charged, which is expected to lower the aggregation number in the cationic micelles relative to the negatively charged silica present in base catalyzed synthesis and lead to a smaller pore diameter in acid catalyzed system. This effect is observed in HFOPC templated silica; the pore diameter for the unprocessed acid catalyzed film is 1.91 nm compared to 2.60 nm for base catalyzed powders.<sup>274</sup> CO<sub>2</sub> processing of an acid catalyzed film is not expected to significantly change the pH of the system; aqueous dispersions of CO<sub>2</sub> is acidic with pH ~ 3.<sup>277</sup> Hence, pore expansion in acid catalyzed systems in the presence of CO<sub>2</sub> is attributed to surfactant solvation by CO<sub>2</sub>. In the case of a base catalyzed system, CO<sub>2</sub> processing may decrease the pH of the system, but the pH is expected to remain well above 3.<sup>278</sup> The CO<sub>2</sub>-based reduction in pH

would compete with the CO<sub>2</sub>-activated expansion of the pores by lowering the aggregation number in the micelles (decreasing the pore diameter).

In addition, CO<sub>2</sub>-activated pore expansion in the acid-catalyzed films occurs during the modifiable steady state (MSS)<sup>274</sup> when the pore structure can still be changed by external forces. The rate of silica condensation is dependent on system pH and is lowest at the isoelectric point of silica (pH ~ 2). Hence, MSS is significantly extended in acidic conditions. However, the base-catalyzed powders experience significant silica condensation prior to CO<sub>2</sub> processing, as demonstrated by the effect of aging time on CO<sub>2</sub> expansion behavior. As discussed above, pH of the base catalyzed system will always be higher than the acid catalyzed films at all CO<sub>2</sub> processing conditions. The increased condensation associated with the higher pH has the effect of restricting pore expansion.

Capturing the kinetically stable structures formed by the pore expansion of templated mesoporous materials has potential for the ex-situ characterization of CO<sub>2</sub> solvation in surfactant aggregates. Understanding and tuning surfactant tail solvation in CO<sub>2</sub> provides insight into the formation CO<sub>2</sub> based microemulsions, emulsions, nanocrystals dispersion, systems which have diverse applications in organic and enzymatic reactions,<sup>51,61</sup> extraction,<sup>249</sup> and the semiconductor industry.<sup>283</sup> However, the effect of pH on self-assembly, in addition to CO<sub>2</sub> solvation, must also be considered.

## 5.5 Conclusions

Mesoporous silica powders with tailored pore sizes were synthesized in a base catalyzed system by combining the favorable solvation of 'CO<sub>2</sub>-philic' fluorinated surfactant tail by CO<sub>2</sub> with the pressure tunable solvent strength of supercritical CO<sub>2</sub>. The long range order of the mesoporous powders was retained after the pore expansion, a significant advantage over some previous investigations using traditional organic solvents for expansion of base catalyzed silica powders. The pore expansion trends in the mesoporous materials can be interpreted from knowledge of CO<sub>2</sub> penetration in surfactants and polymer. However, the important role of pH in self-assembly and sol-gel reaction kinetics is also evident from a comparison of the CO<sub>2</sub> pore expansion behavior of acid-catalyzed thin films and base-catalyzed silica powders.

The demonstration of CO<sub>2</sub> processing of base catalyzed silica powders suggests applications in addition to pore expansion. Sc CO<sub>2</sub> has been used to load and encapsulate drugs into polymers and nanoparticles,<sup>284-286</sup> as well as load small solute molecules in mesoporous silica,<sup>287</sup> while sc CO<sub>2</sub> has also been used in drug delivery applications.<sup>288</sup> The release rate of solutes (e.g., drugs such as ibuprofen) from mesoporous silica can be tailored with pore size.<sup>146</sup> The potential exists to combine CO<sub>2</sub>-based impregnation of mesoporous silica and pore tailoring to control solute release. Alternatively, CO<sub>2</sub> processing may be used to vary the pH to near-neutral conditions during the synthesis of mesoporous silica powders, an approach which may be more amenable to the incorporation of biomolecules,<sup>289</sup> and the adsorption and extraction of metal ions and ionizable species.<sup>290,291</sup>

Copyright © Kaustav Ghosh 2007

## CHAPTER SIX

### SUPERCRITICAL CARBON DIOXIDE SWELLING OF FLUORINATED AND HYDROCARBON SURFACTANT TEMPLATES IN MESOPOROUS SILICA THIN FILMS

#### 6.1 Summary

Differences in the pore expansion behavior of mesoporous silica thin films templated by cationic fluorinated and hydrocarbon surfactants are used to interpret the penetration of CO<sub>2</sub> in straight chain fluorinated and hydrocarbon surfactant micelles. Well-ordered silica thin films are synthesized using cationic surfactants with pyridinium head groups and surfactant tails terminating in an 8-carbon fluorocarbon tail (1, 2 - perfluorohexylethyl pyridinium chloride (HFOPC)), a 16-carbon hydrocarbon tail (cetyl pyridinium bromide (CPB)), and a 16-carbon partially fluorinated tail (1-(11,11,12,12,13,13,14,14,15,15,16,16,16-tridecafluoro-cetyl)-pyridinium bromide (HFCPB)). The high hydrophobicity of the terminal fluorinated segment affects the wetting behavior of solutions of HFOPC and HFCPB dip coating solutions on the hydrophilic glass substrate, resulting in slightly non-uniform thin films. CO<sub>2</sub> processing (69 – 172 bar, 25 °C and 45 °C) immediately after coating of the films results in significant pore expansion for films templated with both fluorinated surfactants. The absolute magnitude of pore expansion is similar for material templated with both HFOPC and HFCPB, which have differing tail length but contains the same number of fluorocarbon groups in their tail. The percentage pore expansion is significantly greater for HFOPC templated silica, which has a higher percentage of fluorocarbon groups compared to HFCPB. Alternatively, pore expansion of the hydrocarbon templated material is negligible at the CO<sub>2</sub> pressures investigated in this study. The significant and preferential penetration of CO<sub>2</sub> in the 'CO<sub>2</sub>-philic' regions of a surfactant tail suggests opportunities to tailor the delivery of CO<sub>2</sub> and solutes dissolved in CO<sub>2</sub> to specific regions of a surfactant aggregates or surfactant templated material.

## 6.2 Introduction

Supercritical (sc) and compressed CO<sub>2</sub> processing has been recently been shown to be useful for tailoring the pore structure of surfactant templated nanoporous silica as a function of CO<sub>2</sub> processing conditions.<sup>75,245,274</sup> The advantageous properties of sc CO<sub>2</sub> for pore tailoring include high diffusivity, a low surface tension, and tunable solvent strength. These properties allow for the rapid CO<sub>2</sub> penetration in the tail of the surfactant templates, negligible pore collapse of the nanometer sized pores during depressurization and control of pore expansion by choice of CO<sub>2</sub> temperature and pressure. Compressed CO<sub>2</sub> is a nontoxic, nonflammable, inexpensive and environmentally friendly alternative to traditional organic solvents. These attractive solvent properties have resulted in the use of CO<sub>2</sub>-based surfactant aggregates (emulsions, microemulsions and dispersions) in a broad range of applications including chemical and enzymatic reactions,<sup>51,61</sup> extraction,<sup>249</sup> nanoparticle syntheses<sup>47,48,250</sup> and microelectronic processing.<sup>53</sup> A limitation of this approach is the ineffective stabilization of water/CO<sub>2</sub> microemulsions<sup>65</sup> or nanocrystal dispersions in CO<sub>2</sub><sup>292</sup> by most hydrocarbon surfactants; the low polarizability of CO<sub>2</sub> leads to weaker solvation of the hydrocarbon tails by CO<sub>2</sub> relative to organic solvents.

Investigations of CO<sub>2</sub>-based self assemblies at low surfactant concentrations (i.e., emulsions, microemulsions and monolayers)<sup>69,70,225,251,293</sup> have resulted in the design of surfactant systems with favorable CO<sub>2</sub> interactions. In contrast to most hydrocarbon-based surfactants,<sup>65</sup> fluorinated surfactants are termed ‘CO<sub>2</sub>-philic’ based on their high solubility in CO<sub>2</sub>.<sup>74,224</sup> ‘CO<sub>2</sub>-philic’ surfactants are characterized by their ability to form water-in-CO<sub>2</sub> microemulsions with significant CO<sub>2</sub> penetration in the fluorinated tails.<sup>64,70,225,226</sup> Compared to analogous hydrocarbon surfactants, the higher hydrophobicity of fluorinated surfactants results in easier self-assembly in water and the large van der Waals radius of fluorine leads to aggregates of lower curvature compared to hydrocarbon surfactants, including novel intermediate mesophases.<sup>113,115,229,294,295</sup> Fluorinated surfactants have been recently used as templates for synthesis of mesoporous silica powders.<sup>31,76,294,296</sup> The advantages of fluorinated surfactant templates have also been explored in mesoporous thin films,<sup>245</sup> where low surface energy and high hydrophobicity present challenges in wetting during coating

CO<sub>2</sub>-based pore expansion of surfactant templated mesoporous silica is hypothesized to occur through the CO<sub>2</sub> solvation of the 'CO<sub>2</sub>-philic' surfactant templates and subsequent capture of the swelling by silica condensation. Hence, pore expansion can potentially be used as an ex-situ technique to study CO<sub>2</sub> penetration in surfactant mesophases. Indeed, pore expansion of hydrocarbon copolymer (Pluronic surfactant, P123) templated mesoporous silica powders was interpreted from CO<sub>2</sub> solvation of P123 liquid crystal and CO<sub>2</sub> solubility in the PPO polymer, as measured by SANS.<sup>75</sup> CO<sub>2</sub> based swelling of fluorinated templates in mesoporous silica films have been correlated with CO<sub>2</sub> penetration in surfactant tails, as interpreted from the interfacial behavior of the surfactants.<sup>245</sup> Similarly, the pore expansion of fluorinated surfactant templated silica powders mirrored the trend of CO<sub>2</sub> swelling observed previously for surfactant tails and polymers, even up to pressures in excess of 340 bar.<sup>297</sup>

The dependence of pore expansion on CO<sub>2</sub> solvation of surfactant templates suggest opportunities to tailor pore expansion by systematically varying template properties from 'CO<sub>2</sub>-philic' to 'non CO<sub>2</sub>-philic'. Molecular simulation have indicated greater CO<sub>2</sub> interaction with fluorocarbon groups (CF<sub>2</sub>) compared to hydrocarbon groups (CH<sub>2</sub>).<sup>298,299</sup> In simulations of both water-in-CO<sub>2</sub> microemulsions<sup>300</sup> and surfactant monolayers at water-CO<sub>2</sub> interfaces,<sup>70</sup> CO<sub>2</sub> solvates the fluorinated tail group throughout the fluorocarbon chain. Fluorinated solvents also demonstrated greater volume expansion by pressurized CO<sub>2</sub> compared to hydrocarbon solvents.<sup>256</sup> The existence of specific interactions between fluorinated groups and CO<sub>2</sub> have been demonstrated using NMR investigations<sup>301</sup> (between C<sub>6</sub>F<sub>14</sub> and CO<sub>2</sub>) and ab-initio studies (C<sub>2</sub>F<sub>6</sub> and CO<sub>2</sub>).<sup>32</sup> However, other NMR (for CHF<sub>3</sub> and CO<sub>2</sub>)<sup>303</sup> and molecular modeling studies (of perfluorinated compounds)<sup>304</sup> have reported contradictory results and suggest no specific interactions between fluorocarbon groups and CO<sub>2</sub>. Recent simulations also suggested similar CO<sub>2</sub> penetration in analogous hydrocarbon and fluorinated surfactants.<sup>234</sup> Few investigations have addressed CO<sub>2</sub> processing in concentrated surfactant mesophases.<sup>75</sup> CO<sub>2</sub>-based pore expansion of fluorinated and hydrocarbon templated silica provides for the experimental comparison of CO<sub>2</sub> solvation of fluorocarbon and hydrocarbon micelles, as captured by the silica structure formed from the concentrated surfactant solutions.



This chapter describes the synthesis of mesoporous silica thin films using three fluorinated and hydrocarbon surfactant templates, HFOPC, HFCPB and CPB (Figure 6.1) and the subsequent processing of these films in gaseous and sc CO<sub>2</sub>. The surfactant

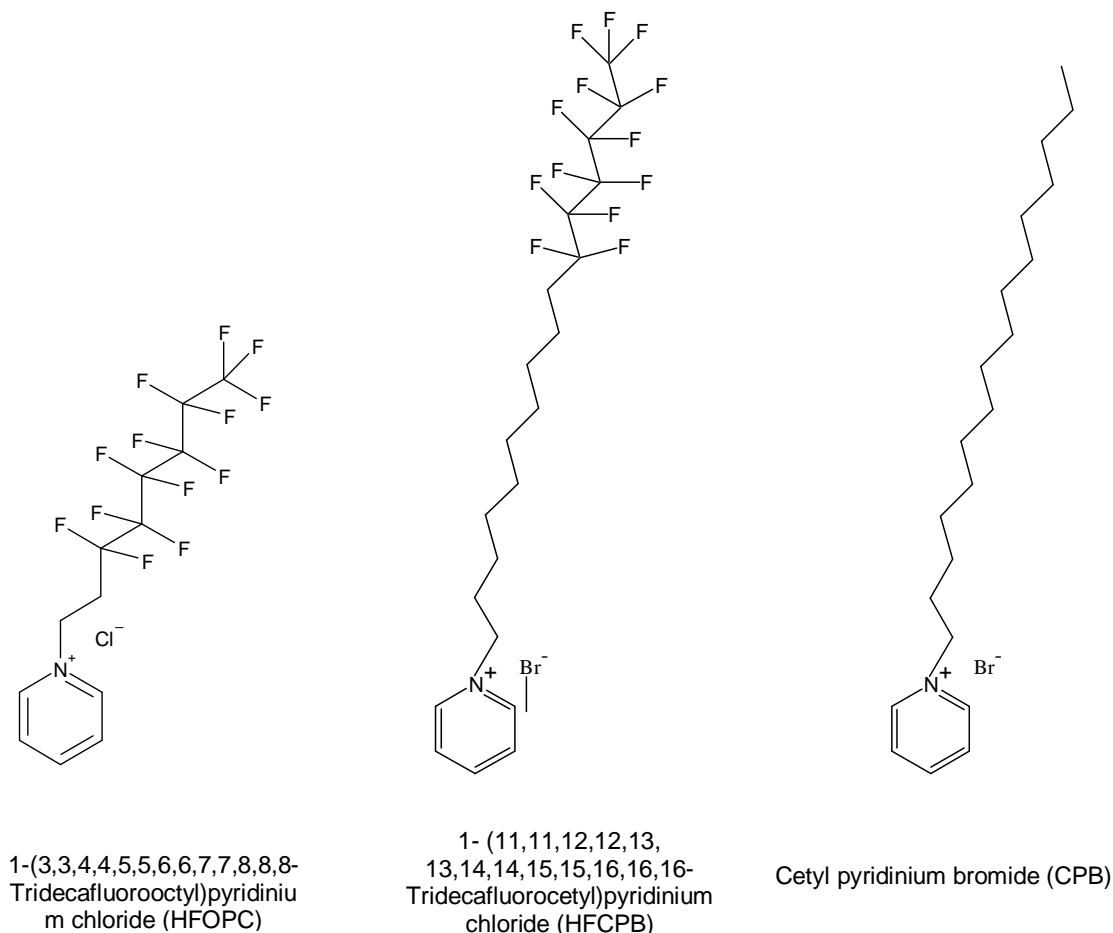


**Figure 6.1.** Schematic of cetyl pyridinium bromide and perfluoroalkylpyridinium halide surfactants

system is designed to provide a comparison of pore expansion behavior based on the hydrocarbon and fluorocarbon segments of the surfactant tail. The relative CO<sub>2</sub> penetration of the hydrocarbon (CH<sub>2</sub>) and fluorocarbon (CF<sub>2</sub>) groups in concentrated surfactant mesophases is investigated by comparing the pore expansion behavior of two surfactants containing a 16 carbon chain length tail: a traditional hydrocarbon surfactant (CPB) and a partially fluorinated surfactant containing both fluorocarbon and hydrocarbon segments (HFCPB; -(CH<sub>2</sub>)<sub>10</sub>(CF<sub>2</sub>)<sub>5</sub>CF<sub>3</sub>) The two fluorinated templates investigated (HFOPC and HFCPB) have the same number of fluorocarbon groups, but

differing number of CH<sub>2</sub> groups. Absolute differences in the pore expansion between these two templates are due to difference in CO<sub>2</sub> uptake by the hydrocarbon (CH<sub>2</sub>) groups. Thin films are obtained for all three templates by dip-coating solutions on glass substrates. For the fluorinated templates, HFOPC and HFCPB, thin films are also successfully coated on low energy fluorinated silane (1H, 1H, 2H, 2H perfluorodecyltrichlorosilane (FDTS)) modified glass substrates. The relative 'CO<sub>2</sub>-philicity' of fluorocarbon and hydrocarbon groups is interpreted from the cohesive energy density and fractional free volume<sup>164</sup> of each surfactant template.

### 6.3 Materials and Methods

**6.3.1 Materials.** The fluorinated surfactants (1, 2 - perfluorohexylethyl pyridinium chloride (HFOPC; C<sub>6</sub>F<sub>13</sub>(CH<sub>2</sub>)<sub>2</sub>NC<sub>5</sub>H<sub>5</sub><sup>+</sup> Cl), and 1-(11,11,12,12,13,13,14,14,15,15,16,16,16-Tridecafluoro-cetyl)-pyridinium bromide (HFCPB; C<sub>6</sub>F<sub>13</sub>(CH<sub>2</sub>)<sub>10</sub>NC<sub>5</sub>H<sub>5</sub><sup>+</sup> Br<sup>-</sup>) were synthesized as described previously.<sup>80,274</sup> The purity of both surfactants were confirmed by mass spectrometry and melting point measurements. Cetyl pyridinium bromide (CPB) was obtained from Aldrich. Tetraethoxysilane (TEOS, purity > 99%) and 1H, 1H, 2H, 2H perfluorodecyltrichlorosilane (FDTS) was purchased from Gelest. Absolute ethyl alcohol purchased from Aaper Alcohol and Chemical Co. (Shelbyville, KY), anhydrous toluene and deionized ultrafiltered water from Fisher Scientific and hydrochloric acid (0.1 N standardized solution) obtained from Alfa Aesar were used for thin film synthesis. Carbon dioxide (Coleman grade, 99.99+%) was purchased from Scott Gross Co. (Lexington, KY). Concentrated aqueous HCl (Fisher Scientific) was used for surfactant extraction.

**6.3.2 Substrate Preparation.** Glass slides were cleaned by immersing them in a NoChromix/sulfuric acid cleaning solution for 1 h and then sequentially rinsed in water, isopropanol and acetone. For fluorinated silane modification of the glass slides, FDTS was added to anhydrous toluene in an atmosphere of nitrogen to achieve a final concentration of 2 wt% FDTS. The clean glass slides were immersed in the solution for 5 min. To complete the surface modification, the silylated substrate was then baked at 120 °C for 2 h.

**6.3.3 Thin Film Synthesis.** Thin porous silica films were synthesized by dip coating on pretreated substrates based on the procedure of Lu et al.<sup>26</sup> Initially, TEOS, ethanol, water and HCl (mole ratio 1: 3.8: 1:  $5 \times 10^{-5}$ ) were refluxed at 65 °C for 90 minutes and a clear solution of partially hydrolyzed silica was formed. The remaining water and HCl were then added in calculated quantities, resulting in a pH of approximately 2 in the final solution, and the mixture was aged at 25 °C for 15 min and then at 50 °C for an additional 15 min. Finally, a solution of the surfactant in ethanol was added to the previously hydrolyzed silica sol under constant stirring. The final mole ratios obtained were 1 TEOS : 12 C<sub>2</sub>H<sub>5</sub>OH : 5 H<sub>2</sub>O : 0.004 HCl :  $x$  surfactant ( $x$  depending on the surfactant). The surfactant mole ratio in the dip-coating solution ( $x$ ) was determined by selecting the mesophase corresponding to the desired pore structure in the surfactant/water phase diagram and equating the surfactant volume fraction in the silica dip coating solution to that in the film after removal of the volatile solvents.<sup>245,257</sup> To obtain a 2D hexagonal mesostructure,  $x$  was calculated to be 0.1 for CPB, 0.14 for HFCPB and 0.2 for HFOPC. The solution was then dip-coated on to the substrates at a withdrawal speed of 6 cm/min.

The thin films were divided into two treatment groups immediately after coating. One treatment group of thin films was pressurized by CO<sub>2</sub> in a 100 ml stainless steel Parr Mini Reactor (rated to 623 K and 207 bar) under controlled temperature and pressure for 48 hours. The effects of CO<sub>2</sub> pressure (69 to 172 bar) and temperature (25 °C or 45 °C) on the final pore structure were observed. The second treatment group of thin films, which was not processed in CO<sub>2</sub>, was dried in an oven at 25 °C or 45 °C for 48 hours. Thus, both treatments of thin films were subject to similar thermal conditions. Both treatment groups were next heated to 150 °C in vacuum (starting at 30 °C and ramping the oven temperature by 5 °C/hr) to ensure condensation of the silica wall. The surfactant was then extracted from the as-synthesized films by washing twice with acidic ethanol (5 ml of concentrated HCl in 45 ml of EtOH).

**6.3.4 Thin Film Characterization.** The thickness and uniformity of each film on glass and FDTs modified glass substrates were estimated using a Dektak 6M Stylus profilometer with a diamond stylus. X-ray diffraction patterns were recorded on a Siemens 5000 diffractometer using Cu K $\alpha$  radiation ( $\lambda = 1.54098 \text{ \AA}$ ) and a graphite

monochromator. Transmission electron microscope (TEM) images were taken with a JEOL 2000FX instrument operating at 200 kV. TEM samples were prepared by scraping the films off the glass substrate and directly depositing them onto a lacey carbon grid. The pore diameters were calculated from the TEM images using ImageJ software, as reported previously.<sup>230,274</sup> Nitrogen sorption measurements were performed on the thin film samples which did not undergo CO<sub>2</sub> processing using a Micromeritics Tristar 3000 system. Samples for nitrogen sorption analysis were prepared by scraping the films off the glass substrate and degassing at 140 °C for 4 hours under flowing nitrogen prior to measurement.

**6.3.5 Contact angle measurement.** Contact angles of CPB- and HFOPC-based silica dip-coating solutions were measured on glass and FDTS modified glass substrates to interpret the wetting behavior of each solution. The contact angles were obtained using a video-based contact angle system (OCA, Future Digital Scientific Co., Bethpage, NY). All experiments were performed in air at temperatures of approximately 23 °C. Sessile drops (1 µL) of each liquid were dispensed and placed on the solid substrates. An image of the drop was taken immediately after placing the drop on the substrate; contact angles on both left and right sides were measured to obtain the initial contact angle. The contact angle measurement was repeated at 10 different areas on each substrate and an average value is reported. The spreading of the drops was also observed and the time for complete spreading was recorded. If a drop did not spread completely after 240 seconds, the solvent was identified to be unsuitable for complete spreading on that particular substrate.

## **6.4 Results and Discussion**

### **6.4.1 Synthesis of Uniform Silica Thin Films by Fluorinated and Hydrocarbon Templates.**

The swelling of fluorinated surfactant templates by CO<sub>2</sub> has the potential to alter both the pore structure (i.e., hexagonal, cubic, intermediate, slit-shaped) and pore size of thin silica films. Our research team has synthesized fluorinated surfactant templated porous silica powders with a broad range of structures including hexagonal,<sup>31</sup> novel

‘intermediate’ mesh phase structures<sup>31</sup> and novel fluoro-functionalized silica for application in chromatography columns and gas adsorbents<sup>77</sup> The synthesis of 2D hexagonally ordered silica thin films using a series of perfluoroalkyl pyridinium chloride surfactants (including HFOPC) as templates has also been demonstrated.<sup>274</sup>

In the synthesis of dip-coated films, the difference in hydrophobic nature between fluorinated and hydrocarbon templates has the potential to cause variation in film uniformity as a function of template. Uniform thin films have been coated on glass substrates from solutions of silica precursor, hydrocarbon surfactant and a good wetting agent like ethanol.<sup>26</sup> However, the greater hydrophobicity of fluorinated surfactants has been observed to cause lower surfactant adsorption on glass substrates during dip coating, resulting in partial dewetting. Indeed, uniform spreading of fluoropolymers and fluorinated solvents or strong adhesion of fluoropolymer film on hydrophilic glass substrates is not possible.<sup>305,306</sup> A competing property which may enhance thin film uniformity and quality is the very low surface tension of the fluorinated surfactant based coating solution, which is associated with decreased liquid hold-up on the film edges and lower capillary pressure and may prevent the collapse of materials during solvent evaporation.<sup>307,308</sup> The low surface tension of fluorinated solutions also makes them suitable in coating low energy substrates, as demonstrated by fluoropolymer coatings in optical<sup>309</sup> and lubrication applications.<sup>310</sup>

The uniformity of silica thin films templated from fluorinated surfactant solutions are interpreted from the wetting properties of the coating solution as a function of substrate hydrophobicity. Contact angle measurements for CPB and HFOPC based solutions on different substrates are summarized in Table 6.1. The low surface tension of ethanol and the strong adsorption of CPB on glass result in complete wetting of the hydrocarbon surfactant CPB based solution on the unmodified glass substrate. In contrast, the initial contact angle is 20° for the HFOPC based solution on glass substrate, due to slower adsorption of the more hydrophobic fluorinated surfactant, but complete wetting is achieved in about 20 s. During dip coating, the contact angle is reduced relative to that obtained from sessile drops on substrates.<sup>311,312</sup> An optimized dip coating speed balances the need for a low contact angle to entrain the film on the substrate (enhanced by increasing the speed) and sufficient time to allow for the spreading of the

solution on the substrate (as suggested by the finite time (~ 20 s) required by the sessile drop to completely spread on glass substrate). An optimized coating speed of 6 cm/min

**Table 6.1:** Average contact angle measurements of CPB and HFOPC based solutions on glass and FDTS modified substrate

Substrate	Surfactant Template Solution	Initial Contact Angle <sup>a</sup>	Spreading time <sup>a</sup>
Glass	CPB	Complete spreading	-
	HFOPC	20° (0.024)	20 s (0.031)
FDTS modified glass	CPB	70° (0.025)	No spreading
	HFOPC	60° (0.027)	30 s (0.033)

<sup>a</sup> Values in the parenthesis are standard deviations of contact angle and spreading times obtained from ten different drops on various regions of the same substrate.

results in fluorinated surfactant (HFOPC) templated films with very slight non-uniformity, as indicated by the presence of small droplets in a few regions in the film. The formation of such droplets and loss of uniformity has been observed previously and is associated with the dewetting of apolar liquid films (e.g., polystyrene) on silicon<sup>313,314</sup> or coating sol-gel silica films using a hydrophobic surfactant template, SPAN 20, as compared to a more hydrophilic template, TWEEN 20.<sup>315</sup>

On FDTS modified glass substrate, the HFOPC based silica solution forms an initial contact angle of 60°, consistent with the extremely low energy of the surface. However, the favorable interaction of the fluorinated surfactants with the fluorocarbon backbone of the silane facilitates complete spreading in about 30 s. The ability of the solution to completely spread on FDTS modified substrate within a brief period of time (< 30 s) translates to the synthesis of dip-coated HFOPC templated thin films with slight non-uniformity on a chemically similar substrate. For CPB solution, the initial contact angle on FDTS modified substrate is 70°, similar to HFOPC solution on the same substrate. However, CPB is not fluorophilic and demonstrates no specific favorable interactions with the fluorinated groups of FDTS. Also, the higher surface tension of CPB compared to HFOPC results in a lesser CPB adsorption at the sol-substrate interface.

Hence, complete spreading of CPB solution is never achieved on the FDTS modified substrates and leads to the inability in coating CPB templated thin films on FDTS modified substrates.

CPB templated films dip coated on glass substrate are uniform with a thickness around 200 nm ( $\pm 20$  nm) for the coating speed of 6 cm/m used in this study. However, at the substrate edges, the thickness for the CPB templated film increases to about 1000 nm ( $\pm 20$  nm) because of high liquid hold up on edges. On a similar glass substrate, thickness HFOPC templated film is about 150 nm ( $\pm 20$  nm) at coating speed of 6 cm/m. The edge thickness is only about 300 nm ( $\pm 20$  nm) and is much smaller than that for CPB films due to the fact that the lower surface tension of HFOPC solution decreases liquid hold up on edges and makes the film thickness more uniform throughout. The thickness and uniformity of films dip-coated with the fluorinated/hydrocarbon segmented template, HFCPB, are very similar to films templated with HFOPC. The similarity in coating indicates that the wetting property of the surfactant solutions is governed by the terminal fluorocarbon groups.

The pore structure of the mesoporous silica thin films synthesized with all three templates (HFOPC, HFCPB, CPB) without CO<sub>2</sub> processing is confirmed to be a well ordered 2D hexagonal structure from XRD plots (Figure 6.2) and TEM images (Figure 6.3). The XRD patterns for HFCPB templated thin film (Fig. 6.2a) and CPB templated

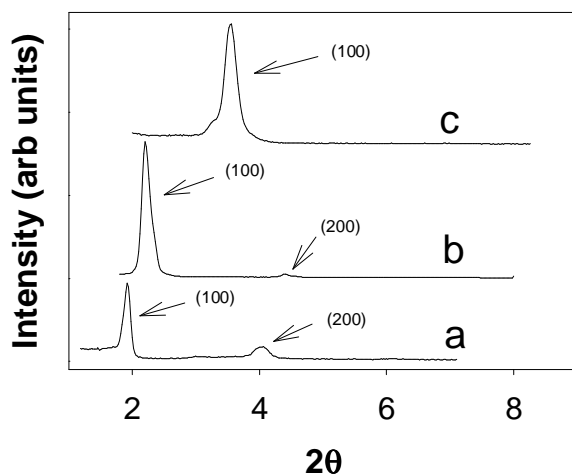


**Figure 6. 2.** XRD patterns of thin films prepared without CO<sub>2</sub> processing templated with (a) HFCPC (b) HFOPC and (c) CPB

films (Fig. 6.2b) after surfactant extraction show the presence of two peaks that can be indexed to the (100) and the (200) reflection of hexagonally ordered structure with parallel orientation of the cylindrical channels.<sup>145</sup> The presence of (100) and (200) peaks can also be indicative of lamellar ordering; however for the porous materials a lamellar structure would have been destroyed after surfactant removal. Representative TEM images of HFCPB templated film (Fig. 6.3a) and CPB templated film (Fig 6.3b) showing cross-sectional views of the hexagonal channels confirm the presence of well-ordered 2D hexagonal structure. The presence of one sharp peak in the XRD plot of HFOPC templated thin film (Fig. 6.2c) indicates an ordered porous materials, This structure is determined to be 2D hexagonal from TEM images of the HFOPC templated film (Fig. 6.3c).

The orientation and order are similar for films templated with both 16-carbon chain length surfactants (the fluorinated/hydrocarbon segmented HFCPB and the hydrocarbon CPB). However, the d-spacing of the HFCPB templated film (4.6 nm) is considerably larger than that of the CPB templated film (4.1 nm). The d-spacing value is dominated by a combination of the template micelle size and the thickness of the silica walls ( $t$ ). The wall thickness ( $t$ ) is calculated from the values of d-spacing ( $d$ ) and pore diameter ( $p$ , Table 1) by using  $t = (2/\sqrt{3}) * d - p$ . Films templated by both the hydrocarbon surfactant, CPB and the fluorinated/hydrocarbon segmented surfactant, HFCPB have a similar silica wall thickness ( $\sim 1.1$  nm) before CO<sub>2</sub> processing. However, the larger van der Waals radius of fluorine compared to hydrogen results in the cylindrical fluorinated micelle having a larger diameter than a hydrocarbon micelle, even when both tails have same number of carbon atoms,<sup>115</sup> which results in the greater d-spacing value for the HFCPB templated film compared to the CPB templated film. The d-spacing for films templated with the shorter chain fluorinated surfactant, HFOPC, is significantly less (2.48 nm) than that of HFCPB and CPB. The d-spacing for mesoporous silica synthesized in an acid-catalyzed medium is not significantly dependent on variation of template counterion from Br<sup>-</sup> to Cl<sup>-</sup> as demonstrated in a previous study for two hydrocarbon templates, cetyl pyridinium chloride (CPC) and CPB.<sup>316</sup> Hence, the decreased d-spacing of HFOPC templated film compared to HFCPB and CPB is mainly due to the presence of



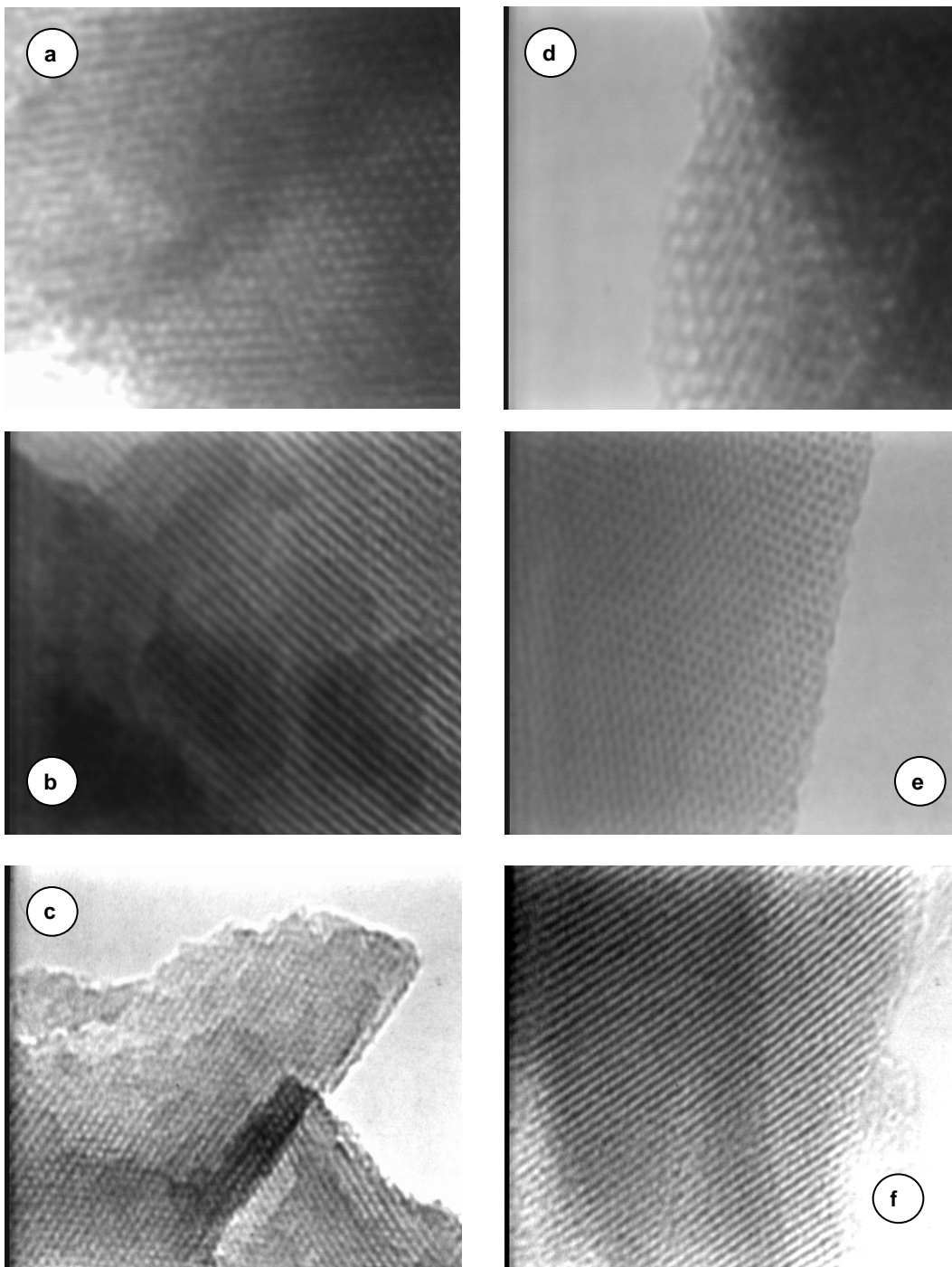


**Figure 6.3.** TEM micrographs of thin films templated with (a) HFCPC, (b) CPB and (c) HFOPC and (d) HFCPC and processed in CO<sub>2</sub> at 172 bar and 45°C, (e) CPB and processed in CO<sub>2</sub> at 172 bar and 45°C and (f) HFOPC and processed in CO<sub>2</sub> at 172 bar and 45°C

only 8 carbon atoms in the HFOPC tail compared to 16 carbons in both HFCPB and CPB.

The pore diameter for films calculated directly from the TEM images using ImageJ software,<sup>230</sup> is estimated to be 4.23 nm ( $\pm$  0.25 nm) for HFCPBC templated film, 1.91 nm ( $\pm$  0.22 nm) for HFOPC templated film, and 3.64 nm ( $\pm$  0.13 nm) for CPB templated film. The pore diameters obtained from TEM images are verified using nitrogen sorption measurements for the films not processed in CO<sub>2</sub>. The resulting pore diameters (4.28 nm for HFCPB templated film, 1.91 nm for HFOPC templated film, and 3.70 nm for CPB) compare favorably with the direct measurements from TEM images. The pore size, which is also dictated by the size of the surfactant micelle, follows the d-spacing trends.

Similar ordering and orientation are also observed for films templated with terminal surfactants with fluorinated segments ((HFOPC and HFCPC) that were coated on the fluorocarbon-modified glass substrate. This is consistent with simulation studies, which have demonstrated that the orientation and ordering of hydrocarbon templated silica films is preserved when the substrates are changed from hydrophilic glass to a complete hydrophobic hydrocarbon silane modified surface.<sup>317</sup> For the hydrophilic glass substrate, the –OH groups of the substrate interact strongly with surfactant headgroup, aligning the channels parallel to the substrate. At the surface of a hydrophobic substrate, the hydrophobic functionalities interact preferentially with the hydrophobic tail of the surfactant to form a monolayer, also resulting in parallel orientation of the channels. The synthesis of hydrocarbon copolymer (P123) templated silica films has been investigated on both glass substrates and hydrocarbon silane modified substrates.<sup>29</sup> For both substrates, synthesized films demonstrated similar 2D hexagonal structure with parallel orientation of porous channels.

#### **6.4.2 Effects of CO<sub>2</sub> Processing on Thin Film Structure**

CO<sub>2</sub> based pore expansion of surfactant templated materials has previously been demonstrated to occur via CO<sub>2</sub> uptake in the template tails to increase the radius of the self-assembled micelles.<sup>75,297</sup> Silica condensation captures this change in self-assembly and subsequent characterization of mesoporous structure after CO<sub>2</sub> processing can be directly correlated to degree of CO<sub>2</sub> solvation of surfactant tail. The series of surfactant

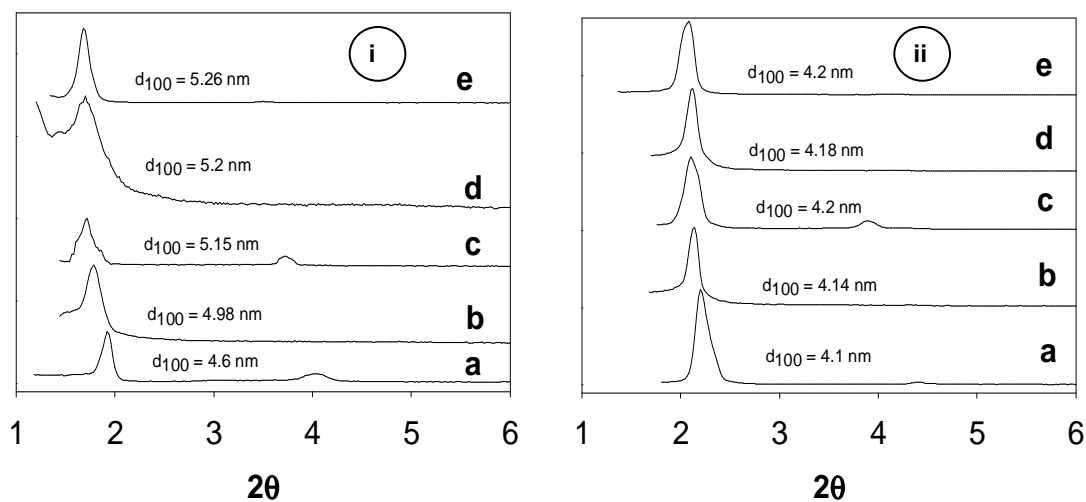


**Figure 4.** XRD spectra of thin films templated with (i) HFCPB and (ii) CPB and (a) not processed in CO<sub>2</sub>, (b) processed in CO<sub>2</sub> at 69 bar and 45 °C, (c) processed in CO<sub>2</sub> at 103 bar and 45 °C, (d) processed in CO<sub>2</sub> at 137 bar and 45 °C, and (e) processed in CO<sub>2</sub> at 172 bar and 45 °C.

templates (HFOPC, HFCPB, and CPB) allows for the systematic study of the solvation of hydrocarbon and fluorocarbon segments in concentrated surfactant mesophases by CO<sub>2</sub> and the localization of CO<sub>2</sub> in these templates.

The swelling of CO<sub>2</sub>-philic surfactant segments as a function of CO<sub>2</sub> processing can be directly related to differences in the pore expansion behavior of films templated with the 16 carbon chain length surfactants, the partially fluorinated HFCPB and its hydrocarbon analogue, CPB. XRD plots of the HFCPB and CPB templated films after surfactant extraction are used to directly measure increases in d-spacing as a function of CO<sub>2</sub> processing conditions. For both templates and at all conditions of CO<sub>2</sub> processing, XRD plots show the presence of at least one sharp peak corresponding to the (100) reflection, indicating that the hexagonal ordering of the films is preserved. A significant increase in d-spacing is observed for films templated with the fluorinated surfactant, HFCPB (Fig. 6.4a) at all conditions of CO<sub>2</sub> processing compared to unprocessed film. The maximum value of d-spacing obtained was 5.26 nm for CO<sub>2</sub> processing at 172 bar and 45°C and represented a 14.3 % expansion compared to the d-spacing of the

unprocessed film (4.6 nm). In contrast, thin films templated with the hydrocarbon analogue, CPB, did not show any significant increase in d-spacing at any CO<sub>2</sub> processing conditions (Fig. 6.4b). The d-spacing varied between 4.1 nm for unprocessed film to only 4.2 nm to film processed in CO<sub>2</sub> at 172 bar and 45°C (2.4% expansion). However, the change in d-spacing values was random as a function of CO<sub>2</sub> pressure and probably reflects experimental error rather than demonstrating any CO<sub>2</sub> based solvation of CPB template.

TEM images confirm the long range order after CO<sub>2</sub> processing for thin films templated with all three surfactants (representative images in Fig. 6.3). The pore diameters measured directly from TEM images at all conditions of CO<sub>2</sub> processing are presented in Table 6.2 and are also used to calculate the percentage pore expansion for films templated with all three surfactants as a function of CO<sub>2</sub> density (Fig. 6.5). At a constant temperature, density rather than pressure is the more physically relevant variable to describe CO<sub>2</sub> solvent strength. For films templated with the surfactant containing fluorinated/hydrocarbon segments, HFCPB, the pore diameter increases as much as 23% at the highest CO<sub>2</sub> density investigated ( $\rho_{\text{CO}_2} = 0.8 \text{ g/ml}$ ). Alternatively, films templated with the corresponding hydrocarbon surfactant, CPB demonstrate insignificant change in pore size for CO<sub>2</sub> densities up to 0.8 g/ml (Fig. 6.5); the absolute pore size varied from 3.64 nm to 3.76 nm (Table 6.2). The small variation is within the experimental error of estimating pore diameter from TEM images (Table 6.1) and suggests negligible CO<sub>2</sub> solvation of the hydrocarbon (CH<sub>2</sub>) groups in concentrated surfactant mesophases. In contrast, the significant increase in d-spacing (Fig. 6.4a) and the pore diameter (from 4.23 nm to 5.21 nm, Table 6.2) of films templated with the HFCPB provides evidence for CO<sub>2</sub> solvation of the fluorocarbon (CF<sub>2</sub>) groups compared to CH<sub>2</sub> groups in surfactant systems at low concentrations. For example, an ionic fluorinated surfactant (perfluoropolyether) was shown to be completely miscible with CO<sub>2</sub><sup>318</sup> whereas the solubility of a corresponding hydrocarbon poly(propylene) oxide was only 0.5 wt% at pressure up to 207 bar.<sup>319</sup>

The ability of CO<sub>2</sub> to selectively solvate 'CO<sub>2</sub>-philic' regions in surfactant mesophases is investigated by comparing pore expansion between films templated with a

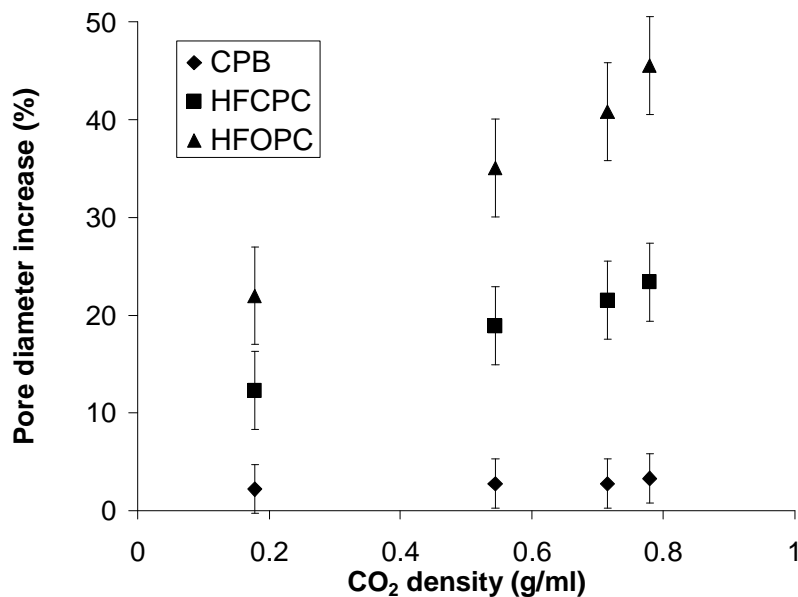


**Figure 6.5.** Percentage increase of pore diameter of thin films templated with all three surfactants as a function of CO<sub>2</sub> processing density

fluorinated surfactant, HFOPC (- (CH<sub>2</sub>)<sub>2</sub>(CF<sub>2</sub>)<sub>5</sub>CF<sub>3</sub>) and a surfactant with fluorocarbon/hydrocarbon segments, HFCPC (- (CH<sub>2</sub>)<sub>10</sub>(CF<sub>2</sub>)<sub>5</sub>CF<sub>3</sub>) containing different percentages of ‘CO<sub>2</sub>-philic’ fluorocarbon segments. The two surfactants have the same number of fluorocarbon groups, but differing number of hydrocarbon groups. Therefore difference in the absolute value of the pore expansion are related to CO<sub>2</sub> solvation of hydrocarbon (CH<sub>2</sub>) groups.

The pore diameter for films templated with the shorter fluorinated surfactant, HFOPC (8 chain length) increases from 1.91 nm for the unprocessed sample to 2.78 nm for CO<sub>2</sub> processed films at 172 bar and 45 °C. At similar conditions, the pore diameter for the film templated with the longer fluorinated surfactant, HFCPC (16 chain length) is much larger and increases from 4.23 nm to 5.21 nm for CO<sub>2</sub> processing at 172 bar and 45°C. However, the absolute magnitude of pore expansion is quite similar at the same CO<sub>2</sub> conditions (within 0.1 nm, Table 6.2) for films templated with both templates. The similar magnitude of pore expansion provides further evidence for negligible CO<sub>2</sub> solvation of the hydrocarbon (CH<sub>2</sub>) groups. The greater number of hydrocarbon groups in HFCPB do not result in a significant increase in pore diameter compared to HFOPC.

**Table 6.2:** Summary of pore diameter and absolute magnitude of pore expansion for thin film templated with all three surfactants as a function of CO<sub>2</sub> density

CO <sub>2</sub> -processing conditions	Density of CO <sub>2</sub> (g/ml) <sup>73</sup>	HFOPC film		HFCPC film		CPB film	
		Pore diameter <sup>a</sup> (nm)	Absolute increase (nm)	Pore diameter <sup>a</sup> (nm)	Absolute increase (nm)	Pore diameter <sup>a</sup> (nm)	Absolute increase (nm)
Unprocessed (45°C)	-	1.91 (0.092)		4.23 (0.084)		3.64 (0.064)	
Unprocessed (25°C)	-	1.90 (0.088)		4.24 (0.092)		3.64 (0.060)	
69 bar and 45°C (gas)	0.178	2.33 (0.086)	0.42	4.75 (0.086)	0.52	3.72 (0.066)	0.08
103 bar and 45°C (sc)	0.544	2.58 (0.098)	0.67	5.01 (0.088)	0.78	3.74 (0.068)	0.1
137 bar and 45°C (sc)	0.715	2.69 (0.094)	0.78	5.12 (0.090)	0.89	3.74 (0.064)	0.1
172 bar and 45°C (sc)	0.779	2.78 (0.090)	0.87	5.21 (0.092)	0.98	3.76 (0.062)	0.12
172 bar and 25°C (liq)	0.894	2.76 (0.094)	0.85	5.19 (0.096)	0.96	3.75 (0.068)	0.11

<sup>a</sup> Values in the parenthesis are standard deviations of pore diameters obtained from ten different TEM images of the same sample.

Favorable CO<sub>2</sub> swelling occurs primarily in the ‘CO<sub>2</sub>-philic’ fluorocarbon (CF<sub>2</sub>) groups of the surfactant tail, leading to similar swelling behavior in the HFOPC and HFCPB templated materials, which have an identical number of fluorocarbon groups in their surfactant tails.

The d-spacing for films templated with the fluorinated surfactant, HFOPC, increase by 23%, from 2.48 nm for the unprocessed film to 3.06 for CO<sub>2</sub> processing at 172 bar and 45°C (results not shown). At similar CO<sub>2</sub> processing conditions, HFCPB templated films undergo a much lesser percentage increase in d-spacing of 14.3%, (Fig. 4(i), from 4.6 nm for the unprocessed film to about 5.26 nm). Similar to increase in d-spacing, the percentage of pore expansion is greater for HFOPC templated film compared to HFCPB templated film at all CO<sub>2</sub> conditions. The largest increase in pore diameter observed for HFOPC templated film is 45.5 % for CO<sub>2</sub> processing at 172 bar and 45°C,

compared to 23.1 % expansion for HFCPB templated films at these conditions. The greatest percentage increase in pore diameter with increasing CO<sub>2</sub> density occurs at low densities ( $\rho_{\text{CO}_2} < 0.2$  g/ml) for both of the fluorinated surfactant templated thin films (Fig. 6.5). The pore size continues to increase with CO<sub>2</sub> density at the higher densities investigated ( $\rho_{\text{CO}_2}$  upto 0.8 g/ml); however the magnitude of increase is smaller than that observed at initial densities. The greater pore expansion for the template with the larger percentage of fluorocarbon segments demonstrates preferential CO<sub>2</sub> solvation of ‘CO<sub>2</sub>-philic’ segments in the mesophases.

Molecular characteristics of a ‘CO<sub>2</sub>-phile’ have been demonstrated to be a low cohesive energy density and flexible geometry with a high free volume.<sup>74</sup> The trends of ‘CO<sub>2</sub>-philicity’ between the three surfactants investigated in this study as measured from pore expansion is interpreted from molecular geometry arguments. The CO<sub>2</sub>-philicity was quantified using the free fractional volume (FFV) paradigm,<sup>164</sup> which is a geometric parameter calculated directly from the surfactant tail geometry and surface coverage of headgroup. FFV is defined as

$$\text{FFV} = 1 - \frac{V_t}{tA_h}$$

where  $V_t$  is van der Waals volume of surfactant tail,  $t$  is the length of the tail in the optimum gas phase configuration.  $A_h$ , the interfacial area per headgroup, is assumed to be a constant, 100 Å<sup>2</sup>, consistent with most measured headgroup areas in CO<sub>2</sub>.<sup>164</sup> Further,  $A_h$  is expected to be similar for all three surfactants investigated in this study (HFCPB, HFOPC, CPB) and considering a constant value of  $A_h$  will not greatly affect the trend of their relative FFV values.  $t$  for each surfactant molecule was calculated from their optimum configuration using SPARTAN.<sup>260</sup> The surfactant molecule was first created in an all trans configuration in SPARTAN. Molecular mechanics energy minimization was performed on the molecule by using the classical MMFF94 force field to obtain the optimum configuration. Finally,  $t$  was measured as the distance between the pyridinium nitrogen atom and the last atom in the surfactant tail and van der Waals volume was directly reported by SPARTAN. For surfactants having a similar headgroup, a lower FFV indicates the potential to form a more stable water/CO<sub>2</sub> aggregate and greater tail solvation by CO<sub>2</sub>.<sup>164</sup> The FFV values for the three surfactants in our study decreased from

CPB (0.79 ) to HFCPC (0.76) and finally to HFOPC (0.67), consistent with increasing 'CO<sub>2</sub>-philic' trend from CPB to HFCPC to HFOPC as determined through pore expansion studies.

Recently, the diversity of 'CO<sub>2</sub>-philic' surfactants has greatly increased beyond fluorinated molecules to include various hydrocarbon surfactants that demonstrates the geometrical properties and molecular interactions discussed above for 'CO<sub>2</sub>-philes'. Stubby methylated branched surfactants have stabilized water-in-CO<sub>2</sub> emulsions and microemulsions and also dispersed silver nanoparticles in CO<sub>2</sub>.<sup>163,165,166,169</sup> Bulky trisiloxane surfactants<sup>168</sup> and small oxygenated hydrocarbon surfactants have also been established as 'CO<sub>2</sub>-philes'.<sup>73</sup> The ability of compressed CO<sub>2</sub> to selectively solvate 'CO<sub>2</sub>-philic' regions of mesophases towards tailoring surfactant templated materials can be potentially extended to include templates containing novel 'CO<sub>2</sub>-philic' groups in specific regions to synthesize materials with tailored pore size, shape and structure and extend the general applicability of CO<sub>2</sub> processing to include a large number of template systems. Additionally, the potential also exists of using CO<sub>2</sub> towards specific delivery of molecules to the novel 'CO<sub>2</sub>-philic' regions in templated materials for synthesis of new functionalized materials.

## 6.5 Conclusions

Ex-situ characterization of pore expansion due to CO<sub>2</sub> processing of surfactant templated mesoporous silica thin films have been used to compare CO<sub>2</sub> solvation of different functional groups (CF<sub>2</sub> and CH<sub>2</sub>). Pore expansion is insignificant for films templated with the hydrocarbon surfactant, CPB, at 45°C and CO<sub>2</sub> pressures up to 172 bar. In contrast, silica thin films templated with HFCPC, a partially fluorinated analogue of CPB containing six fluorocarbon groups. demonstrate significant pore expansion, consistent with significant CO<sub>2</sub> solvation of CF<sub>2</sub> groups in concentrated surfactant systems compared to CH<sub>2</sub> groups. A comparison of the the pore expansion behavior of thin films templated with two fluorinated surfactants reveals an increasing extent of pore expansion with an increasing percentage of 'CO<sub>2</sub>-philic' fluorocarbon groups in the surfactant tail. These results indicate the preferential solvation by CO<sub>2</sub> of 'CO<sub>2</sub>-philic' groups in templates containing both 'CO<sub>2</sub>-philic' and 'non CO<sub>2</sub>-philic' groups. Designing



templates with specific regions of 'CO<sub>2</sub>-philic' groups may be used to tailor pore structure and surfactant mesophases, and potentially deliver CO<sub>2</sub>-soluble substrates to specific regions of a mesostructure..

In addition, the very low surface tension of the fluorinated surfactant coating solution resulted in synthesis of mesoporous silica thin films even on low energy fluorinated silane modified glass substrate. The lower surface tension of the fluorinated surfactant-silica solution also resulted in significantly less liquid hold-up on the edges during formation of the dip-coated film. This suggests the applicability of fluorinated based silica solution in forming coating on porous or high aspect ratio structures or surfaces with small features or patterns such as microelectromechanical systems (MEMS) devices.<sup>320</sup>

Copyright © Kaustav Ghosh 2007

## CHAPTER SEVEN

### IN-SITU FLUORESCENCE SPECTROSCOPY OF SUPERCRITICAL CARBON DIOXIDE PROCESSING OF SURFACTANT TEMPLATED NANO-STRUCTURED SILICA FILMS

#### 7.1 Summary

The local environment and dynamics of compressed carbon dioxide (CO<sub>2</sub>) penetration during surfactant templated silica film synthesis is interpreted from the in-situ fluorescence emission spectra of pyrene (Py) and a modified pyrene probe. Pyrene emission in cetyl trimethyl ammonium bromide (CTAB) and cetyl pyridinium bromide (CPB) templated silica films is monitored immediately after casting and during processing with gaseous and supercritical (sc) CO<sub>2</sub> (17 – 172 bar, 45°C). The solvatochromic emission spectra of pyrene in CTAB templated films suggest CO<sub>2</sub> penetration in both the micelle interface and its interior. An anchored derivative of pyrene, 1- pyrenehexadecanoic acid (C<sub>16</sub>-pyr) (pyrene-(CH<sub>2</sub>)<sub>15</sub>COOH), is established for probing CPB films, where the pyrene moiety is preferentially oriented toward the interior of the micelle, limiting quenching by the pyridine headgroup of CPB. CO<sub>2</sub> penetration occurs in the interior of CPB micelles, as measured from the degree of fluorescence quenching as a function of CO<sub>2</sub> processing conditions. The fluorescence quenching behavior of derivitized pyrene also indicates continuous probe mobility in CPB films and demonstrates an increase in the timescale for silica condensation due to CO<sub>2</sub> processing. The mobility of C<sub>16</sub>-pyr increases with pressure from gaseous to sc CO<sub>2</sub> processing and is greater than 5 h for sc CO<sub>2</sub> processing at 172 bar and 45°C compared to about 25 m for the unprocessed film. The delivery of CO<sub>2</sub> and CO<sub>2</sub> soluble solutes in CTAB templated films is followed through nonradiative energy transfer (NRET) measurements and suggests the potential to engineer the pore functionality and deliver drug and reactant molecules with CO<sub>2</sub> processing.

#### 7.2 Introduction

The synthesis of mesoporous silica occurs through a co-assembly process with the surfactant molecules forming ordered templates and the hydrolyzed silica precursor associating with the surfactant head group to form the solid silica network.<sup>24</sup> Subsequent

removal of the surfactant results in ordered mesoporous materials with the mesostructure replicating the surfactant mesophase. Tailoring the pore structure of surfactant templated materials has been demonstrated to increase the application of such materials.<sup>146-148</sup> Traditional methods of achieving pore expansion in surfactant templated silica has involved the addition of large hydrocarbon solvents (e.g polypropylene oxide, dodecane, mesitylene, etc.) to the surfactant/silica precursor solution directly during the synthesis of porous silica to achieve pore expansion through swelling of the micelle core.<sup>37-40,243</sup>

Supercritical (sc) and compressed CO<sub>2</sub> processing has been recently demonstrated as for the synthesis of tailored mesoporous silica through controlled CO<sub>2</sub> based swelling of the surfactant templates.<sup>75,245,274</sup> Sc CO<sub>2</sub> is an attractive alternative pore tailoring agent due to its tunable solvent strength, high diffusivity and low surface tension, which enables diffusion through the nanometer sized pores while preserving the long range structure. Compressed CO<sub>2</sub> was successfully used to solvate 'CO<sub>2</sub>-philic' fluorinated templates (perfluoroalkyl pyridinium chloride surfactants with 8-10 fluorinated carbon atoms in the surfactant tail).<sup>274</sup> Pore expansion of up to 80% in the fluorinated surfactant templated silica thin films were achieved at processing conditions of 172 bar and 45°C.<sup>274</sup> In contrast, CO<sub>2</sub> pressures of 482 bar resulted in 54% pore expansion for a much longer hydrocarbon copolymer template (P123 with 69 propylene oxide (PPO) groups in its tail) through CO<sub>2</sub> uptake in the PPO core.<sup>75</sup> Negligible pore expansion was achieved for two other hydrocarbon surfactant templates, CTAB<sup>75</sup> and CPB for processing pressures up to 172 bar as demonstrated in Chapter 6. In Chapter 6, we also demonstrated the ability of CO<sub>2</sub> to selectively solvate 'CO<sub>2</sub>-philic' regions of the mesophase compared to 'non CO<sub>2</sub>-philic' areas.

CO<sub>2</sub> based alteration of pore structure of fluorinated surfactant templated dip-coated silica films has been demonstrated to occur during the modulable steady state (MSS) of the film.<sup>274</sup> During this period, which begins a few seconds after sol coating, silica condensation is in progress but is not sufficient to have formed a highly rigid network.<sup>134</sup> MSS is an important stage in the synthesis of dip-coated films because the flexible silica network allows the final structure to be modified through the application of external forces.<sup>29,134,141,321</sup> Knowledge of the dynamics of CO<sub>2</sub> penetration in the surfactant templated materials and the timescales of silica condensation during CO<sub>2</sub> processing can

potentially be used to optimize pore engineering and functionalization during the extended MSS period.

The mechanism of penetration and localization of traditional hydrocarbon swelling agents in surfactant templated silica has been extensively investigated experimentally<sup>37,40,153</sup> and also described based on the free energy of mixing.<sup>154</sup> Long chain alkanes (> C8) form an inner core, resulting in an increase in pore diameter, while shorter alkanes and aromatic hydrocarbons localize directly in tail with no change in micelle size.<sup>40,153</sup> Alternatively, CO<sub>2</sub> processing of surfactant mesophases is not well studied, and have been mostly limited to small angle neutron scattering (SANS).<sup>75</sup> In contrast, the CO<sub>2</sub> penetration of dilute surfactant aggregates (i.e., CO<sub>2</sub>-continuous microemulsions and emulsions) has been investigated more extensively<sup>154,157-159</sup> due to their potential application in enzymatic reactions,<sup>61,159</sup> extraction,<sup>51</sup> solubilizing metal nanoparticles,<sup>47,48,249</sup> metal ions<sup>322</sup> and proteins<sup>323</sup> and 'green' applications of carbon dioxide technology.<sup>251</sup>

The in situ probing of local environment (i.e., through fluorescent spectroscopy probes) may provide additional insight into the localization and dynamics of CO<sub>2</sub> penetration in surfactant aggregates and mesostructures. Previously, fluorescence spectroscopy have been used to investigate the synthesis mechanism of surfactant templated mesoporous ceramics, the change in micelle polarity with addition of additives during the synthesis, the mobility of various probes in sol-gel silica film from microviscosity estimations and demonstrate probe accessibility in three regions of a sol-gel mesostructured silica film namely the silica framework, the micelle core and the micelle interface.<sup>206,324-330</sup> The solvatochromic behavior of pyrene, in particular, has been used in-situ to follow the evolution of the final mesostructure through the formation of intermediates and also the interactions between surfactants and silica precursors. Pyrene<sup>209</sup> and other spectroscopic probe molecules,<sup>154,215,277</sup> have also been incorporated in CO<sub>2</sub>-continuous solutions of surfactant aggregates and CO<sub>2</sub>-swollen micelles as measures of the polarity of their microenvironment.

In extending the use of high pressure fluorescence spectroscopy to the investigation of the effect of CO<sub>2</sub> processing on the mesostructure of templated silica, the constrained thickness of silica thin films have a clear advantage over templated silica powders. At less than 500 nm thickness, these films are expected to absorb very little

intensity of the excitation beam. This advantage has been employed previously in the investigation of CO<sub>2</sub> processing of polymeric thin films. For instance, the local dynamics of probe systems in thin films in the presence of compressed CO<sub>2</sub> has been investigated by determining the diffusivity of pyrene in polystyrene films using steady state fluorescence spectroscopy.<sup>216</sup> The diffusion coefficients and localization of various probes in CO<sub>2</sub> swollen polymer films have also been investigated in real time by high pressure fluorescence nonradiative energy transfer (NRET) using pyrene labeled polystyrene.<sup>217</sup>

This study extends high pressure fluorescence spectroscopy to the in-situ investigation of CO<sub>2</sub> processing (17 bar – 172 bar, 45°C) of hydrocarbon (CTAB and CPB) surfactant templated silica thin films. The suitability of the well studied solvatochromic probe, pyrene, and a pyrene derivative, 1-pyrene hexadecanoic acid (C<sub>16</sub>-pyr) as probes for the effect of CO<sub>2</sub> processing on CTAB templated films is demonstrated, while only C<sub>16</sub>-pyr is suitable to probe the penetration of CO<sub>2</sub> in CPB templated silica films. The timescales of silica condensation are inferred from the probe mobility and the time dependent behavior of CO<sub>2</sub> penetration. CO<sub>2</sub> localization and relative uptake in surfactant templated silica are determined as a function of processing conditions, and the delivery of a solute dissolved in CO<sub>2</sub> to specific regions in surfactant templated films is demonstrated using fluorescence nonradiative energy transfer (NRET).

### 7.3 Materials and Methods

**7.3.1 Chemicals.** The surfactants cetyltrimethylammonium bromide (CTAB) and cetylpyridinium bromide (CPB) were obtained from Aldrich and used without further purification. Tetraethoxysilane (TEOS, purity > 99%) was purchased from Gelest. Absolute ethyl alcohol purchased from Aaper Alcohol and Chemical Co. (Shelbyville, KY), deionized ultrafiltered water from Fisher Scientific and hydrochloric acid (0.1 N standardized solution) obtained from Alfa Aesar were used for thin film synthesis. Carbon dioxide (Coleman grade, 99.99+%) was purchased from Scott Gross Co. (Lexington, KY). The fluorescence probes, 1-pyrenedecanoic acid (pyrene-(CH<sub>2</sub>)<sub>9</sub>COOH) (C<sub>10</sub>-pyr) and 1-pyrenehexadecanoic acid (pyrene-(CH<sub>2</sub>)<sub>15</sub>COOH) (C<sub>16</sub>-pyr) (purity 99+%) were purchased from Molecular Probes. Pyrene was obtained from

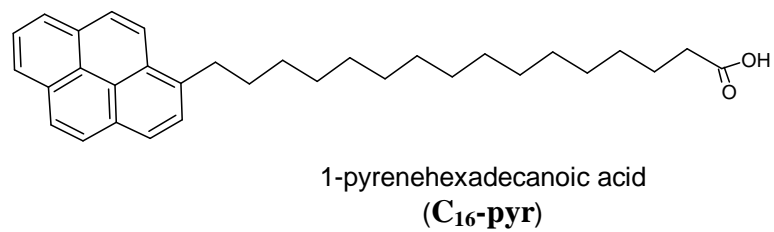
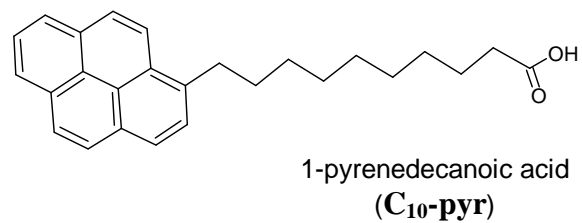
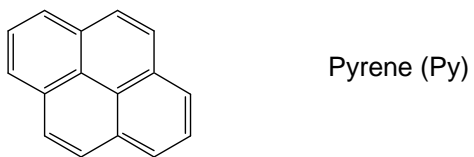
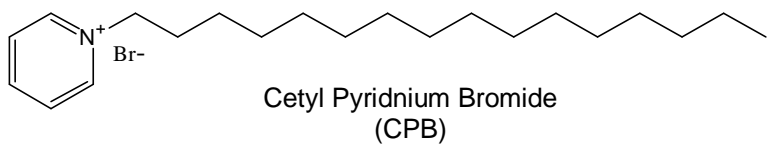
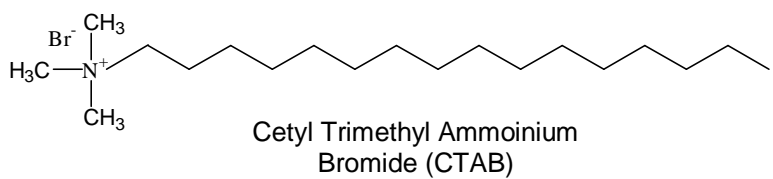


**Figure 7.1** Schematic of CTAB, CPB, naphthalene and pyrene and its derivatives

Sigma (purity ~ 99%) and naphthalene (purity 98+%) from Fisher Scientific. Schematics of all surfactants and probes are presented in Figure 7.1.

**7.3.2 Film Synthesis.** The solution for silica film synthesis was prepared by first refluxing TEOS, ethanol, water and HCl (mole ratio 1: 3.8: 1:  $5 \times 10^{-5}$ ) at 65°C for 90 min to obtain a clear solution of partially hydrolyzed silica. The remainder of the required water and HCl were then added in calculated quantities, resulting in a pH of approximately 2 in the final solution, and the mixture was aged at 25°C for 15 min and then at 50°C for an additional 15 min. Finally, a solution of the surfactant in ethanol was added to the previously hydrolyzed silica sol under constant stirring. The final mole ratios obtained were 1 TEOS : 12 C<sub>2</sub>H<sub>5</sub>OH : 5 H<sub>2</sub>O : 0.004 HCl :  $x$  surfactant ( $x$  0.06 for CTAB<sup>26</sup> and 0.1 for CPB). The fluorescence probe (pyrene, C<sub>10</sub>-pyr or C<sub>16</sub>-pyr) was then added to the solution, resulting in a final probe concentration in the dip-coating solution of  $5 \times 10^{-5}$  M. 500  $\mu$ l of the silica solution was dropped on each side of a clean glass slide and allowed to spread to form a uniform film.

Immediately after coating, the films were divided into two treatment groups. One treatment group was mounted in a high pressure fluorescence view cell (described below), either within 5 min after spreading the film solution (brief-aged film) or after aging the films greater than 25 m (long-aged film). The aging time is defined as the time period between depositing the solution on the glass slide and the initiating the CO<sub>2</sub> processing of the film. CO<sub>2</sub> pressure in the view cell was increased at the rate of 15 bar / min until the pressure reached a desired pressure (17 – 172 bar). Films were maintained at the desired CO<sub>2</sub> pressure at 45°C for up to 24 h, as described in the individual experiments. Fluorescence spectroscopy was performed on the second treatment group of films in a low pressure film holder without any CO<sub>2</sub> processing.

**7.3.3 Atmospheric Fluorescence Measurements.** Steady state fluorescence measurements were performed with a Varian Cary Eclipse fluorescence spectrophotometer (Walnut Creek, CA). Surfactant templated silica films were mounted on the front face of a holder custom designed to fit in a cuvette holder and allow front face illumination by the excitation beam at an angle of 45°. A xenon pulse lamp was used as the light source, with an operational wavelength range of 200-900nm (1.5 nm accuracy; (0.2 nm reproducibility)). Emission spectra of the pyrene or derivatized pyrene

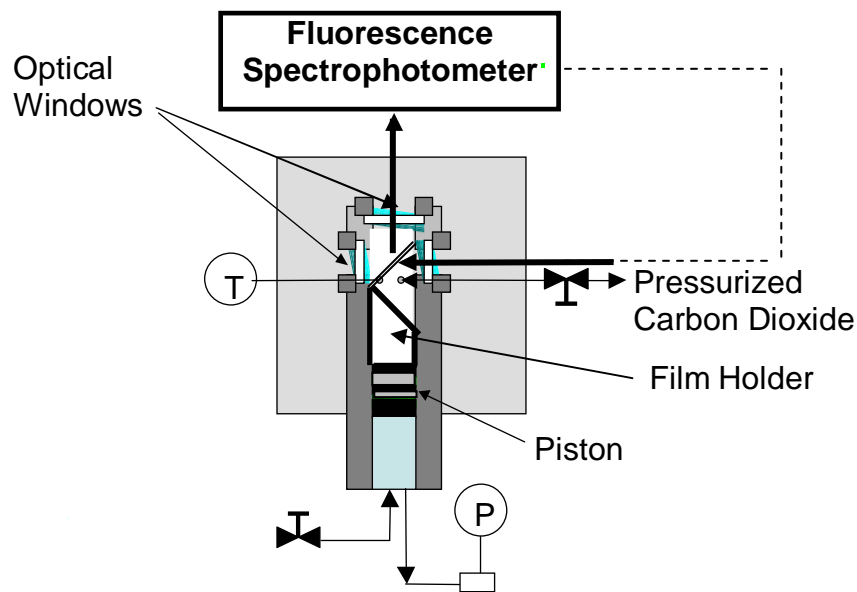


**Fig 7.2** Apparatus for high pressure thin film fluorescence measurements

(C<sub>10</sub>-pyr and C<sub>16</sub>-pyr) in the films was obtained by exciting the probe at 334 nm with an excitation slit width of 5 nm and an emission slit width of 1.5 nm.

**7.3.4 High Pressure Fluorescence Spectroscopy.** In-situ fluorescence measurements of compressed CO<sub>2</sub> processing of silica film was conducted using a custom-designed film holder fitted inside a stainless steel variable volume view cell (10-25 mL working volume, rated to 20.7 MPa) obtained from Thar Technologies (Pittsburgh, PA). The high pressure cell was mounted within the sample compartment of the Varian Cary Eclipse fluorescence spectrophotometer (Figure 7.2). The film holder was placed in line with the quartz windows such that the excitation beam illuminates the film at 45°. The position of the thin film in the path of the beam was kept constant throughout CO<sub>2</sub> pressurization by using a constant volume of an overburden incompressible fluid (water) separated from the film holder by an O-ring piston. The temperature of the spectroscopic cell was controlled using an Omega controller (model CN9000A) with heating tape. CO<sub>2</sub> was deoxygenated by passing it through a high pressure oxygen trap (Alltech, rated to 125 bar) and supplied to the view cell using an Isco syringe pump (Lincoln, NE, model 500D). CO<sub>2</sub> was deoxygenated to prevent the quenching of the probe. Emission spectra of pyrene in CTAB templated film and C<sub>16</sub>-pyr in CPB templated film were obtained at specific intervals during CO<sub>2</sub> processing by exciting the probes at 334 nm.



Nonradiative Energy Transfer (NRET) at high pressure was measured between naphthalene (donor) and C<sub>16</sub>-pyr (acceptor). Naphthalene was dissolved in deoxygenated CO<sub>2</sub> at a fixed concentration of 5\*10<sup>-5</sup> M and supplied to the view cell using the Isco syringe pump. C<sub>16</sub>-pyr labeled CTAB templated films were produced as described above. With naphthalene present in the system, the sample was excited at 290 nm and fluorescence spectra were recorded in the wavelength range 300-550 nm. The ratio of the intensities of C<sub>16</sub>-pyr fluorescence to naphthalene fluorescence (I<sub>P</sub> / I<sub>N</sub>), which is a measure for NRET efficiency, was calculated from fluorescence intensities at 338 and 376 nm for naphthalene and C<sub>16</sub>-pyr emission, respectively.

## 7.4 Results and Discussion

### 7.4.1 Fluorescence Spectroscopy of Silica Films without CO<sub>2</sub> Processing.

Prior to using the fluorescence probe system (pyrene, C<sub>10</sub>-pyr, C<sub>16</sub>-pyr) to investigate the localization and uptake of CO<sub>2</sub> in surfactant templated materials, the applicability of these probes for the thin films templated with the hydrocarbon surfactants CTAB and CPB is demonstrated. The location of pyrene in CTAB micelles<sup>184</sup> has previously been estimated using its solvatochromic behavior, while the change in microviscosity and state of surfactant aggregates in CTAB templated silica films<sup>330</sup> has also been probed by pyrene fluorescence. The ratio of the fluorescence intensities of the vibronic bands of pyrene (intensity ratio of 1<sup>st</sup> to 3<sup>rd</sup> band, I<sub>1</sub>/I<sub>3</sub>) has also been used to probe the micropolarity of its local environment both at low pressure<sup>184-186</sup> and in compressed CO<sub>2</sub> environments.<sup>213,331</sup> The value of the I<sub>1</sub>/I<sub>3</sub> ratio varies from 0.6 for a non-polar solvent, such as hexane, to 1.8 for an aqueous environment.<sup>184</sup>

The emission spectrum of pyrene in a CTAB templated film without CO<sub>2</sub> processing is presented in Figure 7.3a. The spectrum displays five sharp vibronic bands, characteristic of pyrene fluorescence at low probe concentration, with an I<sub>1</sub>/I<sub>3</sub> value of 1.4. The value of I<sub>1</sub>/I<sub>3</sub>, which is intermediate between that for a polar and a non-polar solvent environment, indicates the presence of pyrene at the interface of the CTAB micelle, consistent with previous studies.<sup>184,330</sup> Alternatively, excitation of pyrene in a CPB templated film results in negligible emission intensity (Fig. 7.3b). Similar to CTAB micelles, pyrene is also expected to be present at the CPB micelle interface. However,

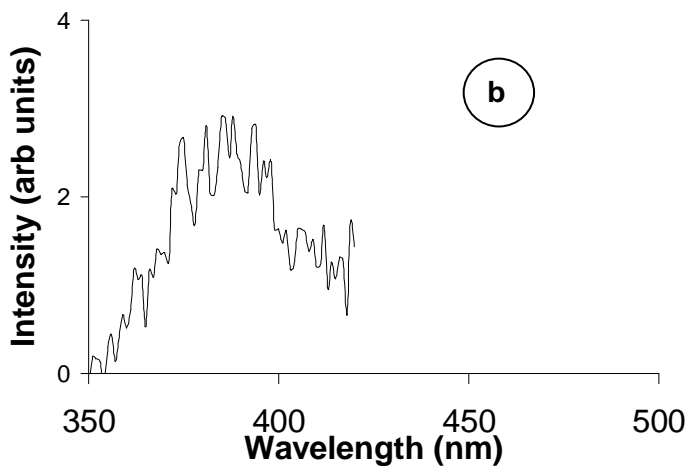
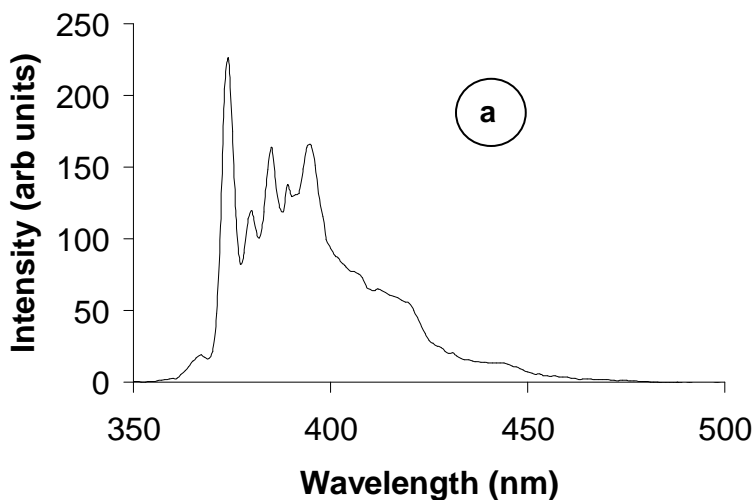


**Fig 7.3.** Emission spectra of pyrene in a) CTAB and b) CPB templated film without CO<sub>2</sub> processing

pyrene fluorescence is effectively quenched by the pyridinium head group of CPB at the interface through electron transfer from the photoexcited state of pyrene to electron deficient pyridine group, leading to the decreased emission intensity.<sup>332,333</sup> In CPB micelles, quenching of pyrene probes occurs through static quenching, in which the electron transfer from the excited probe to the nearest pyridine neighbor requires no pyrene diffusion because of the high local concentration of the quencher.<sup>334,335</sup>

The modification of pyrene with a carboxylic acid tail is expected to significantly alter the location of the pyrene moiety in a CTAB or CPB micelle. In the case of sodium

dodecyl sulfate micelles, the carboxylic acid of these pyrene derivatives associates with the surfactant head group and the pyrene moiety, which is attached to the hydrocarbon chain, is present in the micelle interior.<sup>336</sup> The orientation of derivatized pyrene in the micelle interior is a potential advantage of probing CPB templated films, as it limits the quenching of pyrene by the pyridine head group.

The location of derivatized pyrene C<sub>10</sub>-pyr (pyrene-(CH<sub>2</sub>)<sub>9</sub>COOH) and C<sub>16</sub>-pyr (pyrene-(CH<sub>2</sub>)<sub>15</sub>COOH) is examined from their emission spectra in non-CO<sub>2</sub> processed silica films templated by CTAB and CPB (Figure 7.4). For CTAB templated film, both derivatized probes display emission spectra with high intensity (Fig. 7.4 (a & c)). In contrast, in CPB templated film the intensity of the emission spectra of C<sub>10</sub>-pyr is negligible (Fig. 7.4b), while significant emission intensity is observed for the longer hydrocarbon chain probe, C<sub>16</sub>-pyr in CPB templated film (Fig. 7.4d). The low intensity of the shorter hydrocarbon chain probe may be explained by its ability to bend back to the interface, resulting in quenching due to the proximity of the pyrene moiety and the pyridinium head group of the surfactant. The localization of pyrene and C<sub>10</sub>-pyr has been suggested to be in the same depth in the core of SDS micelles based on their similar quenching rate constants.<sup>336</sup> The location of C<sub>10</sub>-pyr at the interface was attributed to the ability of the hydrocarbon chains to bend in a U-shaped conformation toward the interface. Alternatively, a shorter derivative of pyrene, 1-pyrenebutanoic acid (C<sub>4</sub>-pyr) did not favor a bent conformation and the pyrene moiety of C<sub>4</sub>-pyr was located in the SDS micelle interior.<sup>336</sup>

Alternatively, the significant fluorescent intensity of the longer chain C<sub>16</sub>-pyr in CPB templated material (Fig 7.4d) is consistent with the pyrene moiety being located in the interior of the micelle. Increasing the length of the hydrocarbon tail may increase steric hindrance and limit the pyrene moiety from bending back to the interface. Favorable interactions between the hydrocarbon chains of identical lengths of C<sub>16</sub>-pyr and CPB (16 carbons) have been observed previously for functional group incorporation in surfactant templated materials<sup>77</sup> and may increase incorporation of C<sub>16</sub>-pyr in the micelles and localization of the pyrene moiety in the micelle interior of CPB templated films. While localization and high fluorescent intensities in the CPB templated films are an advantage of the C<sub>16</sub>-pyr probe, a disadvantage is the loss of its solvatochromic

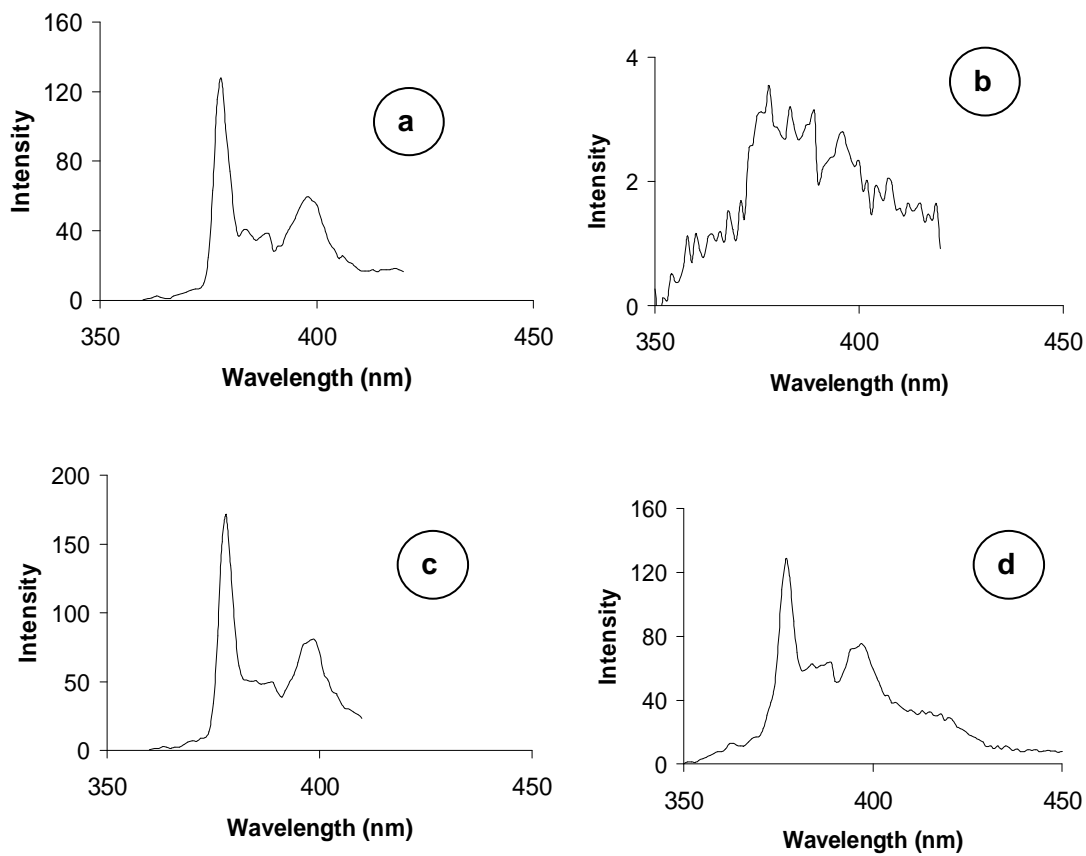


**Fig7. 4.** Emission spectra of C<sub>10</sub>-pyr in a) CTAB and b) CPB and C<sub>16</sub>-pyr in c) CTAB and d) CPB templated film

emission upon functionalization of pyrene. The solvent dependence emission of pyrene is a result of solute-solvent dipole-dipole coupling and  $\pi$ -orbital coupling and is dependent on the symmetry of pyrene,<sup>184</sup> which is lost for C<sub>16</sub>-pyr. However, the location of the pyrene moiety in the micelle interior for the anchored C<sub>16</sub>-pyr suggests other applications, including probing CO<sub>2</sub> interactions and CO<sub>2</sub> based solute delivery in the micelle interior as described below.

#### 7.4.2 Timescales of Silica Condensation with CO<sub>2</sub> processing.

The period of silica condensation in dip-coated surfactant templated thin film synthesis is called the modifiable steady state (MSS)<sup>134</sup> and represents the period when the silica structure can still be modified by external forces. Previously, researchers have modified thin film structure during the MSS by changing system humidity,<sup>134</sup> ethanol vapor concentration,<sup>141</sup> the surface chemistry of the substrate,<sup>29</sup> and by applying an external

magnetic field to alter the thin film orientation.<sup>337</sup> Extending the MSS period may increase opportunities to tailor mesostructure of thin films by directly altering the pore size, structure or functional group incorporation.

Our previous study suggests that alteration of pore structure through compressed CO<sub>2</sub> processing of fluorinated surfactant templated silica film occurs during the MSS period.<sup>274</sup> It was also observed that the x-ray diffraction patterns of fluorinated surfactant templated thin films varied for the first 12 h of CO<sub>2</sub> processing suggesting continuous changes in pore structure due to progressive silica condensation during that period. This observed change is attributed to continuous silica condensation and represents a significant extension in condensation timescales relative to unprocessed films. For example, IR spectra measurements of silanol bond intensity as a function of aging time of silica film aged in ambient conditions have suggested that silica condensation for CTAB templated film is complete after aging times of 20 min.<sup>143</sup> Even though CTAB<sup>75</sup> and CPB (Chapter 6) templated materials do not demonstrate significant CO<sub>2</sub> based pore expansion, the possibility of extending condensation timescales for further pore engineering exists if CO<sub>2</sub> penetration occurs in those templates.

CO<sub>2</sub> localization in the surfactant template is interpreted from the time dependent fluorescence spectra of the pyrene probes in CTAB templated films for both the brief-aged films (aging time < 5 min prior to exposure to CO<sub>2</sub>) and for the long-aged films (aging time > 25 min). Silica condensation is expected to be complete for the long-aged films before being processed in CO<sub>2</sub> compared to incomplete condensation for the brief-aged films.<sup>143</sup> The change in the emission intensity of pyrene is reported as the ratio of the intensity of the third vibronic emission band of pyrene (I<sub>3</sub>, emission at 385 nm) to the initial I<sub>3</sub> value (I<sub>30</sub>) (Fig. 7.5a). I<sub>3</sub> is insensitive to solvent polarity and decrease in the value of I<sub>3</sub> as observed in Figure 7.5a indicates overall decreases in pyrene emission intensity. Since, pyrene quenching is not significant in CTAB micelles,<sup>184,330</sup> the decrease of the emission intensity of pyrene is attributed to CO<sub>2</sub> accessing the pyrene present in the film for both aging times and leaching the pyrene into the bulk CO<sub>2</sub>. The pyrene is leached into the bulk CO<sub>2</sub> is present at a much lower concentration than pyrene in the thin film, suggesting that emission intensity from the bulk pyrene is negligible compared to pyrene emission from the thin film. Hence, most of the contribution to the observed

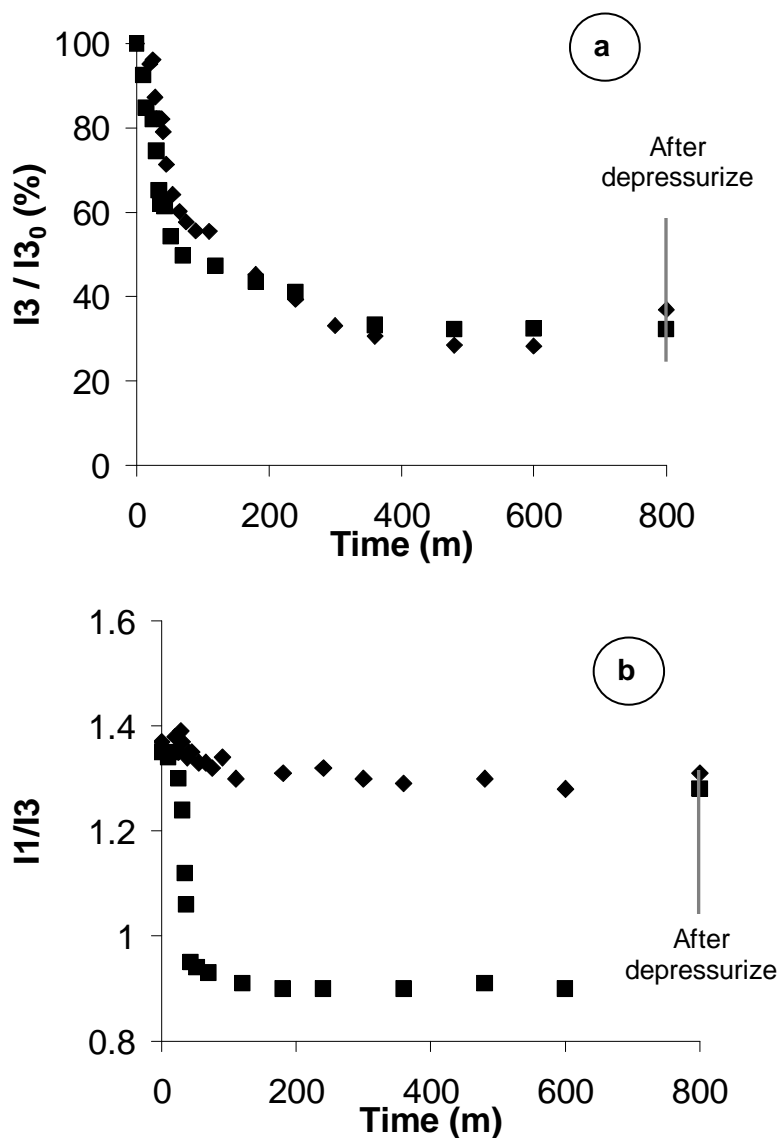


Fig 7.5. a) Change in emission intensity and b) I<sub>1</sub>/I<sub>3</sub> values of pyrene spectra in CTAB templated film and processed in CO<sub>2</sub> at 103 bar and 45°C for aging times less than 5 min (■) and greater than 25 min (◆)

fluorescence emission occurs from the pyrene that remains in the thin film thus resulting in a decrease in emission intensity. The dissolution of pyrene from polymeric films into bulk compressed CO<sub>2</sub> has been previously reported.<sup>217</sup> The rate of pyrene leaching is similar for films of both aging times suggesting that CO<sub>2</sub> accessibility of the CTAB micelle interface to result in pyrene solvation is not significantly dependent on the extent of silica condensation.

The final emission intensity decrease is significant (retaining only 30% of its initial intensity) and similar for films of both aging times and is obtained at processing times greater than 6 hrs. Further, depressurization of the system does not result in an appreciable increase in pyrene intensity. This suggests that pyrene remains dissolved in CO<sub>2</sub> during depressurization and does not re-deposit in the film. To further confirm the dissolution of pyrene in CO<sub>2</sub>, the pyrene dissolved in CO<sub>2</sub> was captured by bubbling in ethanol during depressurization. Significant quantities of pyrene were solubilized in the depressurized CO<sub>2</sub>, as measured by fluorescence spectroscopy of the ethanol solution.

The solvatochromic behavior of pyrene provides further insight into the localization of CO<sub>2</sub> in the surfactant templated films as a function of aging time. The I1/I3 values for pyrene emission in CTAB film at 103 bar and 45°C as a function of CO<sub>2</sub> processing time are presented in Figure 7.5b. The I1/I3 values are plotted both for the brief-aged films (aging time < 5 min prior to exposure to CO<sub>2</sub>) and for the long-aged films (aging time > 25 min.). The I1/I3 value for the brief-aged films decreases from 1.4 (for a non-processed film) to about 0.9 within the first 20 min of CO<sub>2</sub> processing and remains constant thereafter. The decrease is consistent with a change in pyrene localization from a micellar interface to a considerably more non-polar environment. Pyrene emission intensity during CO<sub>2</sub> processing has been demonstrated to have significant contribution only from pyrene fluorescence in the thin film compared to the pyrene present in bulk CO<sub>2</sub>. Thus, the shift in I1/I3 values represent a change in pyrene localization in the thin film suggesting the solubilization of pyrene in a 'CO<sub>2</sub>-like' (non-polar) environment in the micelle interior for the quick-aged film. Indeed, pyrene present at micelle interfaces has been demonstrated to be solubilized by compressed CO<sub>2</sub> into the micelle interior.<sup>154,338</sup> Interestingly, CO<sub>2</sub> penetration in the micelle interior occurs even for this hydrocarbon surfactant template, which shows no significant pore expansion when processed with CO<sub>2</sub>.<sup>75</sup> Similar solvent penetration in surfactant tails without micelle expansion has been observed for alcohols and aromatic hydrocarbons.<sup>40</sup>

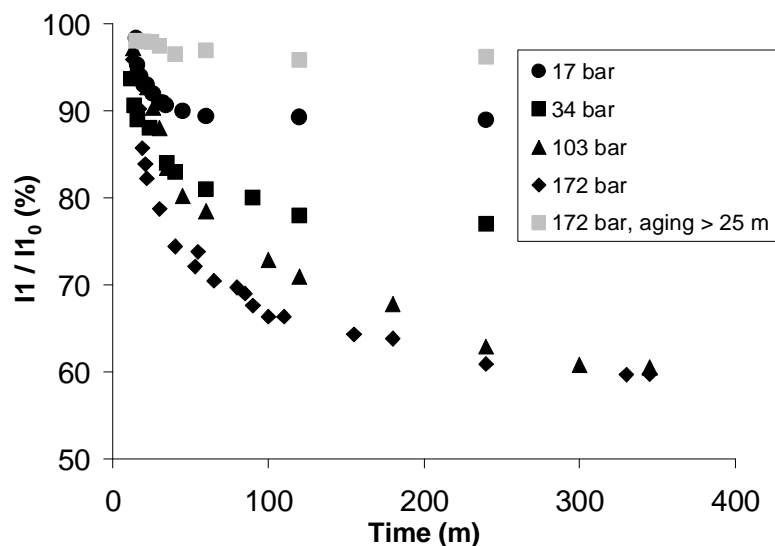


Fig 7.6. Change in emission intensity of  $C_{16}$ -pyr in CPB templated film and processed in  $CO_2$  at different pressures and  $45^\circ C$  as function of processing time

In contrast to the brief-aged films, a decrease in the I1/I3 ratio of pyrene was not observed for the long-aged film, suggesting that  $CO_2$  is incapable of solublizing the pyrene in the micelle interior after complete silica condensation.<sup>143</sup> Thus, the limit for aging times to result in successful  $CO_2$  penetration in surfactant micelle interior may be less than the time period for complete silica condensation. For both film aging times, the I1/I3 value is about 1.35 after  $CO_2$  depressurization, indicating that the environmental change in the vicinity of pyrene is reversible in the quick aged film. During  $CO_2$  depressurization, pyrene returns to the interface from the micelle interior.

The preferential location of  $C_{16}$ -pyr in the micelle interior for CPB templated silica films is used to investigate the localization of  $CO_2$  in the surfactant tails and the dynamics of silica condensation in the films as a function of  $CO_2$  processing time and conditions. Anchoring of the probe system to the micelle interface also results in insignificant  $CO_2$ -based leaching of  $C_{16}$ -pyr from the cationic surfactant templated films, as determined from the negligible change in probe emission intensity in quick aged CTAB templated film for  $CO_2$  processing at 103 bar and  $45^\circ C$  (not shown).

Figure 7.6 plots the change in emission intensity of  $C_{16}$ -pyr in CPB templated film ( $I1 / I1_0$ ;  $I1_0$  is value of I1 before  $CO_2$  processing) due to  $CO_2$  processing time for both the



long-aged films (aging time > 25m) and the brief-aged films (aging time < 5 m) as a function of processing pressure. Significant decreases in C<sub>16</sub>-pyr emission intensity are observed for the quick aged films at all conditions of CO<sub>2</sub> processing compared to the non processed films. In the absence of probe leaching, the decrease in emission intensity of C<sub>16</sub>-pyr is attributed to the quenching of the pyrene moiety by pyridinium head group of the surfactant. This quenching is caused by continued probe mobility in the micelle interior due to the presence of CO<sub>2</sub>, resulting in increased interactions of the probe with pyridine. The magnitude of intensity decrease increases with processing pressure for gaseous CO<sub>2</sub> processing from 17 bar (intensity is about 90% of its original value) to 34 bar (about 80% of original intensity) at 45°C. Emission quenching is even more significant for sc CO<sub>2</sub> processing at 103 bar and 45°C (about 60% of original value) but remains constant thereafter at different sc CO<sub>2</sub> conditions.

The rate of quenching is also a function of CO<sub>2</sub> processing conditions. Similar magnitudes of intensity decrease occurring at a fast rate are observed for all CO<sub>2</sub> conditions during the first 1 h of processing. Thereafter the rate of decrease slows down for both gaseous and sc CO<sub>2</sub> processing and after approximately 1.5 hours, the emission intensity of C<sub>16</sub>-pyr in gaseous CO<sub>2</sub> processed films reaches a constant value. In contrast, the emission intensity continues to decrease for the films processed in sc CO<sub>2</sub> for at least 5 hr. Several factors can limit the rate of quenching of the derivatized pyrene probe with increasing CO<sub>2</sub> processing times. C<sub>16</sub>-pyr mobility in films processed in CO<sub>2</sub> might be decreasing with processing time due to increasing silica condensation, which would limit the association of pyrene moiety with pyridine group. Alternatively, the quenching may be limited by the availability of free pyrene even if the probe is mobile. Quenching of C<sub>16</sub>-pyr in CPB micelle is expected to follow a static quenching mechanism similar to quenching of free pyrene in CPB micelles, i.e. through forming pyrene-pyridine complexes due to electron transfer.<sup>334,335</sup> As an increasing number of pyridine groups form static quenching pairs with C<sub>16</sub>-pyr with processing time, the probability of pyrene moiety finding a free pyridine group decreases (where the initial molar ratio of pyrene to CPB is 9\*10<sup>-3</sup> : 1). Alternately, the emission intensity of C<sub>16</sub>-pyr in the long-aged CPB films remains essentially constant with time for CO<sub>2</sub> processing at 103 bar and 45°C

suggesting that probe mobility is negligible in films having significant silica condensation.

In-situ fluorescence quenching measurements demonstrate that gaseous and sc CO<sub>2</sub> processing of quick-aged CPB templated films is successful in extending silica condensation time from about 25 min for the unprocessed film (as suggested by insignificant quenching for long-aged film) to greater than 5 h depending on processing conditions through CO<sub>2</sub> penetration in the surfactant tails. This technique is applicable to non-CO<sub>2</sub> philic hydrocarbon templates and even gaseous CO<sub>2</sub> is capable of extending the MSS to greater than 1 hour.

### **7.4.3 High Pressure Nonradiative Energy Transfer.**

The preferential localization of the pyrene moiety in the micelle interior for the anchored probe, C<sub>16</sub>-pyr, suggests the opportunity to investigate the delivery of CO<sub>2</sub> dissolved solutes to the micelle interior. NRET involving anchored probes has previously been used to investigate solvent and water uptake in micelle and microemulsion systems.<sup>219,220</sup> Naphthalene and pyrene are often used as an energy donor / acceptor pair;<sup>203,204</sup> naphthalene emission and pyrene absorption have a large spectral overlap and the excitation of the system at 290 nm is selective to naphthalene.<sup>339</sup>

In this study, naphthalene is dissolved in bulk CO<sub>2</sub> and introduced into the film during the CO<sub>2</sub> processing of the CTAB templated film. The pyrene moiety of C<sub>16</sub>-pyr, which is anchored to the film through its carboxylic acid tail, is used as the electron acceptor. The high solubility of naphthalene in compressed CO<sub>2</sub> is well documented<sup>340,341</sup> and is an advantage of this probe system. At the low concentrations of naphthalene required to quantify NRET of the naphthalene/pyrene pair (naphthalene concentration in CO<sub>2</sub> is 5\*10<sup>-5</sup> M), naphthalene can be directly solubilized in CO<sub>2</sub> even at low pressures. Another advantage of the naphthalene/pyrene pair is that the Forster distance (2.9 nm)<sup>342</sup> is greater than the radius of CTAB micelle (~ 2.1 nm).<sup>24</sup> Thus, energy transfer will always occur when naphthalene is localized in the micelle interior, where the pyrene moiety of the anchored C<sub>16</sub>-pyr is also localized.

NRET is confirmed from the emission spectra of a CTAB templated film (labeled with C<sub>16</sub>-pyr) processed with CO<sub>2</sub> (103 bar and 45°C) containing dilute dissolved naphthalene (Fig. 7.7). Even without the presence of naphthalene, excitation of the C<sub>16</sub>-pyr

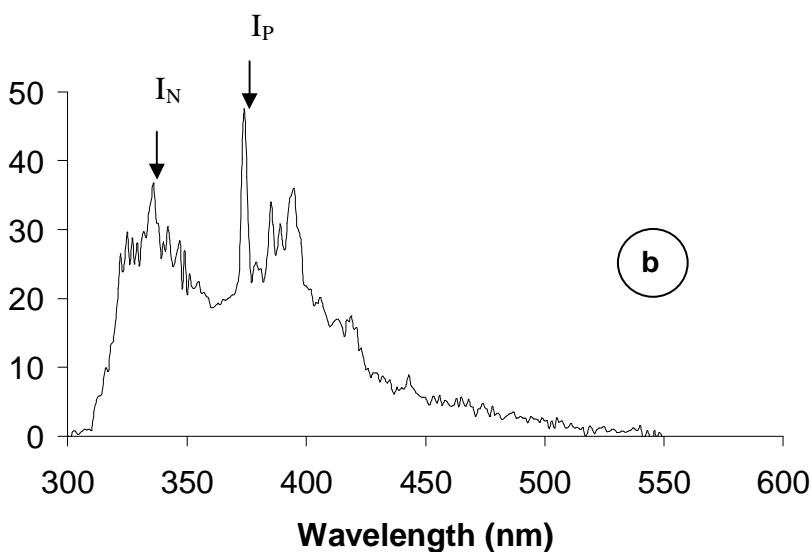
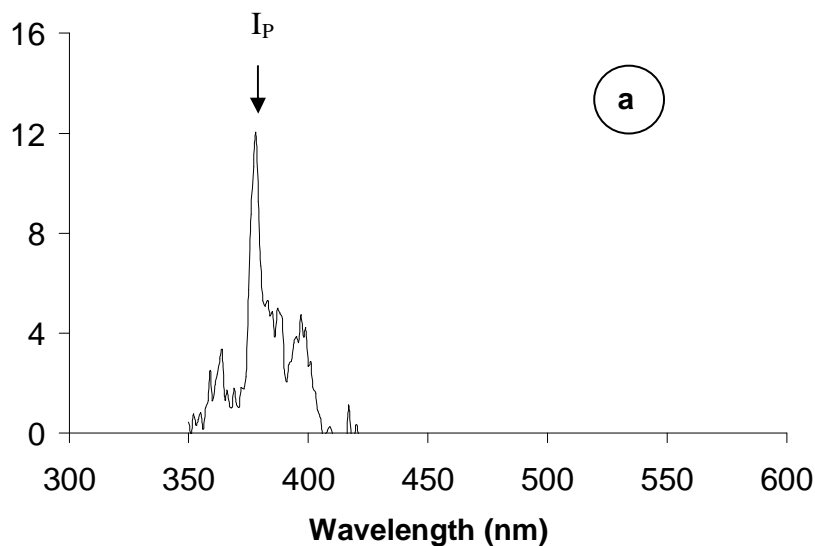


Fig 7.7. Emission spectra of C<sub>16</sub>-pyr in CTAB templated film excited at 290 nm and processed in CO<sub>2</sub> at 103 bar and 45°C (a) without dissolved naphthalene and (b) with naphthalene dissolved in CO<sub>2</sub>

labeled film at 290 nm displays a weak emission around 377 nm (Fig. 7.7a). However, with the introduction of naphthalene dissolved in CO<sub>2</sub>, the emission intensity of C<sub>16</sub>-pyr around 377 nm is significantly increased, along with a corresponding emission from naphthalene around 340 nm (Fig. 7.7b). These emission spectra characteristics demonstrate energy transfer between naphthalene and pyrene moiety of C<sub>16</sub>-pyr.

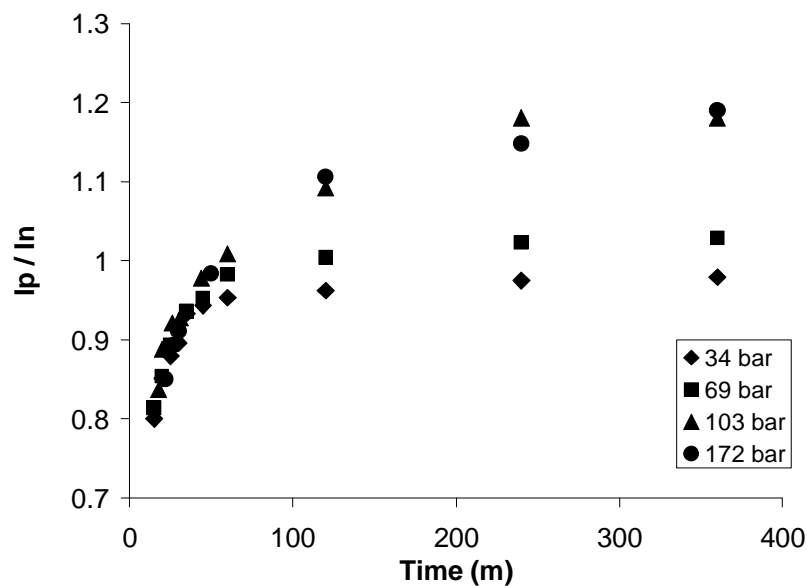


Fig 7.8.  $I_p/I_n$  values due to NRET between naphthalene solubilized in processing  $\text{CO}_2$  and  $\text{C}_{16}$ -pyr in CTAB templated film as a function of time and processing pressure.

Previous studies have reported that in the absence of  $\text{CO}_2$ , the naphthalene probe molecule resides at the micelle interface.<sup>335</sup> For our system, the quenching of the fluorescence emission of naphthalene in CPB templated film without  $\text{CO}_2$  processing also confirms the presence of naphthalene at the micelle interface and near the pyridinium headgroup. Hence, NRET of the pyrene-labeled thin films during  $\text{CO}_2$  processing indicates delivery of naphthalene by dissolved  $\text{CO}_2$  to the micelle interior during the synthesis of templated material. The penetration of naphthalene dissolved in compressed  $\text{CO}_2$  in the micelle interior has been previously demonstrated.<sup>338</sup>

The efficiency of energy transfer between naphthalene and  $\text{C}_{16}$ -pyr can be used to interpret the uptake of the  $\text{CO}_2$ -soluble solute, naphthalene, to the tail region of the surfactant template and changes in the probe localization as a function of  $\text{CO}_2$  processing pressure. Efficiency of energy transfer is calculated using the ratio of the fluorescence intensities of the acceptor to the donor ( $I_p/I_n$ , where  $I_p$  is pyrene emission at 377 nm and  $I_n$  is naphthalene emission at 338 nm) and is plotted in Figure 7.8 as a function of processing pressure and time. The  $I_p/I_n$  ratio increases rapidly and has similar values at all  $\text{CO}_2$  processing conditions for the first 1 h of processing. The  $I_p/I_n$  ratio continues to increase with time and the final values and the processing time required to reach these

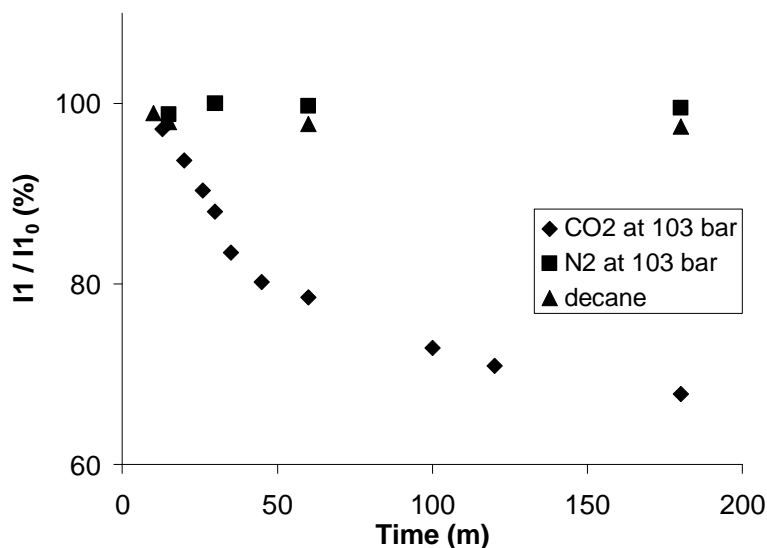
constant values increase with processing pressure from gaseous (from 34 bar to 69 bar at 45°C) to sc CO<sub>2</sub> processing (103 bar and 172 bar at 45°C). Approximately 4 hr of sc CO<sub>2</sub> processing is required to achieve a constant value of  $I_P / I_N$  (~ 1.2) at both 103 bar and 172 bar.

An increase in the  $I_P / I_N$  ratio indicates either a decrease in the average distance between naphthalene and pyrene<sup>203,204,339</sup> or an increase in the naphthalene / C<sub>16</sub>-pyr ratio in the same environment.<sup>343</sup> A decrease in the distance between the probes indicates solute-solute clustering between naphthalene and C<sub>16</sub>-pyr in sc CO<sub>2</sub>.<sup>213,331</sup> However, solute-solute clustering in sc CO<sub>2</sub> has been demonstrated to decrease with increasing CO<sub>2</sub> pressure,<sup>331</sup> which is in contradiction to the trends of  $I_P / I_N$  values in our system ( $I_P/I_N$  values increase with CO<sub>2</sub> pressure). Hence, solute-solute clustering cannot completely explain the increase in energy transfer efficiency with pressure and indicates that increase in the naphthalene / C<sub>16</sub>-pyr ratio is also occurring. For a constant C<sub>16</sub>-pyr concentration, an increase in the naphthalene / C<sub>16</sub>-pyr ratio indicates an increase in naphthalene concentration and suggests an increase in naphthalene uptake in the micelle interior with CO<sub>2</sub> pressure and processing time.

#### **7.4.4 Silica Film Processing in Additional Solvent Environments.**

The combination of steady state fluorescence quenching and NRET measurements has been used to establish that compressed CO<sub>2</sub> is an attractive solvent to alter timescales and transport solute molecules in surfactant templated ceramics. The uniqueness of CO<sub>2</sub> as a process solvent for the pore engineering of mesoporous silica films is investigated in comparison to a pressurized gaseous environment, N<sub>2</sub>, and with a common pore swelling agent, decane. Processing of the dip-coated silica films with compressed N<sub>2</sub> at 103 bar and 45°C is used to determine if pressure contributed to the extension of silica condensation timescales in CO<sub>2</sub> processed films. Figure 7.9 compares the percentage emission intensity for anchored C<sub>16</sub>-pyr in CPB templated film ( $I_1 / I_{10}$ ;  $I_{10}$  is value of  $I_1$  before solvent processing) when processed in CO<sub>2</sub> and N<sub>2</sub> at 103 bar and 45°C and in decane as a function of processing time. Quenching of the emission intensity of C<sub>16</sub>-pyr present in CPB templated film has been correlated to solvent penetration into the CPB micelle interior and incomplete silica condensation. In contrast to compressed CO<sub>2</sub> processing of CPB films, in

which the  $C_{16}$ -pyr intensity decreases over a period of 5 h, no fluorescence intensity change



is

Fig 7. 9. Change in emission intensity of  $C_{16}$ -pyr in CPB templated film and processed 3 different solvents as a function of time.

observed for  $N_2$  processing. This suggests that compressed  $N_2$  is not effective in extending silica condensation timescales and result in a continuous mobility of  $C_{16}$ -pyr in CPB micelles.

Decane has previously been used as a pore swelling agent in the synthesis of CTAB templated silica powders through localization in a separate region inside the micelle core.<sup>37</sup> In the current study, CPB templated silica film with  $C_{16}$ -pyr as probe was immersed in decane after aging for 5 min. The decane to CPB molar ratio was 1:1 and was similar to the ratio previously used to achieve pore expansion in mesoporous silica.<sup>37</sup> Similar to compressed  $N_2$  processing, no change in emission intensity was observed as a function of time (Fig. 7.9). The results indicate the inability of decane processing to result in extension of silica condensation timescales.

## 7.5 Conclusions.

Fluorescence spectroscopy was established as a novel technique to investigate the penetration of compressed  $CO_2$  in surfactant templated silica films. The potential of  $CO_2$  processing to alter templated thin film structures through penetration in the surfactant tail

and extension of silica condensation timescales was demonstrated for hydrocarbon surfactant (CTAB and CPB) templated silica, for which negligible pore expansion has been observed previously.

The ability of fluorescence spectroscopy to successfully follow the delivery of CO<sub>2</sub> solubilized small solutes in mesoporous silica suggests its application in delivery of drug molecules, reactants and novel functional groups. Sc CO<sub>2</sub> is able to access silanol groups in mesoporous silica that are “inaccessible” to traditional liquid solvents due to its favorable transport properties.<sup>344</sup> Sc CO<sub>2</sub> has also been used to load and encapsulate drugs into polymers and nanoparticles,<sup>284-286</sup> while mesoporous silica with tailored pore sizes has been used for adsorption of drugs because the release rate can be tailored with pore size.<sup>146</sup> The potential exists for application of sc CO<sub>2</sub> to load drug molecules and functional groups in mesoporous silica while simultaneously extending silica condensation, thus suggesting a more uniform distribution of solutes and loading in more “inaccessible” regions than possible for CO<sub>2</sub> processing after complete silica condensation. Indeed, it was demonstrated that extension of silica condensation timescales through solvent processing is not a general phenomena for all solvents, but is unique to compressed CO<sub>2</sub> processing of surfactant templated materials. Knowledge of the timescales of silica condensation and the localization of solute/reactant molecules as a function of CO<sub>2</sub> processing time and pressure allows for the optimization of the solute loading and release in mesoporous materials.

Copyright © Kaustav Ghosh 2007

## CHAPTER EIGHT

### CONCLUSIONS AND FUTURE WORK

#### 8.1 CONCLUSIONS

Fluorinated surfactants have been recently demonstrated as templates for the synthesis of ordered mesoporous silica with high surface area. The large van der Waals radius of fluorine favors aggregates with low curvature and results in mesoporous silica with novel intermediate mesh-phase structure.<sup>31</sup> The strong hydrophobicity of fluorocarbon groups allows micelle formation with small chain fluorinated surfactants which was successfully translated to the synthesis of ordered mesoporous silica with pore size in the microporous range<sup>31</sup> and having potential application in catalysis.<sup>89</sup> The synthesis of novel fluorocarbon functionalized mesoporous silica using fluorinated templates towards application in chromatography for separation of fluorocarbon and hydrocarbon compounds has also been demonstrated.<sup>77</sup> This dissertation addresses another major advantage of fluorinated templates, namely their favorable interactions with sc CO<sub>2</sub> to tailor pore structure of the materials directly through sc CO<sub>2</sub> processing during synthesis. In Chapters 3 and 4 we demonstrate the first synthesis of mesoporous silica thin films using three cationic fluorinated surfactants (perfluoralkyl pyridinium chlorides HFOPC, HFDePC, and HFDoMePC) as templates by dip-coating an acid-catalyzed sol-gel solution. A predictive method towards obtaining the dip-coating solution is established by using the phase behavior of the binary fluorinated cationic surfactant/water system to guide the synthesis recipe. Well-ordered silica thin films with 2D hexagonal pore structure are obtained for all three templates. Pore size increases for the longer tailed surfactant, HFDePC (C10 chain) compared to the shorter chain surfactant, HFOPC (C8 tail). Pore size for films templated with the branched surfactant, HFDoMePC and straight chain surfactant HFOPC are very similar, even though HFDoMePC contains an extra CF<sub>2</sub> group in tail compared to HFOPC. This is consistent with the fact that pore size is determined by the length of the hydrophobic tail group of the surfactant.<sup>51</sup> Indeed, the surfactant tail length for HFOPC and HFDoMePC were



demonstrated to be similar, with the extra  $\text{CF}_2$  group for HFDoMePC being part of the terminal branching in the tail.

Compressed  $\text{CO}_2$  processing of these fluorinated surfactant templated thin films (i.e., HFOPC, HFDePC, and HFDoMePC templated material) resulted in significant pore expansion with the degree of pore expansion varying according to template structure and processing conditions. For a particular template, a larger magnitude of pore expansion was observed for  $\text{CO}_2$  processing at lower densities, but pore diameter was nearly constant at higher  $\text{CO}_2$  density ( $\rho_{\text{CO}_2} > 0.6 \text{ g/ml}$ ). At similar  $\text{CO}_2$  processing conditions, pore expansion was greater for the longer tailed surfactant (HFDePC compared to HFOPC) and also increased with template branching when compared between two templates of similar length (i.e., greater expansion for HFDoMePC compared to HFOPC). The significantly different pore expansion behavior observed by varying templates and  $\text{CO}_2$  processing conditions suggest opportunities to tailor processing variables to obtain materials with pre-determined pore size. The relative solubility of the three fluorinated surfactants in  $\text{CO}_2$  and water, as well as their interfacial activity at the  $\text{CO}_2$ -water interface, correlated with the pore expansion. This approach provides a guide to the design surfactant templates that can be solvated by  $\text{CO}_2$  to obtain specific pore sizes.

The successful use of  $\text{CO}_2$  processing to synthesize pore tailored fluorinated surfactant silica films was extended to base-catalyzed silica powders synthesized by using HFOPC as the template.  $\text{CO}_2$  processing of silica powders allowed for the investigation of higher processing pressures than thin film synthesis (up to 344 bar investigated compared to 172 bar for thin film), the effect of pH change on surfactant self-assembly in  $\text{CO}_2$ , and the effect of aging time (sol-gel reaction time before  $\text{CO}_2$  processing) on the final pore structure. The pore expansion in mesoporous silica was dominated by  $\text{CO}_2$  solvation of the surfactant templates. The trends of pore expansion as a function of  $\text{CO}_2$  pressure were very similar to  $\text{CO}_2$  uptake trends in surfactant and polymer systems. The percentage pore expansion in powders is significantly less than observed in the acid-catalyzed films because  $\text{CO}_2$  solvation of surfactant templates in powders has a competing phenomenon, namely a decrease in micelle size due to change of system pH from initial basic condition to acidic with  $\text{CO}_2$  processing. In addition,

whereas silica condensation is delayed in acid-catalyzed film (system pH of 2 is near the isoelectric point of silica), significant silica condensation occurs in the base-catalyzed silica powders even before CO<sub>2</sub> processing. This enhanced silica condensation possibly inhibits pore expansion, which may also be a reason for the lower expansion observed in the powders. A maximum aging time of 20 m was determined to be appropriate for obtaining significant pore expansion while retaining the long range order of the silica, as longer aging times resulted in increased silica condensation and subsequent constrained pore expansion.

Ex-situ characterization of pore expansion between films templated with a fluorinated surfactant, a hydrocarbon surfactant and a surfactant containing hydrocarbon/fluorocarbon segments was used in Chapter 5 used to infer the CO<sub>2</sub> penetration in fluorocarbon (CF<sub>2</sub>) and hydrocarbon (CH<sub>2</sub>) regions of concentrated surfactant mesophases. The higher hydrophobicity of fluorinated surfactants resulted in slight dewetting of the fluorinated surfactant solution on a glass substrate and synthesis of slightly non-uniform thin films compared to hydrocarbon templated films. However, the fluorinated surfactant solution has a lower surface tension and was successful in forming silica films on very low energy substrates, suggesting increased application of such materials. CO<sub>2</sub> processing of a hydrocarbon/fluorocarbon surfactant (HFCPC, -(CH<sub>2</sub>)<sub>10</sub>(CF<sub>2</sub>)<sub>5</sub>CF<sub>3</sub> tail) templated material resulted in significantly greater pore expansion compared to the negligible expansion observed for an analogous hydrocarbon surfactant (CPB, -(CH<sub>2</sub>)<sub>15</sub>CH<sub>3</sub> tail) templated film suggesting greater CO<sub>2</sub> penetration in CH<sub>2</sub> groups compared to CF<sub>2</sub> regions in mesophases. A comparison of the the pore expansion behavior of thin films templated with two fluorinated surfactants reveals an increasing extent of pore expansion with an increasing percentage of 'CO<sub>2</sub>-philic' fluorocarbon groups in the surfactant tail and the preferential CO<sub>2</sub> delivery to 'CO<sub>2</sub>-philic' regions in mesophases.

Finally, real time high pressure fluorescence spectroscopy was used to investigate the extent and localization of CO<sub>2</sub> penetration in surfactant templated materials. In-situ CO<sub>2</sub> processing was probed for two hydrocarbon templated (CTAB and CPB) materials, for which negligible pore expansion after CO<sub>2</sub> processing had been demonstrated. Interestingly, CO<sub>2</sub> penetration was observed in surfactant tails of both templates.

Fluorescence quenching measurements demonstrated that the CO<sub>2</sub> penetration resulted in a pressure dependent extension of silica condensation timescales, suggesting alternative methods for CO<sub>2</sub> to alter porous film structure without significant pore expansion. Fluorescence non radiative energy transfer was successfully used to estimate the localization of CO<sub>2</sub> and follow the delivery of solutes dissolved in CO<sub>2</sub> in surfactant templated silica. These results suggest an approach for in-situ investigation of loading of drug molecules and reactants in porous materials.

The ability to tailor the pore structure of fluorinated surfactant templated silica films through sc CO<sub>2</sub> processing of 'CO<sub>2</sub>-philic' fluorinated templates is established in this study using a series of perfluoroalkyl pyridinium chloride surfactants as model templates. . As hypothesized, pore expansion can be tailored by tuning the solvent strength of CO<sub>2</sub> with pressure and changing template structure. CO<sub>2</sub> processing of hydrocarbon surfactant templated thin films results in negligible pore expansion extending the concept 'CO<sub>2</sub>-philicity' to the processing of concentrated surfactant systems.

## 8.2 FUTURE WORK

An extensive investigation on the effects of CO<sub>2</sub> processing of surfactant templated silica towards tailoring the pore structure has been performed in this study. The ability of CO<sub>2</sub> to selectively solvate the 'CO<sub>2</sub>-philic' regions of surfactant mesophases was demonstrated, suggesting the potential for delivering reactants/drug molecules to specific regions of mesophases. As a first step towards understanding of the mechanism of CO<sub>2</sub> penetration and a predictive guide for template design, the pore expansion has been interpreted from the two basic thermodynamic properties of the templates, solubility and interfacial behavior.

Monte Carlo simulations investigating CO<sub>2</sub> penetration in surfactant mesophases and templated silica will help to increase understanding of the mechanism of CO<sub>2</sub> penetration in such systems. The first step towards this objective is to combine studies of self-assembly and micelle formation of fluorinated surfactants at low concentration in sc CO<sub>2</sub> using large-scale Monte Carlo simulations<sup>345,346</sup> with Monte Carlo studies of solvent-surfactant-inorganic oxide.<sup>347,348</sup> A well-designed simulation system will become a

powerful technique to quickly screen templates and suggest processing conditions for CO<sub>2</sub> processing to result in porous materials with specific pore sizes.

Establishing the procedures for real time spectroscopy probing of CO<sub>2</sub> processing of surfactant templated silica provides a powerful technique towards investigating a variety of important processes in surfactant aggregates and porous materials. The application of fluorescence spectroscopy was initially motivated by the ability of CO<sub>2</sub> processing to swell fluorinated surfactant templates and a need for better understanding of the swelling mechanism. Hence, our immediate future objective is to establish a probe system for the fluorinated surfactant templated materials and to understand the mechanism and uptake of CO<sub>2</sub> in the 'CO<sub>2</sub>-philic' fluorinated tails. Comparison of those results with that obtained for the hydrocarbon template system will allow us to make better design of surfactant templates to obtain a specified tailored pore size.

The release rate of drugs (e.g. ibuprofen) from mesoporous silica has been previously tailored with pore size.<sup>146</sup> Sc CO<sub>2</sub> has been previously used to load and encapsulate drugs into polymers and nanoparticles<sup>284,285</sup> and can be potentially used to dissolve and transport drug molecules into mesoporous silica while at the same time tailoring CO<sub>2</sub> conditions to expand the pore size to obtain the desired release rate. Simultaneous to drug transport, increasing silica condensation timescales through CO<sub>2</sub> processing has potential for a more uniform loading, while designing surfactant templates with specific 'CO<sub>2</sub>-philic' regions will allow increased CO<sub>2</sub> penetration and hence drug loading in those desired regions. Finally, fluorescence spectroscopy established in this study to follow the transport of small solutes (naphthalene) dissolved in compressed CO<sub>2</sub> in mesoporous silica can be extended to monitor the delivery of drug molecules, thus allowing further control over the loading process.

The use of sc CO<sub>2</sub> towards loading solutes in mesoporous silica will potentially have applications in areas beyond drug loading. Mesoporous silica thin films with precise orientation of the porous channels have many applications in addition to those possible for porous silica powders in areas such as membrane separation, sensing and in semiconductor industries. Many of these applications require the use of functionalized silica thin films, for example, carboxy,<sup>349</sup> thiol and amine functionalized films<sup>350</sup> as sensors. The favorable transport property of sc CO<sub>2</sub> has resulted in CO<sub>2</sub> penetration to

regions 'inaccessible' to organic solvents in mesoporous silica<sup>344</sup> and suggests its application as an attractive solvent for post-functionalization of silica film with a variety of 'CO<sub>2</sub>-philic' groups.

Our research group has also synthesized novel fluorocarbon functionalized and amine functionalized mesoporous silica. CO<sub>2</sub> has favorable interactions with both amine groups as demonstrated by CO<sub>2</sub> adsorption on different amine-functionalized compounds<sup>351</sup> and also with fluorocarbon groups as demonstrated in this dissertation. Sc CO<sub>2</sub> processing of the above functionalized materials has potential to provide increased accessibility of the functional groups because of its advantageous transport properties and also the potential to alter surface charge and structure of the materials by either functional group solvation or specific chemisorption.

Copyright © Kaustav Ghosh 2007

## APPENDIX A

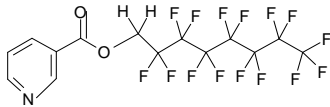
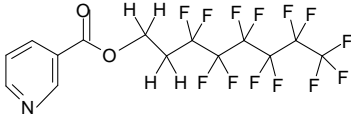
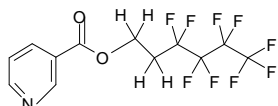
### SOLUBILITY OF NOVEL NONIONIC FLUORINATED ESTERS IN CARBON DIOXIDE

#### A.1 Introduction

This dissertation has extensively investigated methods of tailoring pore size of surfactant templated mesoporous silica materials through compressed CO<sub>2</sub> solvation of custom designed ‘CO<sub>2</sub>-philic’ templates directly during synthesis. The same properties of sc CO<sub>2</sub> making it an attractive processing solvent for tailoring porous silica in this dissertation, namely a high diffusivity for quick transport in the pores and templates, a low surface tension that prevents any pore collapse during depressurization and a pressure tunable solvent strength for controlled solvation of surfactant tail suggests its application for extracting ‘CO<sub>2</sub>-philic’ surfactant templates for obtaining the final porous silica without structure collapse. Indeed, several studies have used sc CO<sub>2</sub> processing to extract surfactant templates from both mesoporous silica powders<sup>275,352,353</sup> and films<sup>354</sup> and have demonstrated that sc CO<sub>2</sub> extraction results in more uniform pore size distribution compared to calcination for MCM-41 samples.<sup>352</sup> However, most of these studies either used very high pressures (> 125 bar) making the process less economic or co-solvents like ethanol<sup>354</sup> introducing solvent separation problems after extraction or had a low efficiency of surfactant removal (< 80 %).<sup>275</sup> Designing surfactant templates with specific ‘CO<sub>2</sub>-philic’ properties has potential to improve extraction with respect to all the problems discussed above. The first step towards designing ‘CO<sub>2</sub>-philic’ templates for extraction by sc CO<sub>2</sub> is to measure the solubility of different surfactants in compressed CO<sub>2</sub> as a screening tool for identifying surfactant systems with high solubility in. The solubility of a homologous series of nonionic fluorinated surfactants (nicotinic acid esters) in compressed CO<sub>2</sub> is reported here as a function of surfactant chain length, concentration and CO<sub>2</sub> pressure and temperature.

## A.2 Experimental Section

**Table A.1** Structures of the nonionic fluorinated nicotinic acid esters in this study

Name	Chemical Name	Structure
FONE-1	1H,1H Perfluoro octyl nicotinate	
FONE-2	1H,1H,2H,2H - Perfluoro-octyl nicotinate	
FHNE-2	1H,1H,2H,2H - Perfluoro-hexyl nicotinate	

Solubility studies in compressed CO<sub>2</sub> were conducted using a Pressure Volume Temperature (PVT) apparatus (DB Robinson Design & Manufacturing Ltd., Edmonton, Canada). The apparatus consists of a temperature-controlled airbath unit ( $\pm 0.1$  °C), which houses a high-pressure variable view cell (total sample volume of 130 mL; rated to 700 bars and 200 °C) equipped with a magnetic mixer. The temperature of the airbath unit is controlled by a digital controller (Omron Corporation, model E5AK; Kyoto, Japan). The system pressure is measured with a digital pressure indicator (Heise Model 901A, Dresser Industries Inc., Newton, CT;  $\pm 0.5$  bar). The temperature of the airbath unit and the PVT cell is measured with two Platinum 100 $\Omega$  ( $\pm 0.3$  °C) Resistance Temperature Devices. The variable volume view cell is pressurized using a syringe pump (ISCO Model 260D, Lincoln, NE) to generate pressure in an overburden fluid (water), sealed from the sample by a O-ring piston. An additional syringe pump (ISCO 500D) is used to inject the desired amount of CO<sub>2</sub> into the view cell.

An experimental run was initiated by loading a measured amount of the sample into the cell. After the system was thermally equilibrated, CO<sub>2</sub> was injected to make a mixture with an initial surfactant concentration of 10 weight %. This mixture was stirred continuously. The pressure of the view cell was then increased slowly until the mixture of

surfactant and CO<sub>2</sub> formed a single, homogenous and optically transparent phase. The formation of a transparent phase was noted both by the naked eye and also with the help of a CCD camera-based measurement system. The pressure of the view cell was then decreased and the cloud-point pressure (CPP) was identified as the pressure at which the solution is no longer transparent. Bubble point pressure (BPP) is the pressure at which a homogenous, one phase liquid on decreasing the pressure starts forming a two phase liquid with the first stream of bubbles coming out of the liquid. In some cases when the surfactant is highly soluble in CO<sub>2</sub>, BPP of the solution is at a higher pressure than the CPP and the bubble point pressure was reported as a measure of surfactant solubility. The procedure of recording the CPP or BPP was duplicated to obtain an averaged pressure reading. Once the CPP was recorded, more CO<sub>2</sub> was injected to decrease the surfactant concentration. CPP for any surfactant at a particular temperature was observed for a range of surfactant concentration from 10 wt% to 1 wt%.

### **A.3 Results and Discussion**

The CPP of the three surfactants, FONE-2 and FHNE-2 is reported in Figure 1 as a function CO<sub>2</sub> temperature (25°C, 35°C and 45°C) and surfactant concentration (10 wt% to 1 wt% in CO<sub>2</sub>). For a given temperature, a single homogenous one phase is present above the CPP whereas the solution turns opaque below the CPP. All three surfactants were soluble in liquid CO<sub>2</sub> at 25°C at any pressure above BPP for all concentrations and hence BPP was identified as a measure of solubility. For all surfactants and at a fixed concentration, CPP increased with an increase in temperature. For example, for FONE-2 at a surfactant concentration of 5 wt%, CPP at 35°C is 80 bar while CPP at 45°C is 95 bar (Figure A.1). The CPP at a particular temperature for this surfactant system is not strongly dependent on the surfactant concentration (Fig. 1) and is consistent with previous reports of solubility of siloxane-based nonionic amphiphiles in CO<sub>2</sub>.<sup>355</sup> However, the trend is not general for all surfactants in CO<sub>2</sub> as demonstrated in another study where an increase in CPP was noted with concentration of fluoroethers at a particular temperature.<sup>356</sup> The CPP for this homologous series of surfactants is not significantly dependent on the length of the fluorinated chain. For example at 35°C and



surfactant concentration of 6 wt%, CPP of FONE-2 (C8 tail) is 80 bar while that for

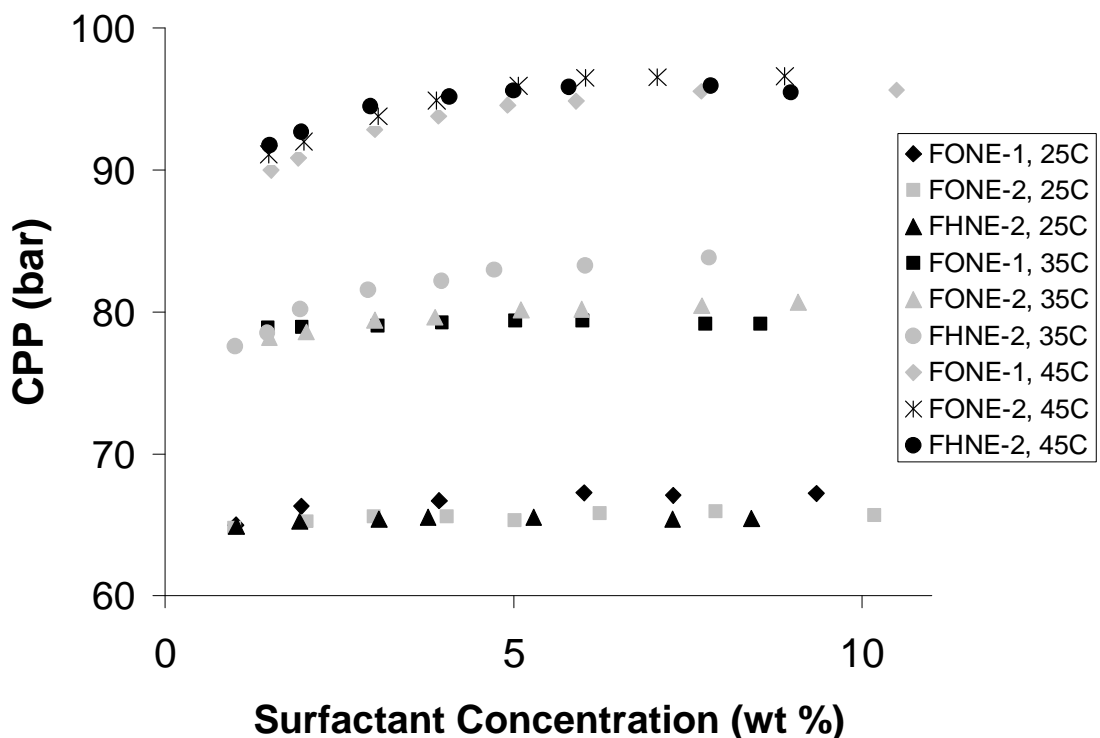


**Figure A.1.** Cloud point and bubble point pressure for FONE-1, FONE-2 and FHNE-2 as a function of surfactant concentration at different temperatures.

FHNE-2 (C6 tail) is 83 bar (Figure A.1). CPP for homologous surfactants is expected to increase with an increase in the molecular weight of the surfactant. However, for this system the additional CO<sub>2</sub>-philicity of FONE-2 due to a greater number of CF<sub>2</sub> groups in its tail may compensate for its increased molecular weight due to its longer chain and result in the final solubility being similar for both surfactants. FONE-1 having the same number of carbon atoms in its tail but with one extra CF<sub>2</sub> group compared to FONE-2 has a CPP very similar to that of FONE-2 (Figure A.1). The negligible difference in CPP between the two surfactants is attributed to the presence of large number 'CO<sub>2</sub>-philic' groups in both tails (all the CF<sub>2</sub> and carbonyl groups) which leads to a very low CPP for both surfactants and the extra CF<sub>2</sub> group in FONE-1 does not make a significant difference in solubility.

#### A.4 Conclusions

We successfully demonstrated the very high solubility of a homologous series of custom designed nonionic fluorinated surfactants in compressed CO<sub>2</sub>. The lowest CPP reported in this study was around 64 bar for all three surfactants at 25°C and for all concentrations and was actually the BPP of CO<sub>2</sub>. This was the result of the very high solubility of all three surfactants in CO<sub>2</sub> resulting from the specific design of ‘CO<sub>2</sub>-philic’ surfactants by combining different ‘CO<sub>2</sub>-philic’ groups. Indeed, CPP’s reported in this study is lower than most reported CPP values in literature.<sup>356,357</sup> However, the surfactants could not be successfully used as templates to form ordered mesoporous silica materials and hence their high solubility in CO<sub>2</sub> could not be extended to template extraction using compressed CO<sub>2</sub>.

## APPENDIX B

### INVESTIGATION TOWARDS ALIGNMENT OF MESOCHANNELS IN MESOPOROUS SILICA FILMS THROUGH APPLICATION OF A MAGNETIC FIELD

#### B.1 Introduction

CO<sub>2</sub> processing of thin films to result in pore expansion and extension of silica condensation timescales has indicated the advantages of the Modulable Steady State (MSS) period (silica condensation period) in silica film synthesis to alter silica structure through application of an external field. Indeed, different studies have modified thin film structure during the MSS period by changing system humidity<sup>134</sup> and ethanol vapor concentration<sup>134</sup> and changed thin film orientation by changing the hydrophilic properties of substrates.<sup>141</sup> External magnetic fields have also been successfully used to alter orientation in silicate-surfactant liquid crystals<sup>358,359</sup> and mesoporous silica monoliths<sup>359</sup> and thin films.<sup>337</sup> Preferential orientation of the channels was obtained based on the interactions between the magnetic field and the collective diamagnetic susceptibilities of all the molecular components in the material. The orientation obtained for mesoporous silica in presence of the magnetic field was demonstrated to remain even after removal of the magnetic field and also extraction of the surfactants. Preferred orientation, especially where the porous channels are oriented orthogonal to the substrate has potential to increase applications of the porous films in membrane separation and photovoltaic cells.<sup>143</sup> However, one problem in all the above studies was the requirement for a magnetic field with very high strength, since the diamagnetic susceptibility of the hydrocarbon groups in the templates is low and application of NMR instruments<sup>358,359</sup> or superconducting magnets with large currents<sup>337</sup> were needed to generate the required magnetic field (about 12 T). The diamagnetic susceptibility of fluorocarbon groups are much larger than hydrocarbon groups and it has been demonstrated that the hexagonal channels of a fluorinated liquid crystal can be preferentially aligned in a magnetic field with strength as low as 2T.<sup>360</sup> Having successfully synthesized for the first time, fluorinated surfactant templated mesoporous silica thin films, the objective was to use a

low strength magnetic field to achieve orthogonally oriented pore arrays in mesoporous silica films.

## **B.2 Experimental Section**

Six permanent Neodymium block magnets (NdFeB, Grade N 42, dimensions 4" x 2" x 1/2" thick) with field strength of about 0.25 T each were obtained from K&J Magnetics, Inc. and placed in a custom designed wooden holder such that 3 magnets were on each side of a narrow slit of width 2 cm. With the field strength being additive, the strength in the narrow slit is expected to be greater than 1T. Mesoporous silica thin films were synthesized using HFOPC as template by dip-coating solution on a hydrophilic glass substrate and immediately after coating was placed inside the slit in the magnetic field. The placement of the film and the block magnets was done to ensure the direction of the magnetic field perpendicular to the substrate.

Characterization of the film structure and orientation was performed using 1D XRD and TEM. Sample preparation was performed in a similar manner as done in the rest of the dissertation. It has been demonstrated previously that when 2D hexagonally structured films have their porous channels oriented orthogonal to the substrate, no X-ray diffraction occurs in the detector plane for a 1D XRD.<sup>145</sup> Previously, the absence of such peaks in 1D XRD spectra combined with the presence of ordered structure in TEM images has been used to confirm the synthesis of mesoporous silica thin films with 2D HCP ordering and orthogonally oriented channels.<sup>143</sup> Alternatively, the presence of peaks in 1D XRD for 2D hexagonally ordered thin films indicate orientation of the porous channels parallel to the substrate.<sup>145</sup>

## **B.3 Results and Discussions**

Surfactant templated mesoporous silica thin film synthesized by dip-coating and without the application of any external field has been demonstrated to result in the porous channels aligned parallel to the substrate for 2D hexagonally ordered materials.<sup>143</sup> It has been previously demonstrated that hexagonal silicate-surfactant liquid crystal domains align their channels parallel to a magnetic field when no other additives are present.<sup>358</sup>

Therefore, our experimental set-up is expected to result in orthogonal orientation of porous channels for 2D hexagonally ordered mesoporous silica thin films.

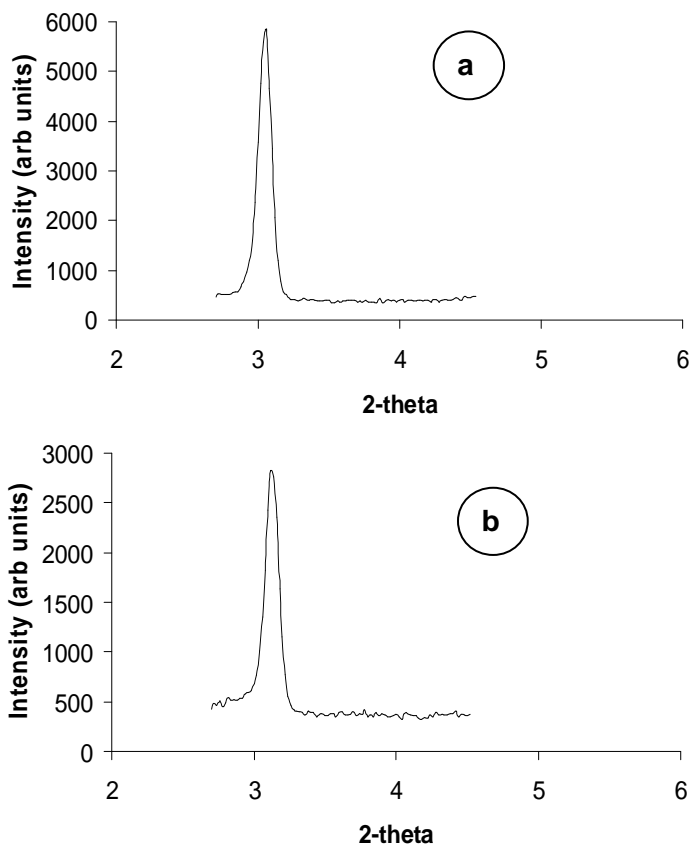


**Figure B.1.** XRD plots of silica thin film templated with HFOPC and with (a) no magnetic field and (b) in the presence of magnetic field of strength  $\sim 1$  T

Figure B.1 reports the XRD plots of HFOPC templated silica thin films without the application of any external field (Figure B.1a) and after processing in the magnetic field immediately after coating for 72 h (Figure B.1b). For both the plots, sharp peaks corresponding to the (100) reflection of 2D hexagonally confirms the synthesis of ordered mesoporous silica. TEM images (not shown) further confirm the long range ordering of the synthesized materials both with and without application of the magnetic field. The presence of the peak further confirms the orientation of the porous channels to be parallel

to the substrate and suggests that the magnetic field was unsuccessful in obtaining orthogonal orientation of the porous channels.

#### **B.4 Conclusions**

The parallel orientation of the porous channels in a 2D hexagonally ordered porous silica thin film was not significantly altered upon application of an external magnetic field during the MSS period. The field strength in the vicinity of the film (expected to be about 1T) was lower than the field strength of about 2T used in a previous study to align channels of a fluorinated hexagonal liquid crystal<sup>360</sup> and was probably too low to significantly alter channel orientation. Future directions of this study should be aimed at increasing the field strength. Also additional characterization methods including 2D XRD would give a better idea of the exact change in orientation of the porous channels compared to 1D XRD which can only identify orientation change when the porous channels are aligned almost perpendicular to the substrate and is not an effective technique to identify partial change in orientation.

## REFERENCES

- (1) Doblin, C.; Mathews, J. F.; Turney, T. W. *Catal. Lett.* **1994**, *23*, 151.
- (2) Clerici, M.C. *Appl. Catal.* **1991**, *68*, 249.
- (3) Dines, M. B.; Digiacomo, P. *Inorg. Chem.* **1981**, *20*, 92.
- (4) Castillo, M. L.; Guil, A.; Grange, P. *Catal. Lett.* **1996**, *36*, 237.
- (5) Xia, H.-Q.; Hidajat, K.; Kawi, S. *Chem. Commun.* **2000**, 2229.
- (6) Matsushashi, H.; Tanaka, M.; Nakamura H.; Arata, K. *Appl. Catal. A.* **2001**, *208*, 1.
- (7) Chen, C.-L.; Cheng, S.; Lin, H.-P.; Wong, S.-T.; Mou, C.-Y. *Appl. Catal. A.* **2001**, *215*, 21.
- (8) White, M.G. *Catal. Today* **1993**, *18*, 73.
- (9) Zhang, Z.; Han, Y.; Xiao, F.-S.; Qiu, S.; Zhu, L.; Wang, R.; Zou, B.; Sun, H.; Zhang, Z.; Zhao, D.; Yen, W. *J. Am. Chem. Soc.* **2001**, *123*, 5014.
- (10) Job, N.; Fernando, M.; Pereira, R.; Lambert, S.; Cabiac, A.; Delahay, G.; Colomer, J.; Marien, J.; Figueiredo, J.; Pirard, J. *Journal of Catalysis* **2006**, *240*, 160.
- (11) Van Der Voort, P.; Baltes, M.; Vansant, E.F.; White, M.G. *Interface Sci.* **1997**, *5*, 209.
- (12) Cheng, Y.L.; Trewyn, B.G.; Jeftinija, D.M.; Jeftinija, K.; Shu, X.; Jeftinija, S.; Lin, V.S.-Y. *J. Am. Chem. Soc.* **2003**, *125*, 4451.
- (13) Rámilia, B.; Muñoz, J.; Pérez-Pariente, M.; Vallet-Regí, J. *Sol-Gel Sci. Technol.* **2003**, *26*, 1199.
- (14) Thomas, K. M. *Catalysis Today*, **2007**, *120*, 389.
- (15) Liu, J.; Fryxell, G. E.; Mattigod, S.; Zemanian, T. S.; Shin, Y.; Wang, L.-Q. *Studies in Surface Science and Catalysis*, **2000**, *129*, 729.
- (16) Liu, A.M.; Hidajat, K.; Kawi, S.; Zhao, D.Y. *Chem. Commun.* **2000**, *13*, 1145.
- (17) Etienne, M.; Sayen, S.; Lebeau, B.; Walcarius, A. *Stud. Surf. Sci. Catal.* **2002**, *141*, 615.
- (18) Park, D.H.; Nishiyama, N.; Egashira, Y.; Ueyama, K. *Ind. Eng. Chem. Res.* **2001**, *40*, 6105.
- (19) Tsuru, T. *Separation and Purification Methods*, **2001**, *30*, 191.
- (20) Kumar, P.; Vijayalaxmi, R. P. *Chemical Industry Digest*, **2005**, *18*, 81.
- (21) Brandon, N. P.; Brett, D. J. *Philosophical Transactions of the Royal Society of London, Series A: Mathematical, Physical and Engineering Sciences*, **2006**, *364*, 147.
- (22) Foell, H.; Carstensen, J.; Frey, S. *Journal of Nanomaterials*, **2006**, 1687.
- (23) Hartmann, M. *Chem. Mater.* **2005**, *17*, 4577.
- (24) Beck, J. S. V., J. C.; Roth, W. J.; Leonowicz, M. E.; Kresge, C. T.; Schmitt, K. T.; Chu, C. T.-W.; Olson, D. H.; Sheppard, E. W.; McCullen, S. B.; Higgins, J. B.; Schlenker, J. L. *J. Am. Chem. Soc.* **1992**, *114*, 10834.
- (25) Ogawa, M. *Langmuir*, **1995**, *11*, 4639.
- (26) Lu, Y.; Ganguli, R.; Drewien, C. A.; Anderson, M. T.; Brinker, C. J.; Gong, W.; Guo, Y.; Soyez, H.; Dunn, B.; Huang, M. H.; Zink, J. I.; *Nature*, **1997**, *389*, 364
- (27) Wu, X.; Ruan, J.; Ohsuna, T.; Terasaki, O.; Che, S. *Chem. Mater.* **2007**, *19*, 1577.
- (28) Ting, C.; Sheu, H.; Wu, W.; Wan, B. *Journal of The Electrochemical Society*, **2007**, *154*.
- (29) Koganti, V.R.; Rankin, S.E. *J. Phys. Chem. B* **2005**, *109*, 3279.

- (30) Meng, X.; Di, Y.; Zhao, L.; Jiang, D.; Li, S. Xiao, F. *Chem. Mater.* **2004**, *16*, 5518.
- (31) Tan, B.; Vyas, S.H.; Lehmler, H.; Knutson, B.L.; Rankin, S.E. *Chem. Mater.*, **2005**, *17*, 916.
- (32) Yang, Y.; Lu, Y.; Lu, M.; Huang, J.; Haddad, R.; Xomeritakis, G.; Liu, N.; Malanoski, A.; Sturmayer, D.; Fan, H.; Sasaki, D.; Assink, R.; Shelnutz, J.; Swol, F.; Lopez, G.; Burns, A.; Brinker, C. J. *J. Am. Chem. Soc.* **2003**, *125*, 1269.
- (33) Zhang, W.; Daly, B.; Callaghan, J.; Zhang, L.; Shi, J.; Li, C.; Morris, M.A.; Holmes, J.D. *Chem. Mater.* **2005**, *17*, 6407.
- (34) Bois, L.; Bonhomme, A.; Ribes, A.; Pais, B.; Raffin, G.; Tessier, F. *Colloids and Surfaces A: Physicochem. Eng. Aspects*, **2003**, *221*, 221.
- (35) Zhang, H.; Sun, Y.; Ye, K.; Zhang, P.; Wang, Y. *J. Mater. Chem.*, **2005**, *15*, 3181.
- (36) Hiyoshi, N.; Yogo, K.; Yashima, T. *Micr. Meso. Mater.*, **2005**, *84*, 357.
- (37) Blin, J.L.; Otjacques, C.; Herrier, G.; and Su, B. *Langmuir* **2000**, *16*, 4229.
- (38) Branton, P.J.; Doughert, J.; Lockhart, G.; White, J.W. *Charact. Porous Solids IV* **1997**, 668.
- (39) Kimura, T.; Sugahara, Y.; Kuroda, K. *Chem. Commun.* **1998**, 559.
- (40) Kunieda, H.; Ozawa, K.; Huang, K.L. *J. Phys. Chem. B* **1998**, *102*, 831.
- (41) Sarkari, M.; Darrat, I.; Knutson, B. L. *Biotechnology Progress*, **2003**, *19*, 448.
- (42) Hanrahan, J. P.; Ziegler, K. J.; Glennon, J.D.; Steytler, D. C.; Eastoe, J.; Dupont, A.; Holmes, J. D. *Langmuir* **2003**, *19*, 3145.
- (43) DeSimone, J.M.; Guan, Z.; Elsbrand, C.S.; *Science*, **1992**, *257*, 945.
- (44) Cooper, A.I. *J. Mater. Chem.* **2000**, *10*, 207.
- (45) Shim, J.; Johnston, K.P. *Ind. Eng. Chem. Res.* **2002**, *41*, 4750.
- (46) Debenedetti, P.G.; Tom, J.W.; Kwauk, X.; Yeo, S.D. *Fluid Phase Equilibria*, **1993**, *82*, 311.
- (47) Ji, M.; Chen, X.; Wai, C. M.; Fulton, J. L. *J. Am. Chem. Soc.* **1999**, *121*, 2631.
- (48) McLeod, M. C.; McHenry, R. S.; Beckman, E. J.; Roberts, C. B. *J. Phys. Chem. B* **2003**, *107*, 2693.
- (49) Novick, B.J.; DeSimone, J.M.; Carbonell, R.G. *Ind. Eng. Chem. Res.* **2004**, *43*, 515.
- (50) Sarkari, M.; Knutson, B. L.; Chen, C-S. *Biotechnology and Bioengineering*, **1999**, *65*, 258.
- (51) Holmes, J. D.; Steytler, D. C.; Rees, G. D.; Robinson, B. H. *Langmuir* **1998**, *14*, 6371.
- (52) Zhang, X.; Pham, J.Q.; Ryza, N.; Green, P.F.; Johnston, K.P. *J. Vac. Sci. Technol. B*, **2004**, *22*, 818.
- (53) DeSimone, J. M. *Science* **2002**, *297*, 799.
- (54) Wakayama, H.; Fukushima, Y. *Ind. Eng. Chem. Res.* **2006**, *45*, 3328.
- (55) Pai, R. A.; Humayun, R.; Schulberg, M. T.; Sengupta, A.; Sun, J.; Watkins, J. J. *Science* **2004**, *303*, 507.
- (56) Xua, Q.; Hea, J.; Changa, Y.; Hanb, B.; Guoc, Y.; Su, Y. *Materials Science and Engineering B*, **2005**, *123*, 41.
- (57) Jackson, M.A.; Mbaraka, I.K.; Shanks, B.H. *Applied Catalysis A: General*, **2006**, *310*, 48.



- (58) Huang, J.; Jiang, T.; Han, B.; Mu, T.; Wang, Y.; Li, X.; Chen, H. *Catalysis Letters*, **98**, 225.
- (59) Huang, L.; Kawib, S.; Pohb, C.; Hidajatb, K.; Ng, S.C. *Talanta*, **2005**, *66*, 943.
- (60) Grieken, R.; Calleja, G.; Stucky, G.D.; Melero, J.A.; Garcia, R.A.; Iglesias, J. *Langmuir* **2003**, *19*, 3966.
- (61) Jacobson, G. B.; Lee, C. T.; Johnston, K. P. *J. Org. Chem.* **1999**, *64*, 1201.
- (62) Chattopadhyay, P.; Gupta, R.B. *Ind. Eng. Chem. Res.* **2003**, *42*, 465.
- (63) Ji, M.; Chen, X.; Wai, C. M.; Fulton, J. L. *J. Am. Chem. Soc.* **1999**, *121*, 2631.
- (64) Lee, C. T.; Johnston, K. P. Dai, H. J.; Cochran, H. D.; Melnichenko, Y. B.; Wignall, G. D. *J. Phys. Chem. B* **2001**, *105*, 3540.
- (65) Consani, K. A.; Smith, R. D. *J. Supercrit. Fluids* **1990**, *3*, 51.
- (66) O'Shea, K.; Kirmse, K.; Fox, M. A.; Johnston, K. P. *J Phys Chem* **1991**, *95*, 7863.
- (67) Psathas, P.A.; Sander, E.A.; Ryoo, W.; Mitchell, D.; Lagow, R.J.; Lim, K.T.; Johnston, K. P. *J. Dispersion Science and Technology*, **2002**, *23*, 81.
- (68) Sagisaka, M.; Fujii, T.; Ozaki, Y.; Yoda, S.; Takebayashi, Y.; Kondo, Y.; Yoshino, N.; Sakai, H.; Abe, M.; Otake, K. *Langmuir* **2004**, *20*, 2560.
- (69) da Rocha, S.R.P.; Harrison, K.L.; Johnston, K. P. *Langmuir* **1999**, *15*, 419.
- (70) da Rocha, S. R. P.; Johnston, K. P.; Rossky, P. J. *J. Phys. Chem. B* **2002**, *106*, 13250.
- (71) Dickson, J.L.; Smith, P.G.; Dhanuka, V.V.; Srinivasan, V.; Stone, M.T.; Rossky, P.J.; Behles, J.A.; Keiper, J.S.; Xu, B.; Johnson, C.; DeSimone, J. M. Johnston, K. P. *Ind. Eng. Chem. Res.* **2005**, *44*, 1370.
- (72) Eastoe, J.; Gold, S.; Steytler, D. C. *Langmuir* **2006**, *22*, 9832.
- (73) Eastoe, J.; Gold, S.; Rogers, S.; Wyatt, P.; Steytler, D. C.; Gurgel, A.; Heenan, R.K.; Fan, X.; Beckman, E.J.; Enick, R.E. *Angew. Chem. Int. Ed.* **2006**, *45*, 3675 .
- (74) Beckman, E.J. *Chem. Commun.* **2004**, 1885.
- (75) Hanrahan, J. P.; Copley, M. P.; Ziegler, K. J.; Spalding, T. R.; Morris, M. A.; Steytler, D. C.; Heenan, R. K.; Schweins, R.; Holmes, J. D. *Langmuir* **2005**, *21*, 4163.
- (76) Osei-Prempeh, G.; Lehmler, H.; Rankin, S.E.; Knutson, B.L.; *Micro. Meso. Mater.* **2005**, *85*, 16.
- (77) Osei-Prempeh, G. *Ph.D. Dissertation*, University of Kentucky, **2007**.
- (78) Han, Y.; Li, D.; Zhao, L.; Song, J.; Yang, X.; Li, N.; Li, C.; Wu, S.; Xu, X.; Meng, X.; Lin, K.; Xiao, F.-S. *Angew. Chem., Int. Ed.* **2003**, *42*, 3633.
- (79) Xing, R. *Ph.D. Dissertation*, University of Kentucky, **2007**.
- (80) Vyas, S.M.; Turanek, J.; Knotigova, P.; Kasna, A.; Kvardova, V.; Koganti, V.R.; Rankin, S.E. Knutson, B.L.; Lehmler, H. *New J. Chem.*, **2006**, *30*, 944.
- (81) Flanigen, E. M., *Pure appl. Chem.*, **1980**, *52*, 2191.
- (82) Guliants, V.V.; Carreon, M.A.; Lin, Y.S. *Journal of Membrane Science*, **2004**, *235*, 53.
- (83) Gottoli, G.; Ayers, R.; Schowengerdt, F.; Moore, J. *Trans. Soc. Biomater.* **2003**, *29*, 239.
- (84) Moore, J.C. *J. Polym. Sc. A2*, **1964**, 835
- (85) Albright, R.L. *React. Polym.* **1986**, *4*, 155
- (86) Coutinho, F.M.; Neves, M.A.; Dias, M.L. *Macromol. Symp.* **2002**, *189*, 27

- (87) Breck, D.W. *Zeolite Molecular Sieves: Structure, Chemistry and Use*, Wiley, New York, **1974**.
- (88) Smith, J.V. *Chem. Rev.* **1988**, 88, 149.
- (89) Corma, A. *Chem. Rev.* **1997**, 97, 2373
- (90) Suib, S. L., *Chem. Rev.*, **1993**, 93, 803
- (91) Occelli, M. L.; Tindawa, R. M. *Clays Clay Miner.* **1983**, 31, 22.
- (92) Brinker, C. J., and Scherer, G. W., *Sol Gel Science. The Physics and Chemistry of Sol Gel Processing* (San Diego, California: Academic Press) **1990**.
- (93) Kresge, C. T.; Leonowicz, M. E.; Roth, W. J.; Vartuli, J. C.; Beck, J. S. *Nature* **1992**, 359, 710.
- (94) Zhao, D.; Huo, Q.; Feng, J.; Chmelka, B. F.; Stucky, G. D. *J. Am. Chem.Soc.* **1998**, 120, 6024.
- (95) Zhao, D.; Feng, J.; Huo, Q.; Melosh, N.; Fredrikson, G.; Chmelka, B.; Stucky, G. D. *Science* **1998**, 279, 548.
- (96) Yang, P.; Zhao, D.; Margolese, D.; Chmelka, B.; Stucky, G. D. *Nature* **1998**, 396, 152.
- (97) Ernst, S.; Hartmann, M.; Munsch, S. *Stud. Surf. Sci. Catal.* **2001**, 135, 4566.
- (98) Cao, J.; Sun, J.-Z.; Li, H.-Y.; Hong, J.; Wang, M. *J. Mater. Chem.* **2004**, 14, 1203.
- (99) Uchida, S.; Chiba, R.; Tomiha, M.; Masaki, N.; Shirai, M. *Electrochemistry* **2002**, 70, 418.
- (100) Qu, F.; Zhu, G.; Lin, H.; Zhang, W.; Sun, J.; Li, S.; Qiu, S. *J. Solid State Chem.* **2006**, 179, 2027.
- (101) Stokes, R.J & Evans, D.F. *Fundamentals of Interfacial Engineering*, John Wiley & Sons, **1997**.
- (102) Hiemenz P. C.; R. Rajagopalan, *Principles of Colloid and Surface Chemistry*, Dekker, New York, NY, 3rd. edn., **1997**.
- (103) Nagarajan, R.; Ruckenstein, E *Langmuir*, **1991**, 7, 2934
- (104) Nagarajan, R.; Ruckenstein, E *Langmuir*, **2000**, 16, 6400
- (105) Nagarajan, R.; Wang, C-C *Langmuir*, **1995**, 11, 4673
- (106) Puvvada, S.; Blankschtein, D. *J. Chem. Phys.* **1990**, 92, 3710
- (107) Srinivasan, V.; Blankschtein, D. *Langmuir*, **2005**, 21, 1647
- (108) Israelachvili, J. N. *Intermolecular and Surface Forces*, Academic Press, New York, 2nd edn., **1992**.
- (109) Israelachvili, J.; Mitchell, D.J.; Ninham, B.W. *J. Chem. Soc. Faraday Trans. 2* **1976**, 72, 1525.
- (110) Nagarajan, R. *Langmuir*, **2002**, 18, 31
- (111) Rosen, M. J.; Tracy, D. J. *J. Surfactants Deterg.*, **1998**, 1, 547.
- (112) Edler, K.; Roser, S. *Int. Reviews in Physical Chemistry*, 2001, 20, 387
- (113) Wang, K.; Karlsson, G.; Almgren, M.; Asakawa, T. *J. Phys. Chem. B* **1999**, 103, 9237.
- (114) Wang, K.; Orädd, G.; Almgren, M.; Asakawa, T.; Bergenståhl, B. *Langmuir* **2000**, 16, 1042.
- (115) Kissa, E. *Fluorinated Surfactants and Repellents*, 2<sup>nd</sup> Edition, CRC; **2001**
- (116) Abe, M. *Curr. Opin. Colloid Interface Sci.*, **1999**, 4, 354.
- (117) Tanev, P.T.; Pinnavaia, T.J. *Science*, **1995**, 267, 86.

- (118)Blin, J.L.; Leonard, A.; Su, B.L. *J. Phys. Chem. B* **2001**, *105*, 6070.
- (119)Ryoo, R.; Kim, J.M.; Ko, C.H.; Shin, C.H. *J. Phys. Chem.* **1996**, *100*, 17718.
- (120)Yanagisawa, T.; Shimizu, T.; Kuroda, K.; Kato, C. *Bull. Chem. Soc. Jpn.* **1990**, *63*, 988.
- (121)Linssen, T.; Cassiers, K.; Cool, P.; Vansant, E.F. *Advances in Colloid and Interface Science* **2003**, *103*, 121
- (122)Hoffmann, F.; Cornelius, M.; Morell, J.; Froba, M. *Angew. Chem. Int. Ed.* **2006**, *45*, 3216
- (123)Tan, B.; Lehmler, H.; Vyas, S.H.; Knutson, B.L.; Rankin, S.E. *Nanotechnology*, **2005**, *16*, 8502.
- (124)Tan, B.; Dozier, A.; Lehmler, H.; Knutson, B.L.; Rankin, *Langmuir*, **2004**, *20*, 6981.
- (125)Li, S.; Sun, J.; Li, Z.; Peng, H.; Gidley, D.; Ryan, T. Yan, Y. *J. Phys. Chem. B*, **2004**, *108*, 11689
- (126)Yang, H; Coombs, N; Sokolov, I; Ozin, G.A. *J Mater Chem* **1997**, *7*, 1285
- (127)Braun AE. *Semiconductor Int* **1999**;56, 25.
- (128)Brinker, C. J. *Curr. Opin. Colloid Interface Sci.* **1998**, *3*, 166.
- (129)Liu, N. G.; Dunphy, D. R.; Atanassov, P.; Bunge, S. D.; Chen, Z.; Lopez, G. P.; Boyle, T. J.; Brinker, C. J. *Nano Lett.* **2004**, *4*, 551.
- (130)Zhao, D.; Yang, P.; Melosh, N.; Feng, J.; Chmelka, B. F.; Stucky, G. D. *Adv. Mater.* **1998**, *10*, 1380
- (131)Brinker, C. J. Lu, Y. Sellinger, A fan, H *Adv. Mater.* **1999**, *11*, 579
- (132)Doshi, D.A.; Huesing, N.K.; Lu, M.; Fan, H.; Lu, Y.; Simmons, P. K.; Potter, B.G. Jr.; Hurd, A.J.; Brinker, C.J.; *Science*, 2000, *290*, 107
- (133) Lu, Y.; Yang, Yi; Sellinger, A.; Lu, M.; Huang, J.; Burns, A. R.; Sasaki, D. Y.; Shelnutt, J.; Brinker, C. J.; et. al.; *Nature*, 2001, *410*, 913
- (134)Cagnol, F; Grosso, D.; Soler-Illia, G.J.A.A.; Crepaldi, E.L.; Babboneau, F.; Amenitsch, H.; Sanchez, C. *J. Mater. Chem.* **2003**, *13*, 61.
- (135)Huo, Q.; Margolese, D.; Ciesla, U.; Feng, P.; Gier, T.E.; Sieger, P.; Leon, R.; Petroff, P.; Schuth, F.; Stucky, G.D. *Nature*, **1994**, *368*, 317.
- (136)Grosso, D.; Balkenende, A. R.; Albouy, P. A.; Lavergne, M.; Babonneau, F. *J. Mater. Chem.* **2000**, *10*, 2085.
- (137)Grosso, D.; Babonneau, F.; Albouy, P. A.; Amenitsch, H.; Balkenende, A. R.; Brunet-Bruneau, A.; Rivory, J. *Chem. Mater.* **2002**, *2*, 931.
- (138)Besson, S.; Gacoin, T.; Jacquot, C.; Ricolleau, C.; Babonneau, D.; Boilot, J.-P. *J. Mater. Chem.* **2000**, *10*, 1331.
- (139)Doshi, D.A.; Gibaud, A.; Liu, N.; Sturmayer, D.; Malanoski, A.P.; Dunphy, D.R.; Chen, H.; Narayanan, S.; MacPhee, A.; Wang, J.; Reed, S.T.; Hurd, A.J.; Swol, F.; Brinker, C.J. *J. Phys. Chem. B* **2003**, *107*, 7683.
- (140)Grosso, D.; Babonneau, F.; Soler-Illia, G. J. d. A. A.; Albouy, P.-A.; Amenitsch, H. *Chem. Commun.* **2002**, 748.
- (141)Alonso, B.; Balkenende, A. R.; Albouy, P. A.; Durand, D.; Babonneau, F.; *New J. Chem.*, **2002**, *26*, 1270
- (142)Crepaldi, E.; Soler-Illia, G.; Grosso, D.; Cagnol, F.; Ribot, F.; Sanchez, C. *J. Am. Chem. Soc.* **2003**, *125*, 9770
- (143)Koganti, V.R. *Ph.D. Dissertation*, University of Kentucky, **2006**.

- (144) Cullity, B.D.; Stock, S.R. *Elements of X-Ray Diffraction*, Prentice Hall, **2001**.
- (145) Hillhouse, H. W.; van Egmond, J. W.; Tsapatsis, M.; Hanson, J. C.; Larese, J. Z. *Micropor. Mesopor. Mater.* **2001**, *44*, 639.
- (146) Qu, F.; Zhu, G.; Lin, H.; Zhang, W.; Sun, J.; Li, S.; Qiu, S. *J. Solid State Chem.* **2006**, *179*, 2027.
- (147) Ma, Y.; Qi, L.; Ma, J.; Wu, Y.; Liu, O.; Cheng, H. *Colloids and Surfaces A: Physicochem. Eng. Aspects* **2003**, *229*, 1.
- (148) Fuertes, A. B.; Lotaa, G.; Centeno, T. A.; Frackowiak, E. *Electrochimica Acta* **2005**, *50*, 2799.
- (149) Liu, K.; Fu, H.; Shi, K.; Xiao, F.; Jing, L.; Xin, B. *J. Phys. Chem. B*, **2005**, *109*, 18719.
- (150) Kruk, M.; Jaroniec, M.; Sayari, A. *Micropor. Mesopor. Mater.* **2000**, *35-36*, 543
- (151) Jana, S.K.; Nishida, R.; Shindo, K.; Kugita, T.; Namba, S. *Microporous and Mesoporous Materials*, **2004**, *68*, 133
- (152) Blin, J. L.; Stebe, M. J. *J. Phys. Chem. B*, **2004**, *108*, 11399
- (153) Ulagappan, N.; Rao, C. N. R. *Chem. Commun.* **1996**, 2759.
- (154) Lee, C. T. Jr.; Johnston, K. P. *J. Am. Chem. Soc.* **2003**, *125*, 3181.
- (155) Butler, R.; Hopkinson, I.; Cooper, A. I. *J. Am. Chem. Soc.* **2003**, *125*, 14473.
- (156) Butler, R.; Davies, C. M.; Cooper, A. I. *Adv. Mater.* **2001**, *13*, 1459
- (157) Johnston, K. P.; Harrison, K. L.; Clarke, M. J.; Howdle, S. M.; Heitz, M. P.; Bright, F. V.; Carlier, C.; Randolph, T. W. *Science* **1996**, *271*, 624-626.
- (158) Clarke, M. J.; Harrison, K. L.; Johnston, K. P.; Howdle, S. M. *J. Am. Chem. Soc.* **1997**, *119*, 6399-6406.
- (159) da Rocha, S. R.; Johnston, K. P. *Langmuir* **2000**, *16*, 3690-3695.
- (160) Lee, C. T., Jr.; Psathas, P. A.; Ziegler, K. J.; Johnston, K. P.; Dai, H. J.; Cochran, H. D.; Melnichenko, Y. B.; Wignall, G. D. *J. Phys. Chem. B* **2000**, *104*, 11094.
- (161) Eastoe, J.; Bayazit, Z.; Martel, S.; Steytler, D. C.; Heenan, R. K. *Langmuir* **1996**, *12*, 1423-1424.
- (162) Harrison, K. L.; Johnston, K. P.; Sanchez, I. C. *Langmuir* **1996**, *12*, 2637.
- (163) Ryoo, W.; Webber, S.E.; Johnston, K. P. *Ind. Eng. Chem. Res.* **2003**, *42*, 6348
- (164) Stone, M. T.; Smith, P. G.; da Rocha, S. R. P.; Rossky, P. J.; Johnston, K. P. *J. Phys. Chem. B* **2004**, *108*, 1962.
- (165) Dhanuka, V.V.; Dickson, J.L.; Ryoo, W.; Johnston, K. P. *Journal of Colloid and Interface Science* **2006**, *298*, 406
- (166) Dickson, J.L.; Smith, P.G.; Dhanuka, V.V.; Srinivasan, V.; Stone, M. T.; Rossky, P. J.; Johnston, K. P.; J.A. Behles, J.A.; Xu, B.; DeSimone, J.M. *Ind. Eng. Chem. Res.* **2005**, *44*, 1370.
- (167) Dickson, J.L.; Psathas, P.; Salinas, B.; Ortiz-Estrada, C.; Luna-Barcenas, G.; Hwang, H.; Lim, K.T.; Johnston, K. P. *Langmuir* **2003**, *19*, 4895
- (168) da Rocha, S. R. P.; Dickson, J.L.; Cho, D.; Rossky, P. J.; Johnston, K. P. *Langmuir* **2003**, *19*, 3114
- (169) Anand, M.; Bell, P.; Fan, X.; Enick, R.M.; Roberts, C.B. *J. Phys. Chem. B*, **2006**, *110*, 14693.
- (170) Kalyanasundaram, K. *Langmuir* **1988**, *4*, 942.
- (171) Behera, G. B.; Mishra, B. K.; Behera, P. K.; Panda, M. *Adv. Colloid Interface Sci.* **1999**, *82*, 1.

- (172)Goto, Y.; Hagihara, Y. *Biochemistry*, **1992**, *31*, 732
- (173)Parkhurst, K.M.; Parkhurst, L.J. *J. Biomed. Opt.* **1996**, *1*, 435
- (174)Hu, Y.; Kramer, M.C.; Boudreaux, C.J.; McCormick, C.L. *Macromolecules*, **1995**, *28*, 7100.
- (175)Huang, H.; Verrall, R.E.; Skalski, B. *Langmuir*, **1997**, *13*, 4821.
- (176)Owen, C. S. *J. Membrane Biology*, **1980**, *54*, 13.
- (177)Lakowicz, J.R. *Principles of Fluorescence Spectroscopy*, New York, Kluwer Academic, Plenum, **1999**.
- (178)Suppam, P.; Ghoneim, N. *Solvatochromism*, Royal Society of Chemistry, **1997**.
- (179)Kim, S.Y.; Semyonov, A.N.; Twieg, R.J.; Horwich, A.L.; Frydman, J.; Moerner, W.E. *J. Phys. Chem. B* **2005**, *109*, 24517
- (180)Mchedlov-Petrosyan, N.; Vodolazkaya, N.A.; Kornienko, A.; Karyakina, E.L.; Reichardt, C. *Langmuir* **2005**, *21*, 7090
- (181)Kosower, E.M. *An Introduction to Physical Organic Chemistry*, John Wiley and Sons, New York, **1968**.
- (182)Reichardt, C. *Chem. Rev.* **1994**, *94*, 2319
- (183)Kamlet, M.J.; Abboud, J.L.M.; Taft, R.W. *J. Am. Chem. Soc.* **1977**, *99*, 6027
- (184)Kalyanasundaram K.; Thomas J. K. *J. Am. Chem. Soc.* **1977**, *99*, 2039
- (185)Nakajima, A. *Bull. Chem. Soc. Jpn.* **1971**, *44*, 3272
- (186)Nakajima, A. *Spectrochim. Acta Part A*, **1974**, *30*, 860
- (187)Zana, R. *J. Phys. Chem. B* **1999**, *103*, 9117.
- (188)Almgren, M. *Adv. Colloid Interface Sci.* **1992**, *41*, 9. → first two together then correct order
- (189)Lebedeva, N.; Ranganathan, R.; Bales, B.L. *J. Phys. Chem. B* **2007**, *111*, 5781
- (190)Tachiya, M. *Kinetics of Non-homogeneous Processes: A Practical Introduction for Chemists, Biologists, Physicists and Materials Scientists*, G. R. Freeman, Ed. Wiley, New York, **1987**.
- (191)Melo, E. C. C.; Costa, S. M. B. *J. Chem. Soc. Faraday Trans.* **1990**, *86*, 2155.
- (192)Velazquez, M. M.; Costa, S. M. B. *Chem. Phys. Lett.* **1992**, *190*, 247.
- (193)Lehrer, S.S. *Biochemistry*, **1971**, *10*, 3254
- (194)Wasylewski, M.; Malecki, J.; Wasylewski, Z. *J. Protein Chem.* **1995**, *14*, 299
- (195)Poulos, A.T.; Kuzmin, V.; Gaecintov, N.E. *J. Biochem. Biophys. Methods*, **1982**, *6*, 269
- (196)Forster, T. *Ann. Phys.* **1948**, *2*, 55
- (197)Cai, K.; Schircht, V. *J. Biol. Chem.* **1996**, *271*, 27311
- (198)Chapman, E.R.; Alexander, K.; Vorherr, T.; Carafoli, E.; Storm, D.R. *Biochemistry*, **1992**, *31*, 12819
- (199)Adams, S.R.; Backskai, B.J.; Taylor, S.S.; Tsien, R.Y. *Fluorescent and Luminescent Probes for Biological Activity*, W.T. Mason, Academic Press, New York.
- (200)Cardullo, R.A.; Agarwal, S.; Flores, C.; Zamechnik, P.C.; Wolf, D.E. *Proc. Natl. Acad. Sci. U.S.A.* **1988**, *85*, 8790
- (201)Stryer, L. *Biochemistry* 4<sup>th</sup> ed. **1992**, W.H. Freeman and Co. , New York
- (202)Shahrokh, Z.; Verkman, A.S.; Shohet, S.B. *J. Biol. Chem.* **1991**, *266*, 12082
- (203)Yusa, S.; Sakakibara, A.; Yamamoto, T.; Morishima, Y. *Macromolecules*, **2002**, *35*, 10182.

- (204)Kujawa, P.; Liu, R.C.W.; Winnik, F.M. *J. Phys. Chem. B* **2002**, *106*, 5578.
- (205)Fung, B.; Stryer, L. Lateral Energy Transfer in Membranes, 1978, 17, 5241
- (206)Huang, M.H.; Dunn, B.S.; Zink, J.I. *J. Am. Chem. Soc.* **2000**, *122*, 3739
- (207)Zana, R.; Frasc, J.; Soulard, M.; Lebeau, B.; Patarin, J. *Langmuir* **1999**, *15*, 2603
- (208)Vautier-Giongo, C.; Pastore, H.O. *Journal of Colloid and Interface Science*, **2006**, *299*, 874
- (209)Caragheorghopol, A.; Caldararu, H.; Vasilescu, M.; Khan, A.; Angelescu, D.; Zilkova, N.; Cejka, Z. *J. Phys. Chem. B* **2004**, *108*, 7735
- (210)Gilliland, J.W.; Yokoyama, K.; Yip, W.T. *Chem. Mater.* **2005**, *17*, 6702
- (211)Hyatt, J.A. *J. Org. Chem.* **1984**, *49*, 5097.
- (212)Sun, Y-P.; Bunker, C.E.; Hamilton, N.B. *Chem Phys. Lett.* 1993, 210, 111.
- (213)Brennecke, J.F.; Tomasko, D.L.; Peshkin, J.; Eckert, C.A. *Ind. Eng. Chem. Res.* **1990**, *29*, 1682.
- (214)Sun, Y-P. *Supercritical Fluid Technology in Materials Science and Engineering*, Marcel Dekker, Inc. New York, **2002**
- (215)Liu, D.; Zhang, J.; Fan, J.; Han, B.; Chen, J. *J. Phys. Chem. B* **2004**, *108*, 2851
- (216)Cao, T.; Johnston, K.P.; Webber, S.E. *Macromoleules* **2004**, *37*, 1897.
- (217)Gupta, R.R.; RamachandraRao, V.S.; Watkins, J.J. *Macromoleules* **2003**, *36*, 1295.
- (218)Prochazka, K.; Bednar, B.; Mukhtar, E.; Svoboda, P.; Trnena, J.; Almgren, M. *J. Phys. Chem.* **1991**, *95*,4563
- (219)Lissi, E. A.; Abuin, E. B.; Rubio, M. A.; Ceron, A. *Langmuir* **2000**, *16*, 178
- (220)Hasegawa, M.; Yamasaki, Y.; Sonta, N.; Shindo, Y.; Sugimura, T.; Kitahara, A. *J. Phys. Chem.* **1996**, *100*, 15575
- (221)Bein, T., *Chemistry of Materials*, **1996**, *8*, 1636
- (222)Huang, M.H.; Kartono, F.; Dunn, B.; Zink, J.I.; *Chem. Mater.*, **2002**, *14*, 5153
- (223)Hanrahan, J. P.; Copley, M. P.; Ryan, K. M.; Spalding, T. R.; Morris, M. A.; Holmes, J. D. *Chemistry of Materials*, **2004**, *16*, 424
- (224)Beckman, E. J.; *Journal of Supercritical Fluids*, **2004**, *28*, 121
- (225)Harrison, K.; Goveas, J.; Johnston, K. P.; O'Rear, E. A. III.; *Langmuir*, **1994**, *10*, 3536
- (226)Keiper, J. S.; Simhan, R.; DeSimone, J. M.; Wignall, G. D.; Melnichenko, Y. B.; Frielinghaus, H.; *J. Am. Chem. Soc.*, **2002**, *124*, 1834
- (227)Kekicheff, P.; Tiddy, G.J.T.; *J. Phys. Chem.*, **1989**, *93*, 2520
- (228)Giuleri, F.; Krafft, M.P.; *Thin Solid Films*, **1996**, *284-285*, 195
- (229)Asakawa, T.; Hisamatsu H.; Miyagishi, S.; *Langmuir*, 1995, *11*, 478
- (230)ImageJ 'Image processing and analysis in Java', Retrieved Aug 5, **2007**, from <http://rsb.info.nih.gov/ij/>
- (231)Sirard, S. M.; Green, P. F.; Johnston, K. P.; *J. Phys. Chem. B*, **2001**, *105*, 766
- (232)Aksay, I.A.; Trau, M.; Manne, S.; Honma, I.; Yao, N.; Zhou, L.; Fenter, P.; Eisenberger P.M.; Guner, S.M.; *Science*, **1996**, *273*, 892
- (233)NIST Chemistry Webbook 'NIST Standard Reference Database Number 69 - March, 2003 Release', Retrieved Aug 5, **2007**, from <http://webbook.nist.gov/chemistry/>
- (234)Stone, M.T.; da Rocha, S.R.P.; Rossky P.J.; Johnston, K.P.; *J. Phys. Chem. B*, **2003**, *107*, 10185

- (235) Lin, Hong-Ping; Cheng, Yah-Ru; Liu, Shang-Bin; Mou, Chung-Yuan; *Journal of Materials Chemistry*, **1999**, *9*, 1197
- (236) Wong, E. M.; Markowitz, M. A.; Qadri, S. B.; Golledge, S.; Castner, D. G.; Gaber, B. P. *J. Phys. Chem. B* **2002**, *106*, 6652.
- (237) Garnweitner, G.; Smarsly, B.; Assink, R.; Ruland, W.; Bond, E.; Brinker, C. J. *J. Am. Chem. Soc.* **2003**, *125*, 5626.
- (238) Nicole, L.; Boissière, C.; Grosso, D.; Hesemann, P.; Moreau, J.; Sanchez, C. *Chem. Commun.* **2004**, 2312.
- (239) Fan, H.; Reed, S.; Baer, T.; Schunk, R.; Lopez, G. P.; Brinker, C. J. *Micro. Meso. Mater.* **2001**, *44-45*, 625.
- (240) Chen, J. Y.; Pan, F. M.; Chang, L.; Cho, A. T.; Chao, K. J. *Journal of Vacuum Science & Technology, B: Microelectronics and Nanometer Structures--Processing, Measurement, and Phenomena* **2005**, *23*, 2034.
- (241) Ciaramella, F.; Jousseau, V.; Maitrejean, S.; Verdier, M.; Remiat, B.; Zenasni, A.; Passemard, G. *Thin Solid Films* **2006**, *495*, 124.
- (242) Jang, K.; Song, M.; Cho, S.; Kim, J. *Chem. Commun.*, **2004**, 1514.
- (243) Hwang, Y. K.; Patil, K. R.; Jhung, S. H.; Chang, J.; Ko, Y. J.; Park, S. *Micro. Meso. Mater.* **2005**, *78*, 245.
- (244) Gupta, G.; Shah, P. S.; Zhang, X.; Saunders, A. E.; Korgel, B. A.; Johnston, K. P. *Chem. Mater.* **2005**, *17*, 6728.
- (245) Ghosh, K.; Lehmler, H.; Rankin, S. E.; Knutson, B. L. *Langmuir* **2005**, *21*, 6145.
- (246) Cao, C. T.; Fadeev, A. Y.; McCarthy, T. J. *Langmuir* **2001**, *17*, 757.
- (247) Combes, J. R.; White, L. D.; Tripp, C. P. *Langmuir* **1999**, *15*, 7870.
- (248) Pai, R. A.; Watkins, J. J. *Advanced Materials* **2006**, *18*, 241.
- (249) Yazdi, A. V.; Beckman, E. J. *Mater. Res.* **1995**, *10*, 530.
- (250) Ye, W.; Keiper, J. S.; DeSimone, J. M. *Chinese Journal of Polymer Science* **2006**, *24*, 95.
- (251) Eastoe, J.; Dupont, A.; Steytler, D. C. *Current Opinion in Colloid & Interface Science* **2003**, *8*, 267.
- (252) Kruk, M.; Jaroniec, M.; Gadkaree, K. P. *Langmuir* **1999**, *15*, 1442.
- (253) Kruk, M.; Jaroniec, M.; Sayari, A. *Langmuir* **1997**, *13*, 6267.
- (254) Bothun, D. G.; Kho, Y. W.; Berberich, J. A.; Shofner, J. P.; Robertson, T.; Tatum, K. J.; Knutson, B. L. *J. Phys. Chem. B* **2005**, *109*, 24495.
- (255) Andreas, J. M.; Hauser, E. A.; Tucker, W. B. *J. Phys. Chem.* **1938**, *42*, 1001.
- (256) Kho, Y. W.; Conrad, D. C.; Knutson, B. L. *Fluid Phase Equilibria* **2003**, *206*, 179.
- (257) Alberius, P. C. A.; Frindell, K. L.; Hayward, R. C.; Kramer, E. J.; Stucky, G. D.; Chmelka, B. F. *Chem. Mater.* **2002**, *14*, 3284.
- (258) Klotz, M.; Ayrat, A.; Guizard, C.; Cot, L. *J. Mater. Chem.* **2000**, *10*, 663.
- (259) Rankin, S. E.; Tan, B.; Lehmler, H.; Hindman, K. P.; Knutson, B. L. *Micro. Meso. Mater.* **2004**, *73*, 197.
- (260) SPARTAN, student version; Wavefunction, Inc.: Irvine, CA, 1998.
- (261) Oates, J. D. *J. Colloid Interface Sci.* **1989**, *131*, 307.
- (262) Wissinger, R. G.; Paulaitis, M. E. *J. Polym. Sci., Polym. Phys. Ed.* **1987**, *25*, 2497.
- (263) Zhang, Y.; Gangwani, K. K.; Lemert, R. M. *J. Supercrit. Fluids* **1997**, *11*, 115.
- (264) Goel, S. K.; Beckman, E. J. *Polymer* **1993**, *34*, 1410.

- (265) Fleming, G. K.; Koros, W. J. *Macromolecules* **1986**, *19*, 2285.
- (266) Chun, B.-S.; Wilkinson, G. T. *Ind. Eng. Chem. Res.* **1995**, *34*, 4371.
- (267) Psathas, P.; Sander, E. A.; Lee, M. Y.; Lim, K. T.; Johnston, K. P. *J. Disp. Sci. Tech.* **2002**, *23*, 65.
- (268) Bancroft, W. D. *J. Phys. Chem.* **1913**, *17*, 501.
- (269) Kahlweit, M. *Microemulsions in Chemical Thermo*, Letcher, T. Ed. Blackwell, Oxford, UK, **1999**, 37.
- (270) Hentze, H.; Kaler, E.W. *Chem. Mater.* **2003**, *15*, 708.
- (271) Hentze, H.; Co, C. C.; McKelvey, C. A.; Kaler, E. W. *Topics in Curr. Chem.* **2003**, *226*, 197.
- (272) Turner, C; Topgaard, D; Sivik, B.; Bergenstahl, B. *Colloids and Surfaces A: Physichem. Eng. Aspects* **2003**, *213*, 69.
- (273) Scanu, L. F.; Gubbins, K. E.; Hall, C. K. *Langmuir* **2004**, *20*, 514.
- (274) Ghosh, K.; Vyas, S.H.; Lehmler, H.; Rankin, S.E.; Knutson, B.L. *J. Phys. Chem. B* **2007**, *111*, 363.
- (275) Grieken, R.; Stucky, G. D.; Melero, J. A.; Iglesias, J. *Langmuir* **2002**, *18*, 10.
- (276) Lu, X.B.; Zhang, W. H.; He, R.; Li, X. *Ind. Eng. Chem. Res.* **2003**, *42*, 653.
- (277) Niemeyer, E.D.; Bright, F.V. *J. Phys. Chem.* **1998** *102*, 1474.
- (278) Ziegler, K.J.; Hanrahan, J. P.; Glennon, J. D.; Holmes, J.D. *J. Supercrit. Fluids* **2003**, *27*, 109.
- (279) Chang, S. H.; Park, S. C.; Shim, J. J.; *J. Supercrit. Fluids* **1998**, *13*, 113.
- (280) Garg, A.; Gulari, E.; Manke, W. *Macromolecules*, **1994**, *27*, 5643.
- (281) Zhang, Y.; Gangwani, K.K.; Lemert, R.M. *J. Supercrit. Fluids* **1997**, *11*, 115.
- (282) Koga, T.; Seo, Y.; Shin, K.; Zhang, Y.; Rafailovich, M.H.; Sokolov, J.C.; Chu, B.; Satija, S.K. *Macromolecules*, **2003**, *36*, 5236.
- (283) Shah, P.S.; Hanrath, T.; Johnston, K. P.; Korgel, B.A. *J. Phys. Chem. B*, **2004**, *108* 9574.
- (284) Guney, O.; Akgerman, A. *AIChE J.* **2002**, *48*, 856.
- (285) Pathak, P.; Mezziani, M.J.; Desai, T.; Sun, Y. *J. Am. Chem. Soc.* **2004**, *126*, 10842.
- (286) Liu, H.; Finn, N.; Yates, M. Z. *Langmuir*, **2005**, *21* 379.
- (287) Zang, J.; Han, B.; Hou, Z.; Liu, Z.; He, J.; Jiang, T. *Langmuir*, **2003**, *19* 7616.
- (288) Lee, S.; Kim, M. S.; Kim, J. S. ; Park, H. J.; Woo, J. S. ; Lee, B. C.; Hwang, S. J. *J. Microencapsulation*, **2006**, *23* 741.
- (289) Fletcher, P. D. I.; Robinson, B. H.; Freedman, R. B.; Oldfield, C. J. *Chem. Soc. Faraday Trans.* **1985**, *81*, 2667.
- (290) Toews, K. L.; Shroll, R. M.; Wai, C. M.; Smart, N. G. *Anal. Chem.* **1995**, *67*, 4040.
- (291) Ashraf-Khorassani, M.; Combs, M. T.; Taylor, L. T. *J. Chromatogr. A* **1997**, *774* 37.
- (292) Shah, P. S.; Holmes, J. D.; Doty, R. C.; Johnston, K. P.; Korgel, B. A. *J. Am. Chem. Soc.* **2000**, *122*, 4245.
- (293) Senapati, S.; Keiper, J. S.; DeSimone, J. M.; Wignall, G. D.; Melnichenko, Y. B.; Frielinghaus, H.; Berkowitz, M. L. *Langmuir* **2002**, *18*, 7371
- (294) Meng, X.; Di, Y.; Zhao, L.; Ziang, D.; Li, S. Xao, F. *Chem. Mater.* **2004**, *16*, 5518.
- (295) Krafft, M. P.; Riess, J. G. *Biochemie* **1998**, *80*, 489.



- (296)Blin, J. L.; Lesieur, P.; Ste'be', M. J. *Langmuir* **2004**, *20*, 491.
- (297)Ghosh,K; Bashadi, S.; Lehmler, H.; Rankin, S.E.; Knutson, B.L. *submitted to Micro. Meso. Mater.*
- (298)Senapati, S.; Berkowitz, M. L. *J. Phys. Chem. B* **2003**, *107*, 12906.
- (299)Kirmizialtin, S.; Menciloglu, Y.Z.; Baysal, C. *J. Chem. Phys.* **2003**, *119*, 4953.
- (300)Senapati, S; Berkowitz, M.L. *J. Chem. Phys.* **2003**, *118*, 1937.
- (301)Dardin, A.; Desimone, J.M.; Samulski, E.T. *J. Phys. Chem. B* **1998**, *102*, 1775.
- (302)Cece, A.; Jureller, S.H.; Kerscher, J.L.; Moschner, K.F. *J. Phys. Chem.* **1996**, *100*, 7435.
- (303)Yonker, C.R.; Palmer, B.J. *J. Phys. Chem. A* **2001**, *105*, 308.
- (304)Diep, P.; Jordan, K.D.; Johnson, J.K.; Beckman, E.J. *J. Phys. Chem. A* **1998**, *102*, 2231.
- (305)Yabu, H.; Shimomura, M. *Chem. Mater.*, **2005**, *17*, 5231.
- (306)Zou, X.P.; Kang, E.T.; Neoh, K.G.; Huang, W. *J. Adhesion Science and Technology* **2001**, *15*, 1655
- (307)Kheshgi, H. S. In *Liquid film coating: scientific principles and their technological implications*; Kistler, S. F., Schweizer, P. M., Eds.; Chapman and Hall: New York, 1997; pp 183-205.
- (308)Kim, J.; Novick, B.J.; DeSimone, J.M.; Carbonell, R.G. *Langmuir* **2006**, *22*, 642.
- (309)U. S. Patent 5,851,674 (1999).
- (310)Choi, J.; Kawaguchi, M.; Kato, T. *IEEE Transactions on Magnetics*, **2004**, *40*, 3189
- (311)Diaz, M.E.; Cerro, R.L. *Thin Solid Films*, **2004**, *460*, 274
- (312)Cerro, R.L. *J. Colloid Interface Sci* **2003**, *257*, 276
- (313)Yerushalmi-Rozen, R.; Klein, J. *Langmuir* 1995, *11*, 2806.
- (314)Thiele, U.; Mertig, M.; Pompe, W. *Phys. Rev. Lett.* **1998**, *80*, 2869.
- (315)Wongcharee, K.; Brings, M.; Chaplin, R.; Hong, Y. J.; Sizgek, E. *J. Sol-Gel Science and Technology*, **2004**, *29*, 115.
- (316)Setoguchi, Y.; Teraoka, Y.; Moriguchi, I.; Kagawa, S.; Tomonaga, N.; Yasutake, A.; Izumi, J. *J. Porous Materials*, **1997**, *4*, 129
- (317)Rankin, S. E.; Malanoski, A.; Van, P.; Swol, F. *Materials Research Society Symposium Proceedings* **2001**, *636*, D1.2/1.
- (318)Lee, C. T.; Bhargava, P.; Johnston, K. P. *J. Phys. Chem. B* **2000**, *104*, 4448
- (319)O'Neill, M. L.; Cao, Q.; Fang, M.; Johnston, K. P.; Wilkinson, S. P.; Smith, C. D.; Kerschner, J. L.; Jureller, S. H. *Ind. Eng. Chem. Res.* **1998**, *37*, 3067
- (320)Bunker, B. C.; Carpick, R. W.; Assink, R. A.; Thomas, M. L.; Hankins, M. G.; Voigt, J. A.; Sipola, D.; de Boer, M. P.; Gulley, G. L. *Langmuir* **2000**, *16*, 7742.
- (321)Yamayauchi, Y.; Sawada, M.; Noma, T.; Ito, H.; Furumi, S.; Sakka, Y.; Kuroda, K. *J. Mater. Chem.* **2005**, *15*, 1137.
- (322)Yates, M. Z.; Apodaca, D. L.; Campbell, M. L.; Birnbaum, E. R.; McCleskey, T. M. *Chem. Commun.* **2001**, 25.
- (323)Ghenciu, E. G.; Russell, A. J.; Beckman, E. J. *Biotechnol. Bioeng.* **1998**, *58*, 572.
- (324)Fernandez, R.; Franville, A.; Minoofar, P.; Dunn, B.; Zink, J. *J. Am. Chem. Soc.* **2001**, *123*, 1248
- (325)Minoofar, P.N.; Hernandez, R.; Chia, S.; Dunn, B.; Zink, J.I.; Franville, A-C *J. Am. Chem. Soc.* **2002**, *124*, 14388.

- (326) Meng, Q.; Fu, L.; Lin, J.; Zhang, H.; Wang, S.; Zhou, Y.; Yu, M.; Liu, F. *J of Phys. And Chem. of Solid* **2003**, *64*, 63.
- (327) Bartl, M.H.; Scott, B.J.; Wirnsberger, G.; Popitsch, A.; Stucky, G.D. *Chem Phys Chem* **2003**, 392.
- (328) Gilliland, J.W.; Yokoyama, K.; Yip, W.T. *Chem. Mater.* **2005**, *17*, 6702.
- (329) Yao, Y.; Zhang, M.; Shi, J.; Gong, M.; Zhang, H.; Yang, Y. *Materials Letters*, **2001**, *48*, 44.
- (330) Ogawa, M.; Igarashi, T.; Kuroda, K. *Chem. Mater.* **1998**, *10*, 1382
- (331) Zagrobelny, J.; Bright, F.V. *J. Am. Chem. Soc.* **1993**, *115*, 701.
- (332) Davis, G.A. *J.C.S. Chem. Comm.* **1973**, 728.
- (333) Wade, D.A.; Tucker, S.A. *Talanta*, **2000**, *53*, 571
- (334) Miola, L.; Ab akerli, R. B.; Ginani, M. F.; Filho, P. B.; Toscano, V. G.; Quina, F. *H. J. Phys. Chem.* **1983**, *87*, 4417
- (335) Ayala, J.H.; Afonso, A.M.; Gonzalez, V. *App. Spectroscopy*, **1997**, *51*, 380.
- (336) Angelescu, D.; Vasilescu, M. *J. Colloid and Interface Science* **2001**, *244*, 139.
- (337) Yamayauchi, Y.; Sawada, M.; Noma, T.; Ito, H.; Furumi, S.; Sakka, Y.; Kuroda, K. *J. Mater. Chem.* **2005**, *15*, 1137.
- (338) McFann, G.J. *Ph.D. Dissertation*, The University of Texas at Austin, **1993**.
- (339) Suwa, M.; Hashidzume, A.; Morishima, Y.; Nakato, T.; Tomida, M. *Macromolecules*, **2000**, *33*, 7884.
- (340) Gonzalez-Garcia, J.; Molina, M.J.; Rodriguez, F.; Mirada, F. *J. Chem. Eng. Data* **2001**, *46*, 918.
- (341) Zuniga-Moreno, A.; Galicia-Luna, L.A.; Camacho-Camacho, L.E. *Fluid Phase Equilibria*, **2005**, *234*, 151.
- (342) Winnik, F.M. *Polymer*, **1990**, *31*, 2125.
- (343) Kramer, M.C.; Steger, J.R.; Hu, Y.; McCormick, C.L. *Macromolecules*, **1996**, *29*, 1992.
- (344) McCool, B.; Tripp, C.P. *J. Phys. Chem. B* **2005**, *109*, 8914
- (345) Lisal, M.; Hall, C.K.; Gubbins, K.E.; Panagiotopoulos, A. *J. Chem. Phys.*, **2002**, *116*, 1171.
- (346) Lisal, M.; Hall, C.K.; Gubbins, K.E.; Panagiotopoulos, A. *Molecular Simulation*, **2003**, *29*, 139
- (347) Siperstein, F. R.; Gubbins, K. E. *Molecular Simulation* **2001**, *27*, 339.
- (348) Siperstein, F. R.; Gubbins, K. E. *Langmuir* **2003**, *19*, 2049.
- (349) Liu, N.; Assink, R. A.; Brinker, C. J. *Chem. Commun.* **2003**, 370.
- (350) Petkov, N.; Mintova, S.; Jean, B.; Metzger, T.; Bein, T. *Mater. Sci. Eng. C* **2003**, *23*, 827.
- (351) Hiyoshi, N.; Yogo, K.; Yashima, T. *Micr. Meso. Mater.* **2005**, *84*, 357.
- (352) Kawi, S.; Lai, M. *Chem. Commun.*, 1998, 1407
- (353) Kluson, P.; Kacer, P.; Cajthaml, T.; Kalaj, M. *J. Mater. Chem.*, **2001**, *11*, 644.
- (354) Huang, L.; Poh, C.; Ng, S. C.; Hidajat, K.; Kawi, S. *Langmuir* **2005**, *21*, 1171
- (355) Fink, R.; Beckman, E.J. *Journal of Supercritical Fluids*, **2000**, *13*, 101.
- (356) Singley, E.J.; Wei, L.; Beckman, E.J. *Fluid Phase Equilibria* **1997**, *128*, 199.
- (357) Hoefling, T.; Stofesky, D.; Reid, M.; Beckman E.; Enick, R.E. *Journal of Supercritical Fluids*, **1992**, *5*, 237.

- (358) Firouzi, A.; Schaefer, D. J.; Tolbert, S. H.; Stucky, G. D.; Chmelka B. F. *J. Am. Chem. Soc.* **1997**, *119*, 9466.
- (359) Tolbert, S. H.; Firouzi, A.; Stucky, G. D.; Chmelka B. F. *Science*, **1997**, *278*, 264
- (360) Froba, G.; Kalus, J. J. *Phys. Chem.* 1995, *99*, 14450.

## VITA

**Date of Birth:**

February 26, 1979

**Place of Birth:**

Calcutta, India

**EDUCATION**

B.S. Chemical Engineering, Jadavpur University, Calcutta, India, 2001

**PROFESSIONAL POSITION**

Summer Intern: July 2002 – July 2002, Haldia Petrochemicals Limited, Haldia, India

**PUBLICATIONS**

Kaustav Ghosh; Hans-Joachim Lehmler; Stephen E. Rankin; Barbara L. Knutson  
“Supercritical Carbon Dioxide Processing of Fluorinated Surfactant Templated  
Mesoporous Silica Thin Films”, *Langmuir*, 2005, 21, 6145-6149.

Kaustav Ghosh; Sandhya H. Vyas; Hans-Joachim Lehmler; Stephen E. Rankin; Barbara  
L. Knutson “Carbon Dioxide Controlled Pore Tailoring of Ordered Mesoporous Silica  
Thin Films Templated by Homologous Series of Fluorinated Surfactants” *Journal of  
Physical Chemistry B*, 2007, 111, 363-370.

Kaustav Ghosh; Sarah Bashadi; Hans-Joachim Lehmler; Stephen E. Rankin; Barbara L.  
Knutson “Surfactant Tail Solvation in Mesoporous Ceramics as a Function of  
Supercritical Carbon Dioxide Processing Conditions ” submitted to *Microporous and  
Mesoporous Materials*..

**PRESENTATIONS (underlined represents presenter)**

Barbara Knutson, Kaustav Ghosh, Stephen Rankin and Hans-Joachim Lehmler, “Carbon  
Dioxide Processing of Surfactant Templates in Porous Silica Probed by In-Situ  
Spectroscopy”, 2007 ACS Colloid & Surface Science Symposium, Newark, DE.

Kaustav Ghosh, Barbara Knutson, Stephen Rankin and Hans-Joachim Lehmler, “In-Situ  
Fluorescence Spectroscopy of Supercritical Carbon Dioxide Swelling of Surfactant  
Templates in Porous Silica Films”, 2006 Annual Meeting of American Institute of  
Chemical Engineers, San Francisco, CA.

Sarah Bashadi, Barbara Knutson, Kaustav Ghosh, Stephen Rankin and Hans-Joachim Lehmler, “Pore Expansion in Fluorinated Surfactant Templated Silica Powders by Supercritical Carbon Dioxide Processing”, 2006 Annual Meeting of American Institute of Chemical Engineers, San Francisco, CA.

Barbara Knutson, Kaustav Ghosh, Sarah Bashadi, Stephen Rankin and Hans-Joachim Lehmler, “Supercritical Carbon Dioxide Processing of Mesoporous Silica Templated by Fluorinated Surfactants”, 2006 Interamerican Congress of Chemical Engineering, Buenos Aires, Argentina.

Kaustav Ghosh, Barbara Knutson, Stephen Rankin and Hans-Joachim Lehmler, “Pore Expansion in Cationic Fluorinated Surfactant Templated Porous Silica Thin Films through Supercritical Carbon Dioxide Processing”, 2005 Annual Meeting of American Institute of Chemical Engineers, Cincinnati, OH.

Kaustav Ghosh, Barbara Knutson, Stephen Rankin and Hans-Joachim Lehmler, “Tailored Thin Films through CO<sub>2</sub> Processing of Fluorinated Surfactant Templated Silica”, 2005 Chemical Engineering Graduate Student Symposium, Morgantown, WV.

Kaustav Ghosh, Barbara Knutson, Stephen Rankin and Hans-Joachim Lehmler, “Pore Expansion in Fluorinated Surfactant Templated Porous Silica Thin Films through Supercritical CO<sub>2</sub> Processing”, 2005 ACS Colloid & Surface Science Symposium, Potsdam, NY.

Kaustav Ghosh, Barbara Knutson, Stephen Rankin and Hans-Joachim Lehmler, “Supercritical Carbon Dioxide Processing of Fluorinated Surfactant-Templated Mesoporous Silica Thin Films”, 2004 Annual Meeting of American Institute of Chemical Engineers, Austin, TX.